UNIVERSITY OF OKLAHOMA

GRADUATE COLLEGE

INTRODUCING THE CONNECTED RESERVOIR STORAGE CONCEPT FOR RESERVOIR CHARACTERIZATION AND PRODUCTION FORECAST

A DISSERTATION

SUBMITTED TO THE GRADUATE FACULTY

in partial fulfillment of the requirements for the

Degree of

DOCTOR OF PHILOSOPHY

By

DAVID R. CHILDERS
Norman, Oklahoma
2020

INTRODUCING THE CONNECTED RESERVOIR STORAGE CONCEPT FOR RESERVOIR CHARACTERIZATION AND PRODUCTION FORECAST

A DISSERTATION APPROVED FOR THE
MEWBOURNE SCHOOL OF PETROLEUM AND GEOLOGICAL ENGINEERING

BY THE COMMITTEE CONSISTING OF

Dr. Xingru Wu, Chair

Dr. Peter Attar

Dr. Deepak Devegowda

Dr. Ahmed Ghassemi

Dr. Zulfiquar Reza

© Copyright by DAVID R. CHILDERS 2020
All Rights Reserved.

For my wife Paula and my son Vonn without you this journey could not be possible.

Acknowledgements

To my doctoral advisor and mentor Dr. Wu thank you for all that you have given me. I would also like to express my sincere gratitude to all the committee members on my doctoral advisory board, and Pengiu Wang for his research contributions, while at British Petroleum.

Table of Contents

List of Tables

List of Figures

Abstract

This research presents a novel concept of the connected reservoir storage (CRSM) with which we can characterize the reservoir and accurately predict the production performance of hydrocarbon reservoirs, which have a complex reservoir geometry and have a considerable uncertainty of reservoir energy support. Based on the deconvolution of measured pressures and rate data from a well, both a liquid and gas reservoir performance can be modeled using a group of normalized quantities with which the behavior of the well can be accurately predicted in all flow regimes. No foreknowledge of reservoir geometries, petro-physical properties, or fluid properties is required to develop this analysis.

Reservoir storage is a time function defined as the product of the total compressibility and the reservoir volume at a particular time. Unlike with classical or curve fitting decline curve analysis, the CRSM is based on the pressure diffusivity theory by the normalized production rate and normalized cumulative production volume through deconvolution methods. With the knowledge of reservoir volumes, the long term well performance of liquid or gas reservoirs can be predicted. Through the development of the CRSM, three profiles can be ascertained and are interrelated to shed valuable insight into the production potential and health of a liquid or gas reservoir that exhibits complex formation geometries. The three curves are the reservoir response curve (RPC), normalized decline curve (NDC), and connected reservoir storage curve (CRSC). Utilizing the three curves stated above embodies a more powerful reservoir performance analysis technique for predicting the production potential of complex reservoirs.

The CRSM will be presented from the fundamental material balance approach and mathematical equations will be derived for the model related to both liquid and gas reservoir production. The CRSM concept will be validated through the development of numerical simulation

models, conventional well application, with varying permeabilities, porosities and well geometries through the use of a reservoir simulation suite with known reservoir parameters and the utilization of deconvolution techniques to develop the CRSM. The CRSM will then be used to evaluate the reservoir response behavior to better approximate and characterize the flow and pressure behavior utilizing simulated production data of a bi-wing hydraulically fractured undersaturated oil reservoir, tight well application, and compare the CRSM to two classical forecasting methods. Additional studies using the CRSM will be applied to shale gas well performance comprised of a formation where the matrix is made up of very low permeable media (Kim and Lee, 2015). Moreover, this research will conclude by applying the CRSM to evaluate the reservoir response behavior to characterize the fracture network system in a shale gas reservoir with multi-stage hydraulic fracturing along the horizontal segment.

The application ability of the CRSM allows for the bridging of the production decline and reservoir pressure response from production data found in the public domain. This concept enables one to evaluate and forecast current and future volume production, reservoir pressure behavior, average reservoir pressure and determine original fluids in place with no prior knowledge of reservoir geometries, petro-physical or fluid properties. With the development of this model, decline curve analysis (DCA) can be extended into the transient regime of the production period.

Chapter 1: Introduction

1.1 Connected Reservoir Storage Model (CRSM)

The CRSM will be presented from the fundamental material balance approach and mathematical equations will be derived for this model as it relates to both liquid and gas reservoirs. The primary objective of completing or stimulating reservoirs is to bypass formation damage encountered in the drilling and completion phase of a new well and by opening highly conductive fractures to increase the contacting surface area such that a well can be economically produced from a very low permeable media (Bybee, 2011). Tight reservoirs require a stimulation process such that recoverable resources can be produced economically due to flow behavior in tight reservoirs with multistage fractured horizontal wells being acutely complex (Wu, 2015). The actual physics behind the flow and transport processes regarding tight formations is insufficiently understood; therefore, at this time there is not an effective way of modeling the dynamic flow behaviors during the process of development (Spivey and Lee, 2013). One common approach regarding production performance analysis and forecasting is using conventional reservoir simulation to approximate hydrocarbon migration and rate forecast. This method is usually time-consuming and contains large uncertainties due to poor reservoir characterization of its heterogeneity. Another practical way is to use decline curve analysis (DCA), such as the Arps' model (Arps, 1945), which is often used to evaluate tight formation performance, even though the fundamental assumptions are highly questionable for reservoirs with permeability in the order of nano-Darcy's. Therefore, there is a need to develop physics-based mathematical models as well as associated modeling tools for assisting in the development and quantification of tight formation oil and gas resources.

Tight formation wells that are completed with hydraulic fractures exhibit multiple flow regimes including linear flow, boundary dominated flow via fracture interface, linear flow in the unstimulated matrix that may or may not appear during the life of the well (Joshi and Lee, 2013). Currently, several methods have been empirically formulated for shale and tight formation wells. These methods are Power Law Exponential Decline (PLE) (Ilk et al., 2008), Stretched Exponential Decline (SEPD), (Valkó and Lee, 2010), the Duong model (Duong, 2011) and the logistic growth model (LGM) (Clark et al., 2011b) and each method has different parameters used for history matching for the goodness of fit using numerical regression (Agarwal et al., 1999; Duong, 2011; Freeborn and Russell, 2012; Kanfar and Wattenbarger, 2012). Other curve fitting based models that have been developed for tight formations in the past five years are the composite type curve model (Childers and Callard, 2015), and the combined capacities resistance model (CRM), which was developed as a data-driven approach using the physics of the reservoir to find a collaboration between analytical and empirical methodologies, which was initially designed for waterflood performance with an application for unconventional wells (Pan, 2016), the Fracture Decline Model (FDC) based on uncharacteristic anomalous diffusion principles (Zuo et al., 2016). The Variable Decline Modified Arps' model (Gupta et al., 2018) modifies the existing Arps' exponential decline curve by replacing the constant decline rate with power-law function for variable decline rates, which in turn has been applied to existing shale reservoir. Ravikumar and Lee (2019) proposed Bayesian estimations and prior probability distributions to facilitate noise reduction for better estimates in the loss ratio and Arps' b-factor to understand reservoir flow regimes when applied to tight formation reservoirs. Currently, one aspect that is challenging for empirical models to reconcile is due to the high initial production from a tight reservoir, which is caused by the fracture network unloading, which results in early production in two transient flow phenomena, fracture linear flow followed by bilinear flow (Wasaki and Akkutlu, 2015). Flow characteristics in tight formations are still not well understood; therefore, most of the empirical curve-fitting techniques cannot be used to accurately predict reservoir behavior in the long term and lose accuracy when production schedules are modified (Childers and Wu, 2017). Uncertainty in reserve estimates using DCA techniques has led to the need for probabilistic methods to overcome shortcomings with tight formation reservoirs (Holdaway, 2013).

This research focuses on production forecast from a reservoir system comprised of low permeable matrix and fracture networks, which features multiple flow regions and complex reservoir energy charging. The CRSM differs from the empirical methods as it relies on the actual physics of the reservoir, lending itself to more acceptable reservoir forecasting results with the novelty being the implementation through deconvolution to converge on a solution that will update in real-time and forgoes the need to use tuning parameters as in classical empirical methods. The model utilizes production rate history and well flowing bottom-hole pressure that can be readily found or determined in practice. Utilizing the CRSM allows for production performance prediction to be applied to a well with varying operational conditions, which will exceed the current curve fitting based models. The CRSM was first developed using numerical simulation models with variable reservoir parameters via reservoir simulation and deconvolution techniques. The CRSM was then used to evaluate the reservoir response behavior to better approximate and characterize the flow and pressure behavior utilizing simulated production data of a bi-wing hydraulically fractured undersaturated oil reservoir. The CRSM was then applied to shale gas well performance where the matrix is made up of very low permeable media to predict future production behavior. Lastly, the CRSM was applied to characterize the fracture network system in a shale gas reservoir with multi-stage hydraulic fracturing along the horizontal segment.

1.2 Research Motivation:

The motivation of this research is to present a new approach of evaluating reservoir response behavior to accurately predict well production performance through the concept of the CRSM as it relies on the actual physics of the reservoir; thereby, lending itself to more accurate reservoir forecasting results. This model utilizes production rate history and well flowing bottom-hole pressure from numerical simulation models and actual production data from a shale reservoir. This research continues the efforts of DCA but utilizes the CRSM that allows for the extension of DCA into the transient and pseudosteady state (PSS) flow regimes.

1.3 Research Objectives:

The limitations of the empirically formulated methods previously mentioned have led to the development of the CRSM bypassing the ambiguous nature when using empirical methods by incorporating reservoir diffusivity theory and to allow for rate forecasting with changes in operational conditions. The CRSM determines a unit response behavior of a producing reservoir - through the utilization of deconvolution techniques - from measured transient pressure and production rate data (Kuchuk et al., 2010a). Deconvolution has been used to determine a wide variety of reservoir parameters such as the minimum tested reservoir volume (Whittle and Gringarten, 2008), enhanced reservoir characterization (Ahmad et al., 2016), and used in the minimization and removal of wellbore storage effects (Dastkhan et al., 2015). Details and other applications in the determination of reservoir characteristics as well as pressure transient analysis applications can be found in the literature (Levitan, 2005; Levitan and Wilson, 2012).

1.4 Layout of Chapters:

Chapter 2 is a literature review of the various production forecasting methodologies and fracture diagnostic methods used in tight formations that exhibit low permeable media. The mathematical models, assumptions, limitations, and applications will be discussed. This chapter intends to help the reader understand the various methodologies of the existing problems when utilizing these methods with production forecasting and fracture diagnostics.

Chapter 3 is the introduction of the CRSM. This chapter will detail how the CRSM was derived and how it should be implemented to aid in production forecasting and fracture diagnostics along with model validation.

Chapter 4 applies the CRSM to a bi-wing hydraulically fractured undersaturated oil reservoir to predict production performance and compare the results to two classical empirical techniques currently used in unconventional reservoir predictions. The validation is done via numerical simulation.

Chapter 5 will demonstrate the interrelated paradigms among well performance, increasing reservoir connected volume, and rate forecasts with uncertainties. This research uses the operational history of a shale gas well to demonstrate the CRSM's capability in rate prediction under variable operating conditions.

Chapter 6 applies the CRSM to the actual production rate and pressure of a shale gas reservoir free of subsurface uncertainties and can be used efficiently to characterize the flow regimes and reservoir boundaries, derive the reservoir behavior, and predict production performance to quantify hydraulic fractures using the CRSM. This chapter will demonstrate that the CRSM can be used in lieu of stimulated reservoir volume (SRV) for multiple stage fracture characterization. The CRSM allows for estimating the efficiency of a stimulation program through production decline and reservoir pressure response from production data and is strongly physics-based.

Chapter 7 presents conclusion, recommendations, and future research endeavors.

Chapter 2: Literature Review

This chapter will review the current methodologies, mathematical models, and practices regarding prediction models used in tight formations such as reservoirs classified as shales and sandstones. This review will also look at the current technologies used to characterize fractures after undergoing a hydraulic stimulation process. Fracture technologies will be reviewed based on mechanisms, advantages, limitations, and uncertainties when evaluating hydraulic fracture treatment. Hydraulic fracturing of a reservoir has two motivations. (1) To accelerate the production potential of oil or gas reservoirs through the increase of the productivity index, while unlocking trapped hydrocarbons in tight formations that would not otherwise be economically viable to produce, in this case, tight formations. (2) To bypass the near-wellbore skin damage induced by drilling and completion practices to allow better communication with the reservoir, in this case conventional wells. Whichever well classification, conventional or unconventional, one is evaluating, the need for understanding fracture characterization is imperative to surmise how hydraulic fractures interface with natural fractures in the reservoir, example shales, and understand how the induced hydraulic fractures propagate near the wellbore and far away from the wellbore.

2.1 Current Production Forecasting Methods:

Throughout the literature, there have been many research efforts to develop mathematical models such that the behavior of tight formation production can be estimated and projected into the future. Projecting production from tight formations has been an ongoing challenge due to the uncertainties one encounters when evaluating shales and sandstones, which are deemed unconventional due to their very low permeable media. Some of the uncertainties of hydrocarbon production reside in the fluid transport mechanism when encountering hydraulic fractures and the natural fractures in the formation (Tan et al., 2018). Reservoir simulation methods are arguably the most efficient method for production forecasting; however, this can be time consuming and expensive. Many production models have been developed, mostly empirical except for the combined capacities resistance model (CRM), which was developed as a data-driven approach using the physics of the reservoir to find a collaboration between analytical and empirical methodologies (Pan, 2016). The following review will look at the most common models used in production forecasting of tight formations and discuss their governing assumptions, applications, and limitations.

2.1.1 Reservoir Simulation

Perhaps the most efficient way to develop production forecasting models is through reservoir simulation; however, simulators are predicated on classical diffusivity equations based on Darcy flow mechanisms and the complexity of the tight formation wells regarding organic matter, petrophysical properties and nanopores make it extremely challenging to develop simulation models to capture all of the multifaceted flow mechanism one would encounter. Moreover, gathering the needed information to properly develop a reservoir simulation model can be expensive and time consuming and one needs to evaluate the economic feasibility to determine if the information needed to conduct reservoir simulation is warranted (Tan et al., 2018). Lastly, in depth experience is paramount to developing a good reservoir simulation model where one needs a good foundational understanding of conservation of mass, energy and momentum as well equations of state and constitutive equation, which is the foundation of reservoir simulation and each element can contribute to uncertainty in reservoir simulation analysis (Ertekin et al., 2019).

2.1.2 Hydrocarbon Tight Formation Production Models

Many models have been developed or have been adapted to predict the production performance of tight reservoirs. This section will discuss the most commonly used foundational models found in the literature and emphasize their applications and limitations.

The most often used classical production forecasting model used in evaluating tight formation production has been the Arps model introduced in 1945 (Arps, 1945). The governing assumptions regarding the Arps model state that the bottom-hole flowing pressure (BHFP), skin factor and drainage area must be constant, and the flow regime has reached boundary dominated flow. Arps defined the change in flow rate by Eq. (2-1) where D the continuous decline rate per unit time, for liquid flow rate in STB per unit of time and gas flow rate in Mscf per unit of time.

$$D = -\frac{d(\ln q)}{dt} \tag{2-1}$$

The Arps exponent b is described as the time rate of change to the reciprocal rate of the decline rate Eq. (2-2) and should remain constant throughout the life of the well.

$$b = \frac{d\left(1/D\right)}{dt} \tag{2-2}$$

Integrating Eq. (2-2) for 0 to t, a unit of time, and assuming at $t = 0$ that $D = D_i$, where D_i is the initial decline rate at $t = 0$, then Eq. (2-2) becomes Eq. (2-3) as follows:

$$D = \frac{D_i}{1 + bD_i t} \tag{2-3}$$

Setting Eq. (2-1) equal to Eq. (2-3) gives the general differential expression of the Arps equation:

$$-\frac{d(\ln q)}{dt}=\frac{D_i}{1+bD_it} \tag{2-4}$$

From this expression, Eq. (2-4), three cases where assessed for Arps exponent values of $b = 0$, exponential case, $0 < b < 1$, hyperbolic case, and b=1, harmonic case. From the Arps model a few observations should be discussed. (1) The assumption that the Arps exponent b remains constant throughout the life of the reservoir is an impracticality for any well especially that of tight formations as Arps fails to fit early time production of tight formation performance. (2) The Arps is essentially only applicable to medium or high permeable reservoirs as one of the governing assumptions is that it has reached boundary dominated flow rather quickly, which is not the case for tight formation reservoirs as this may take months if not years to reach boundary dominated flow. The Arps model is mathematically simple and is easy to implement with non-linear regression methods and is one of the reasons it is still so widely used in production forecasting applications especially those wells that are considered tight formation. Using the Arps model for tight formation production will lead to overestimates of production performance and ultimately in estimated ultimate recovery's (EUR's) (Akbarnejad-Nesheli et al., 2012). Other works that where developed from the Arps model where the Fetkovich dimensionless type curves (Fetkovich, 1980a) that combined the infinite acting flow regime and boundary dominated flow regimes to the Arps model in the same coordinate system, which helped to extend the Arps model to cover a wider range of conditions one would encounter during well life.

Another model that is predicated on the original Arps model is the Modified Hyperbolic Decline (MDH) model. The MDH model was developed to overcome the original Arps model's issues for boundary-dominated flow. However, the original assumptions of the Arps model still apply as this model utilizes two equations based on the Arps model with a transition from the transient flow regime to boundary dominated flow occurring at a predetermined decline rate given by $D_{\circ}$. It should be noted that $D_{\circ}$ can be ascertained from empirical correlations and has no physical foundation, according to Meyet Me Ndong et al. (2013). To determine the transition point, one would employ a computer program that would transition from the hyperbolic equation to the exponential equation once a certain decline limit has been reached. For tight formations when the original Arps model Arps' exponent is greater than unity the predicted cumulative productions could be unbounded for tight reservoirs in the transient flow regime, which would lead to overestimations of EUR (Lee and Sidle, 2010; Valkó and Lee, 2010). With this knowledge, Robertson (1988) developed the modified hyperbolic model and was later adapted to the current form by (Seshadri and Mattar, 2010). The hyperbolic equation is used in the early stages of well life Eq. (2-5). Once it has reached a specific predetermined decline rate, or time domain, which is the end of the transient flow regime, the equation will transition to the exponential decline equation, Eq. (2-6), as boundary dominated flow now governs the flow behavior:

For $D < D_{\circ}$

$$q(t) = \frac{q_i}{\left(q + bD_1 t\right)^{1/b}} \tag{2-5}$$

For $D \geq D_{\circ}$

$$q(t) = q_i e^{-D_2 t} \tag{2-6}$$

One application of the MDH model was presented in the work by (Childers and Callard, 2015) of the composite type curve model to analyze the time to end of linear flow for tight formations in the Bakken basin. Limitations of the MDH model is in the overestimation of the EUR's and Paryani et al. (2016) showed through evaluation of oil shale wells that the MDH model yields over expectant reserve estimates. Moreover, there are additional variants to this model such as the Variable Exponential Decline (VED) model, which modifies the existing Arps exponential decline equation where the decline rate is allowed to very per a power law function (Gupta et al., 2018), The Transient Hyperbolic Model (THM) which uses a logistical Arps exponent that will transition between flow regime states during well life (Fulford and Blasingame, 2013).

An additional expansion regarding the original Arps model, Ilk et al. (2008) suggested a modification to the Arps hyperbolic model such that the loss ratio would be estimated by a decaying power function at later production times Eq. (2-7), where D_∞, D_1 are the decline constant at infinite time and initial time respectively, and n is the time exponent. Since this model is predicated on the governing assumptions of the original Arps model then those assumptions would apply to this model as well unless modifications to the model have been made like with the decline rate.

Ilk et al. (2008) proposed the modification to the Arps decline constant as follows:

$$D = D_\infty + D_1 t^{-(1-n)} \tag{2-7}$$

Eq. (2-8) is defined as the Power Law Exponential Decline (PLE) model where Eq. (2-7) is substituted into the decline rate of the Arps model Eq. (2-1):

$$q(t) = q_i e^{\left[-D_\infty t - D_i t^n\right]} \tag{2-8}$$

where D_i is defined as the ratio of the initial decline constant to the time exponent which is defined as follows, Eq. (2-9):

$$D_i = {D_1}/{n} \tag{2-9}$$

Eq. (2-8) use the power law to allow for approximation of the production rate which was specifically introduced to handle shale gas well production to account for both transient and boundary dominated flow regimes. Mattar and Moghadam (2009) found that Eq. (2-9) is only applicable in transient flow regime applications. Furthermore, McNeil et al. (2009) through studying production data that the PLE model performs well when applied to wells that are in transient and boundary dominated flow regimes and the PLE model has shown to perform better than the original Arps model. The limitation of this method is that it will initially overestimate the production flow rate when using Eq. (2-8). However, Paryani et al. (2016) found that the PLE model yields the most conservative forecasts when compared to other decline curve models. Kanfar and Wattenbarger (2012), found that the PLE model has the capability of being applied to linear, bilinear and boundary dominated flow regimes, with the first two regimes being important to understand production behavior from the fractures in early stages of well life.

The Duong model was introduced to allow for a better approximation of EUR from wells that produce primarily from fracture dominate flow with very little contribution being realized from the formation matrix (Duong, 2011). The model is derived from the relationship of the ratio of the production rate to the cumulative production ${q}/{G_P}$ vs time t on a log-log plot that will reveal a straight line. This relationship is expressed as the material balance time and time retention expressed as Eq. (2-10), where the parameters m and a are the Duong slope, range of $1 \le m \le 2$, and Duong intercept, range $0 \le a \le 2$ respectively. Although Duong derived the equation for shale gas reservoirs, the model can be adapted for use in oil reservoirs as well. The primary assumption with this method is that there is a long term linear flow affect and this flow regime dominates all others. The limitations of this method requires at least a year and a half of production history before applying this model and that some wells may not be applicable as they may violate the constraints of the Duong parameters for the slope and intercept of Eq. (2-10) when using non-linear regression methods to determine the Duong parameters (Zuo et al., 2016).

$$\frac{q(t)}{G_P(t)} = at^{-m} \tag{2-10}$$

From Eq. (2-10), Duong derived equations that represent the production rate and cumulative production Eq. (2-11) and Eq. (2-12) respectively.

$$q = q_i t^{-m} e^{\frac{a}{1-m}\left(t^{1-m}-1\right)} \tag{2-11}$$

$$G_P = \frac{q_i}{a} e^{\frac{a}{1-m}\left(t^{1-m}-1\right)} \tag{2-12}$$

One limitation found in the work conducted by Wang et al. (2017) when comparing empirical models is that the Duong model can overestimate reserves. The Duong model appears to best fit both linear and bilinear flow regimes (Kanfar and Wattenbarger, 2012), which makes a good model for understanding and analyzing early production data.

The Logistic Growth (LG) Model is an empirical model that was adapted by (Clark et al., 2011a) from liver growth models and applied to gas wells with very low permeable media. The main assumptions that governs the LG model is that the cumulative production increases to a maximum bearing capacity and once this capacity has been reached future growth is impeded. However, this model also has an assumption that the reservoir will be depleted by a single well over a long period of time (Paryani et al., 2016), which is very difficult to achieve in practice. The parameters for the LG model are the cumulative production $Q(t)$ with respect to time in bbls, K is the carrying capacity, a is a constant of t^n, n is the hyperbolic exponent that characterizes the curvature of the LG model with a constraint of $0 \le n \le 1$, and t is the time, in days. Nonlinear regression analysis can be implemented to determine the parameters of the LG model for K, a, and n. According to Clark et al. (2011b) the main advantage in utilizing the LG model is that the overall reserve estimate is controlled by the carrying capacity parameter as well as the production rate, which ends as time goes to infinity.

The LG model cumulative production is expressed as follows:

$$Q(t) = \frac{Kt^n}{a + t^n} \tag{2-13}$$

The production rate for the LG model can be found by the expression as follows:

$$q(t) = \frac{Knat^{n-1}}{\left(a + t^n\right)^2} \tag{2-14}$$

The Extended Exponential Decline Curve (EEDC) model was introduced by Zhang et al. (2016) and is predicated on the assumption of a growing drainage volume that models the performance of tight formations like shales. The EEDC model couples the exponential form of the decline equation that was proposed by Fetkovich (1980b). The parameter β_e illustrates early production life of the well that exhibits a quick decline, which is defined as the transient flow regime; whereas, the parameter β_l illustrates the moderate decline that is shallow in nature at later times in well life and both parameters are determined through non-linear regression methods. The moderate decline during late life illustrates how the growing drainage volume will be the dominant behavior at late stages of well life. The main assumptions to this model should follow the same assumption outlined by Fetkovich (1980b), which assumes constant bottom-hole flowing pressure and boundary dominated flow.

Zhang et al. (2016) coupled the exponential form of the Arps decline equation that was originally proposed by Fetkovich (1980b), Eq, (2-15), and the empirical equation that illustrate the growing drainage volume, Eq. (2-16):

$$q = q_o e^{-\alpha t} \tag{2-15}$$

$$\alpha = \beta_l + \beta_e e^{-t^n} \tag{2-16}$$

Combining Eq, (2-15) and Eq. (2-16) the following mathematical expression can be formed for the EEDC model.

$$\frac{\ln\left(q/q_o\right)}{t} = \beta_l + \beta_e e^{-t^n} \tag{2-17}$$

From Eq. (2-17) some important observations should be discussed. (1) at early stages of well life $\beta_e e^{-t^n}$ is the dominant factor, which is characterized as a quick decline, which is indicative of tight formation wells like shales with early production from the fractures. (2) β_l becomes the dominate parameter at late stages of well life, which is characterized by boundary dominated flow. One of the main advantages of using the EEDC model is that it does not require the determination to find the transition point at which transient flow ends and boundary dominated flow begins like when using the MHD and composite type curve models. Moreover, values of β_e, β_l are unique to the well being studied and may not be applicable to project these parameters on wells in the surrounding area. Therefore, a large sample of wells may be required to develop appropriate type curves of a basin of interest.

The Stretched Exponential Decline (SEPD) model was introduced by Valko (2009) and Valkó and Lee (2010) as an alternative to the Arps model. The main assumption with the SEPD model is that the production rate will comply with the stretched exponential decay defined by Eq. (2-18):

$$dq/dt = -n\left(\frac{t}{\tau}\right)^n \frac{q}{t} \tag{2-18}$$

where τ and n are the characteristic time constant and exponent respectively. Additional assumptions for the SEPD model are that the actual production decline will be determined by many contributing volumes and these volumes will all exhibit exponential decay rates with a specific characteristic of time constant.

To develop the SEPD model two parameters τ and n will need to be ascertained through the utilization of the gamma function and incomplete gamma function, Eq. (2-19) and Eq. (2-20) respectively, where r_{21} and r_{31} are the cumulative production ratios of two and three years respectively.

$$\frac{\Gamma\left[\frac{1}{n}\right]-\Gamma\left[\frac{1}{n},\left(\frac{23.5}{\tau}\right)^{n}\right]}{\Gamma\left[\frac{1}{n}\right]-\Gamma\left[\frac{1}{n},\left(\frac{11.5}{\tau}\right)^{n}\right]}=r_{21} \tag{2-19}$$

$$\frac{\Gamma\left[\frac{1}{n}\right]-\Gamma\left[\frac{1}{n},\left(\frac{35.5}{\tau}\right)^{n}\right]}{\Gamma\left[\frac{1}{n}\right]-\Gamma\left[\frac{1}{n},\left(\frac{11.5}{\tau}\right)^{n}\right]}=r_{31} \tag{2-20}$$

An important advantage of the SEPD model is that it has the ability to couple the sharp decline and shallow decline segments of the decline curve model while minimizing model parameters and provide a finite value of EUR without limits in rate or time according to the study by (Akbarnejad-Nesheli et al., 2012). Unlike the Arps model, which is predicated on boundary dominated flow, the SEPD model actually models the transient flow regime. The only downside to using the SEPD is that it requires a long time interval of production data, approximately three years or longer, to provided sufficient approximations of τ and n , and the SEPD model is computationally intensive (Zuo et al., 2016). Moreover, one additional limitation when using the SEPD model is that it has limited ability to project production performance in late well life of shales (Lee, 2015).

The Fracture Decline Curve (FDC) model was introduced by Zuo et al. (2016) based on anomalous diffusions that was used in designing a model that captured the late production life phenomena characteristics of shale gas wells where the production rate declines at a slower rate than observed when using exponential decline models. Challenges with the modeling of tight formations such as shales are due to the slower production rate decline, at late times, and may not be modeled adequately using the beforementioned production forecasting methods. Moreover, anomalous diffusion is prescribed by the nonlinear relationship between the mean square displacement and time, where ordinary diffusion is linear. Therefore, Zuo et al. (2016) proposed the use of fractional diffusion equations using three fitting parameters α, λ, and m that are a special case of the Mittag-Leffler function (Mittag-Leffler, 1903). Taking the special case of $\beta = 1$ when using the Mittag-Leffler function the following FDC model can be formed, Eq. (2-21) and Eq. (2-22) respectively.

$$q = mE_{\alpha,1}(-\lambda t^{\alpha}) \tag{2-21}$$

$$q = m\sum_{k=0}^{\infty}\frac{(-\lambda t^{\alpha})^{k}}{\Gamma\left(\alpha k+1\right)} \tag{2-22}$$

Zuo et al. (2016) surmised that the fractional diffusion equation replaces the conventional pressure equation when utilizing the general solution of fractional diffusion. The results of this new model illustrated improved matching performance with historical production and exhibited a more confident EUR result. Zuo et al. (2016) validated the FDC model using production wells that where from the Fayetteville Shale through a four step implementation process that will not be repeated here; however, has been outlined in the original work. One limitation when using the FDC model is that it requires and iterative process to calibrate the three fitting parameters from historical production data and determining the EUR can be complicated when employing the FDC model.

2.1.3 Production Forecasting Model's Summary

Regardless of which production forecasting method one uses the underlying issue is that the parameters for one model, studying one well, will almost always not be efficient to apply those parameters to existing or future wells. One should think of wells similar to human beings as every human being is unique. Furthermore, using one method that is easy and convenient such as the Arps equation will yield a result; however, the result will most definitely be unreliable in tight formations over the course of well life as the Arps model was never designed for applications in tight formation analysis. Therefore, one usually needs to apply a stochastic approach along with probabilistic models when using production forecasting methods. The models presented in this review are deterministic in nature and are subject to various uncertainties, which range from the quality of the data being analyzed to the complexities of implementing a model such as the FDC model, as well as understanding the formation one is studying. Production forecasting models are good for aiding the understanding of future behavior of production performance; however, physical models are needed as understanding flow mechanism when dealing with tight formation reservoirs is very complex and most, if not all, empirical models will fail due to the lack physics.

Table 2 - 1 Comparison table showing the various empirical models used in assessing tight formation production. Computational complexity increases as one descends down the list.

Empirical Models for Production Forecasting

	Model	Mathematical Expression	Advantage	Limitations
Computational Complexity	Arps	Eq (2-4)	Simplest DCA Method	Overestimates EUR's. Only accurate at late time.
	Modified Arps	Eq (2-5) & Eq (2-6)	Determines a time to end of linear flow and changes from hyperbolic to exponential	Overestimates EUR's Only accurate at late time.
	PLE	Eq (2-8)	Applicable to linear, bilinear and boundary dominated flow regimes	Will overestimate production flow rate. Provides conservative forecasts when compared DCA models
	Duong	Eq (2-11) & Eq (2-15)	Good fit for both linear and bilinear flow regimes	Short term forecast is needed to determine parameters
	LGM	Eq (2-16) & Eq (2-17)	Reserve estimate is controlled by the carrying capacity parameter as well as the production rate	Assumes only one well will drain the entire reservoir
	EEDC	Eq (2-17)	Models transient and boundary flow regimes	May need to study many wells to determine parameters
	SEPD	Eq (2-18)	Couples the concave and convex segments of the decline curve model while minimizing model parameters	Medium term forecast needed to determine parameters Difficulty in prediction production performance of shales in late well life.
	FDC	Eq (2-21) & Eq (2-22)	Models the long tail behavior of shales	Mathematically Complex

*Short term forecast > 1.5 years
*Medium term forecast > 3 years

2.2 Fracture Diagnostic Methods

Fracture diagnostic methods have been developed to aid producers in optimizing the recoverable potential of a hydrocarbon reservoirs by allowing insight into fracture genesis through the propped fracture and net pay zone (Cipolla and Wright, 2000c). In this section, a detailed review will be conducted of all the fracture diagnostic methods available to aid in the quantification of fracture initiation. The fracture diagnostic methods will be split into three segments starting with direct near-wellbore diagnostic methods, direct far-field methods, and conclude with indirect methods. Figure (2-1) illustrates a synopsis of the available methods currently used in field applications and has been extensively discussed in the literature. It should be emphasized that one fracture diagnostic technique may not be adequate to reveal pertinent information about a fracture but only reveal a small portion of the fracture genesis puzzle. Therefore, many fracture diagnostic techniques will be needed to sufficiently quantify fracture geometry as fracture diagnostic techniques should be thought of as a toolbox to allow for deeper understanding of fracture genesis such that trapped hydrocarbons can be produced efficiently and economically.

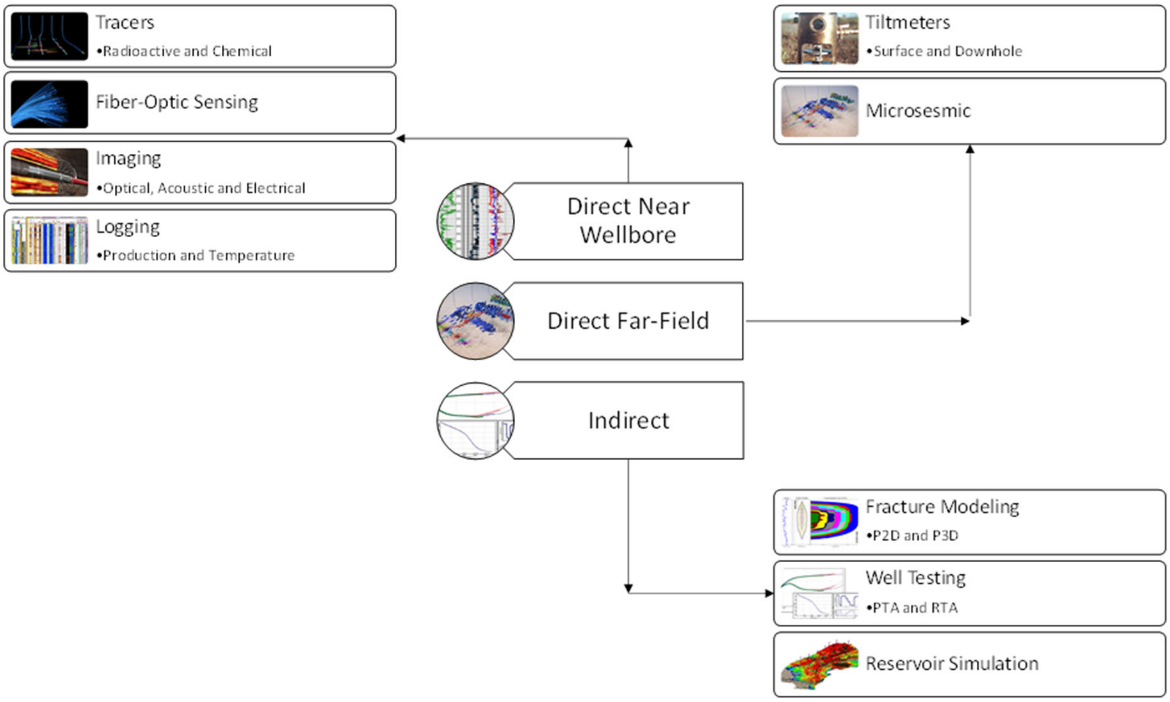

Figure 2 - 1: Diagram of the of the fracture diagnostic methods currently available today. This diagram breaks down the individual elements that make up the fracture diagnostic method for direct methods that are near the wellbore, direct methods that are used to analyze fractures far away from the wellbore and indirect methods that analyze the fractures through field production.

2.2.1 Hydraulic Fracturing Fundamentals

Before fracture diagnostic methods can be discussed one needs to understand hydraulic fracturing and why it is needed. Heydarabadi et al. (2010) asserted that the purpose of hydraulic fracturing is to induce fractures into the target formation such that a highly conductive flow path can be created to allow for hydrocarbons to flow through the created fractures and natural fractures of the rock. Generating artificial fractures is an important component in tight formation reservoirs such that hydrocarbons can be produced economically that are currently locked in hydrocarbon-rich areas in the subsurface of the Earth. According to (API, 2020) the United States Department of Energy stated that 95% of all new wells drilled in the United States will require some form of stimulation. No shale or tight reservoir can be produced economically without some form of stimulation process such as hydraulic fracturing. One of the most challenging aspects of hydraulic fracturing, is understanding how fractures propagate in the formation of interest after undergoing a stimulation process. Stimulating a reservoir has two motivations: (1) to bypass the near-wellbore formation damage that has occurred during the drilling and completion phase of a new well and (2) to create high conductive flow paths such that hydrocarbons locked in the tight pore space of a tight formation can be produced. It should be emphasized that not every well requires treatment as this is predicated on several key factors regarding fracture propagation, which include: ease of penetration into layers outside of the target zone, fracture conductivity loss due to high in-situ stresses on fracture faces, and fluid leak off during fracture initiation (Heydarabadi et al., 2010). Additionally, reservoirs that are comprised of thin formation layers with reservoir pressures that are minimal would be averse to implementing a hydraulic fracturing treatment. Many fracture diagnostic technologies are mechanical in application and are applied in field settings; however, some fracture diagnostic technologies can be limited based on the environment one encounters.

Moreover, there are indirect technologies that are more theory based to help understand the fracture propagation environment, and there have been substantial research efforts regarding indirect technologies that can be found in the literature. However, there may be challenges when using indirect technologies during field applications based on the complexity of some of the indirect theories. Understanding the process of fracture genesis is critical to determine reserves and to understand the production potential of the reservoir.

A hydraulic fracturing process is illustrated in Figure (2-2). Fracturing fluid (pad fluid) is first pumped into the formation causing the pressure to increase at the perforated zones along the wellbore. As the pressure increases above the formation parting pressure, fractures will begin to propagate in the direction of the minimum stress, which is usually orthogonal to the wellbore. The next stage will be to pump a slurry comprised of fluid and proppant agent not only to increase the fracture but to allow for the fractures to remain open due to the utilization of the proppant agents. During the hydraulic fracture operation, the fracture growth may intersect natural fractures and form a complex fracture network. Figure (2-2) also depicts a modeled view projection of just how a theoretical hydraulic fracture stimulation should look. The wellbore will have multiple stages represented by the five compartments that would represent the hydraulically induced fractures. During the pumping of the slurry mixture into the formation these fractures will open and intersect with other natural fractures that will constitute what is known as the stimulated reservoir volume (SRV), which is the stimulated portion of the formation matrix that is in contact with the hydraulic fractures. A few comments are need regarding SRV. First, SRV has several names that are sometimes used interchangeably such as effective stimulated volume (ESV) Cipolla et al. (2011), and the stimulated reservoir area (SRA) Mayerhofer et al. (2010). In essence, SRV is assumed to be the volume of the formation that has been affected by a stimulation treatment that interacts with the fractures within the formation. Moreover, it is believed that as the SRV increases the ultimate recovery of hydrocarbons will also increase. Research conducted by Cipolla and Wallace (2014) found that the hydrocarbon recovery increases due to hydraulic fracture area, reservoir properties and how well fracture conductivity has been dispersed in the formation to quantify the hydrocarbon recovery increase, not SRV. Therefore, trying to quantify SRV has been a challenge for the industry.

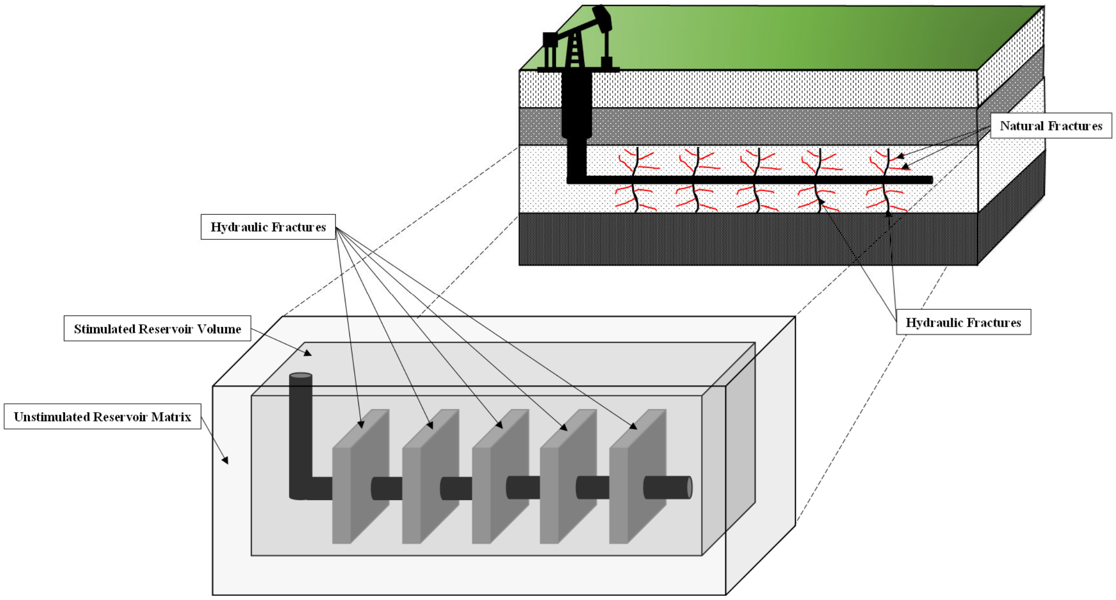

Figure 2 - 2: Diagram of hydraulic fracturing treatment. The black lines in the main diagram represent the induced hydraulic fractures. The red lines, small lines that branch off the induced hydraulic fractures, represents the natural fractures that will be encountered during stimulation treatment. The projected image represents a theoretical model of the hydraulic fracturing treatment design process. The projected image depicts the five stimulated compartments of the hydraulic fracture and illustrates the stimulated reservoir volume (SRV), which is the volume that has been theoretically affected by the stimulation treatment and assumed that it will contribute to production.

Some of the common challenges for hydraulically stimulating tight formation reservoirs is in the complex development of hydraulic fracture networks not being distributed uniformly. The reason for nonuniform development may be related to the heterogeneity of the reservoir, how the natural fractures are distributed in the target formation, deficient hydraulic fracture treatment, and interference relative to clusters and staging. As the lithology in the reservoir can change from one location in the reservoir to another, the effect on the minimum horizontal stress can cause variations in parting pressure that would lead to nonuniform distributions of the hydraulic fractures. To overcome these complexities many fracture models have been proposed in the literature such as the planar model, the wire-mesh model, and the complex-fracture-network model (Cipolla et al., 2010; Crockett et al., 1989; Xu et al., 2009) and are used to help understand the physics of fracture genesis. The planar model, commonly referred to as the planar hydraulic fracture growth model, the projected theoretical model illustrated in Figure (2-2), depicts hydraulic fractures that are orthogonal to the horizontal wellbore and has been utilized as the principal model to describe hydraulic fracturing. The validity of the planar model is only pertinent when the difference between maximum and minimum horizontal stresses in the field are significant (Cipolla et al., 2011). The presence of natural fractures in the formation can aid in the development of complex fracture networks through hydraulic stimulation that can be an elusive parameter to identify, which may require, in almost all cases, a stochastic approach to account for the ambiguous nature in the fracture distribution and connectivity. Most fracture accessing methods, which have been discussed extensively in the literature, use data-assimilation approach employing production data, such as the Kalman Filter (EnKF), to better approximate fracture geometry and to better understand and characterize fracture genesis in real-time (Aanonsen et al., 2009; Crestani, 2013; Evensen and Van Leeuwen, 1996; Ghods and Zhang, 2012; Huseby et al., 2010; Marquart et al., 2013; Moreno et al., 2014). Features that are critical involving hydraulic fracture design are in the estimation of the fracture geometry, which includes: azimuth, fracture height, and fracture half-length, with respect to lateral orientation, see Figure (2-3). There has been a surplus of work in prefracture design assessments such that an approximate model can be developed to enable the ability to design an effective fracture treatment program. Many fracture propagation models have been developed to understand the governing physics of fractures and have been calibrated with actual field data to validate the models accuracy; however, some of the calibrations may result in conflicts when discerning fracture physics (Weijers and De Pater, 2019).

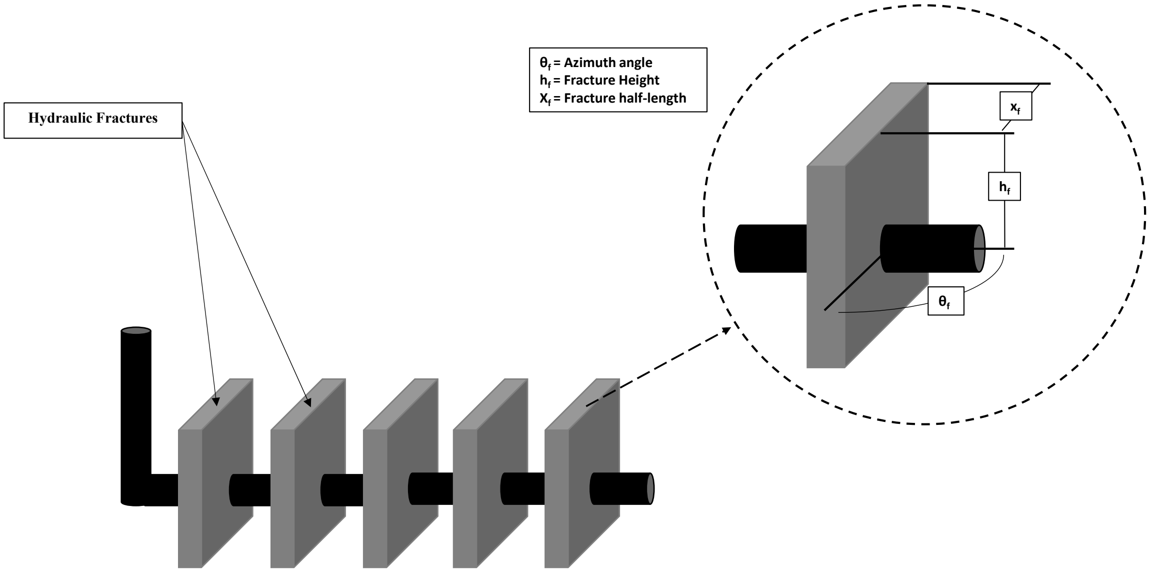

Figure 2 - 3: Diagram of hydraulic fracturing showing the critical geometry that is required for fracture design. The azimuth angle is showing the orientation of the fracture from the horizontal wellbore in addition to the fracture height and fracture half-length.

2.2.2 Fracture Diagnostic Methods Direct Near-Wellbore

Near wellbore diagnostic tools are ran downhole and can be used to understand and characterize fractures less than two feet from the wellbore. The major limitation is its short investigation depth regarding fracture geometry when the fracture is not aligned with the wellbore (Cipolla and Wright, 2000a). Direct near-wellbore techniques consist of tracers, temperature logging, production analysis, borehole imaging, and caliper logs. If a hydraulic fracture traverses the wellbore, these direct near-wellbore techniques can be of some benefit in locating the hydraulic fracture. However, these near-wellbore techniques are not unique and cannot supply information on the size or shape of the fracture once the fracture propagates two to three wellbore diameters from the wellbore. In a naturally fractured reservoirs, in which multiple fractures are likely to exist, the reliability of direct near-wellbore techniques is even more subjective. As such, direct near-wellbore techniques are used only to find where the hydraulic fracture exited the wellbore and to map the fracture that is essentially connected directly to the wellbore (Warpinski, 2019).

Radioactive (RA) proppant tracers can be used as a fracture diagnostic method that allows for an approximation of the fracture height near the wellbore. Figure (2-4) is an illustration of how RA tracers are being injected or tagged with the stimulation fluid and it is pumped downhole into the induced fractures. Gamma-ray logging tools are used to detect the RA tracer downhole to help quantify fracture height and potentially other features in the reservoir of interest. RA tracers can also aid in the understanding of zonal isolation to assess fracture staging efficiencies, evaluate the effectiveness of the perforations around the wellbore and give insight into the completion system by understating its mechanical integrity. RA tracers use embedded tracers, which can be a ceramic material, and through gamma ray logging, provides quantitative information when evaluating important features near the wellbore (Barree et al., 2002).

The most common types of isotopes used in RA tracer applications are Iridium, Scandium and Antimony and each have specific half-life and mean energy peaks, see table 15.1 of Warpinski (2019) for half-life and mean energy peak data. The isotopes of the RA tracers will radiate gamma rays , which can be identified by applying a gamma ray logging tool, spectral gamma ray logging tool, to distinguish the energy peaks of the various isotopes. Logging tools transmit information via a sensor output to a multichannel analyzer, which assess the amount of radiation within a limited spectral window. Common issues that arise regarding RA tracers are the tracers depositing onto the formation and interacting with the mineralogy thereby, in essence, getting trapped as well as potentially compromising the coating that incase the RA tracer. Public concerns when using RA tracers, in wellbore diagnostics, is the perception of the radioactivity emitted from RA tracers maybe harmful to the environment or the public. Therefore, it is important to have good open communicative dialogue with the operating companies and the communities for which RA tracers will be implemented to help prevent concern. Moreover, RA tracers maybe unrecoverable in some stimulation applications as some of the stimulation fluid that is tagged with RA tracers are lost due to fracture conductivity and fracture closure during flowback (Barree and Mukherjee, 1995; Veatch and Crowell, 1982). However, even though some of the RA tracers maybe unrecoverable, studies observed by Smith et al. (1987) and (Gardien et al., 1996) that the quantity of recovered RA tracers can surmise fracture efficiency. One item of note is that since RA tracers are deployed with stimulation fluid it may yield only early time flow information and may not be able to fully evaluate fracture growth.

Applications regarding RA tracers have been used to measure fracture height near the wellbore and assess isolation stages and efficiency in vertical wells (Warpinski, 2019). Other applications looked at monitoring fracture fluid, quantify fracture width and estimating the amount of proppant near the wellbore through studies conducted by Holditch et al. (1993) and McDaniel et al. (2009). RA tracers are also used in understanding of fluid migration in the subsurface, impediments to fluid migration and saturations (Zemel, 1995). Studies conducted by (Lange et al., 2005; Parney et al., 2000) used Interwell tests to understand the transmissivity of active fractures as well as aide in the understanding how fluids are dispersed between the fracture and the formation matrix. RA tracers have been used to conjecture residual oil saturations and to assess the heterogeneity, rock wettability, understanding fluid breakouts, and marking of fracture points in the reservoir (Descant et al., 1989; Ferreira et al., 1992; Kumar et al., 2020; Silber et al., 2003; Woodroof et al., 2003).

RA tracers have also found applications in horizontal wells to differentiate the stages and assess transverse fracture behavior and zonal isolation.

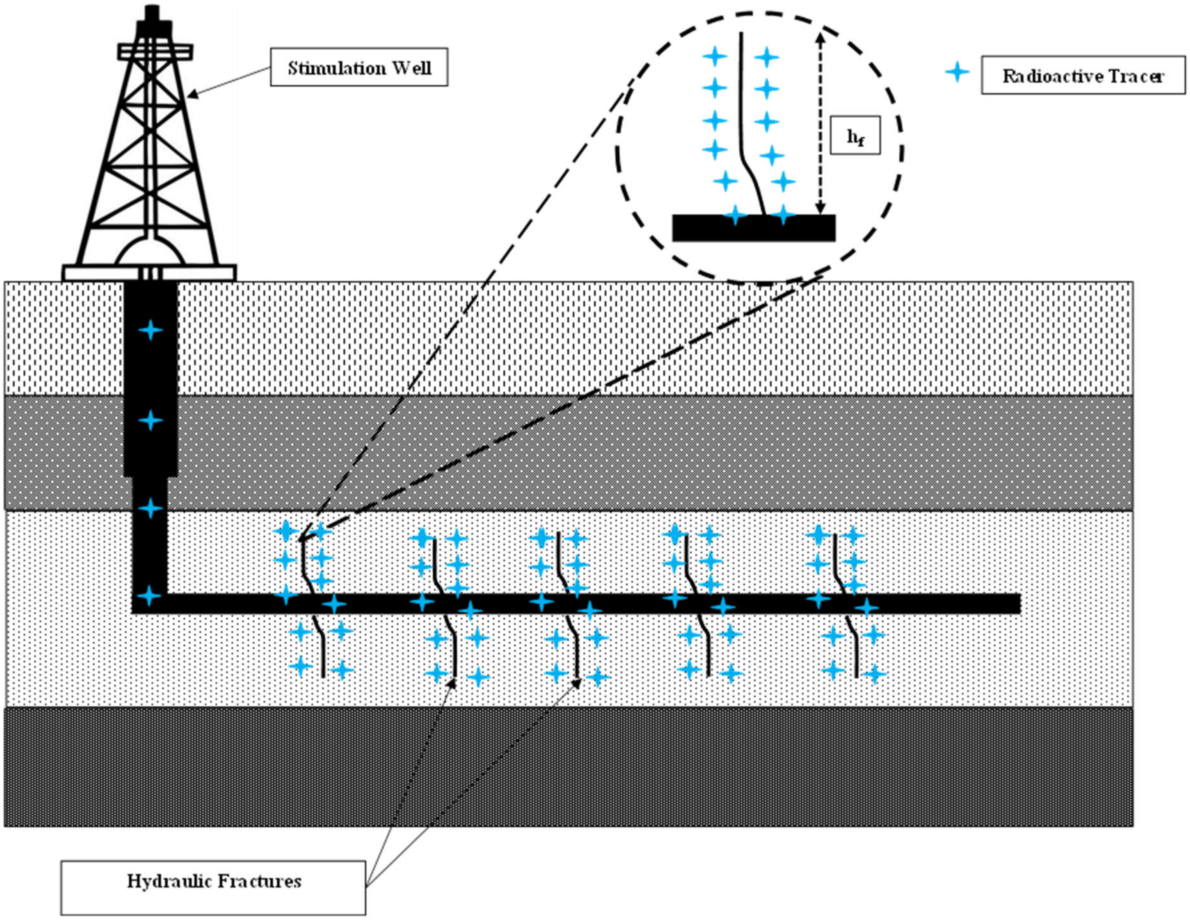

Figure 2 - 4: Diagram illustrating how tracers are dispensed in a reservoir. RA tracer is injected or tagged with the stimulation fluid and is pumped down hole into the induced fractures. Using gamma ray logging tools to detect the energy peaks one can estimate fracture height.

Chemical fracture tracers (CF) are commonly used in multi-stage hydraulic fracturing treatment and are comprised of a chemical compound that is soluble in the presence of water and in both phases of oil and gas. Unlike RA tracers, CF tracers are deemed environmentally safe as they are non-toxic and can be easily implemented in a fracture stimulation program. CF tracers are injected at a specified concentration and traverses with the hydraulic fracturing fluid into the formation. As the CF tracer migrates into the formation it will flow into each fracture stage and allow for assessments of the inter-well connectivity, flow patterns and quantification of the fracture system, see figure (2-4) for illustration. Three types of CF tracers are commonly used in the industry such as emulsion tracers, oil and water soluble tracers commingle with the hydraulic fracturing fluid, perforation tracers, metallic solid used in high temperature applications along with plug-and-perf operations, and controlled-release tracers, which are a polymer compound that release the chemical tracers in the formation once they are in contact with the formation, see Figure (2-5) for CF tracer summary, which has been adapted from Salman et al. (2014). CF tracers are either in a liquid or solid form and must be stable under reservoir conditions, non-absorbent and the partitioning of the CF tracer must be kept to a minimum when encountering multiple phases with low detection limits and stewardship to the environment must be adhered (Dugstad, 2007).

Oil or water soluble tracers can be placed in the fracturing stimulation fluid to provide information regarding the production potential, oil-soluble case, and to evaluate the effectiveness of the stimulation treatment, water soluble case. Tracers allow for the understanding of how the fluids cleanup, zonal distributions, production and well-to-well interference during multistage completions (Warpinski, 2019). CF tracers are comprised of unique characteristics such that one can monitor their propagation using a gas chromatography and mass spectrometry and are usually mixed at a given concentration and pumped into the fracture fluid media using a peristaltic pump (Munoz et al., 2009). One advantage in using CF tracers is that they are usually found to be inert and are not susceptible with temperature or time. Additional advantages of using CF tracers is in examining the staging of a single fracture treatment as different tracers for pad and individual sand stages have different concentrations of different fluid characteristics (Warpinski, 2019). From the research conducted by Woodroof Jr et al. (2003) regarding tracer applications found that by inserting crosslinked gel treatments in the fracture fluid media more complicated flow behavior was observed that was unexpected during the design phase due to convection and leak off. The information that was gained by Woodroof Jr et al. (2003) allowed for optimization of fracture fluid placement and proppant scheduling to enhance overall production. Stegent et al. (2011) used CF tracers in comparing plug-and-perf completions, which indicated that one perforated zone was highly productive versus others.

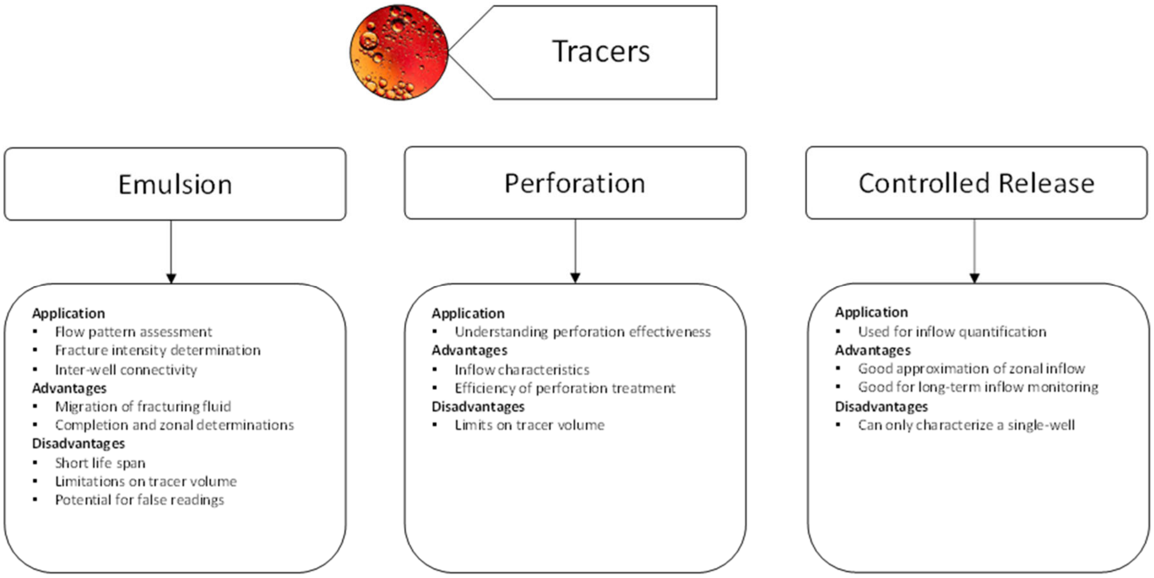

Figure 2 - 5: There are three common chemical tracers used in fracture diagnostic applications: emulsion tracers, perforation tracers, and controlled-release tracers. This chart has been adapted from (Salman et al., 2014).

Distributed fiber-optic sensing (DFOS) has been used in downhole applications, which was introduced to the industry back in the latter half of the twentieth century (Hartog, 1983; Hartog et al., 1985), providing measurements of reservoir information in-real time along the length of the fiber optic cable, which is comprised of glass fibers. The primary use of distributed fiber-optic cables was for use in geothermal studies (Förster et al., 1997; Hurtig, 1993). DFOS application uses the fiber as the sensing element, which is predicated on refraction physics that conveys a series of light pulses through the fiber and measures the natural occurring scattered signal with respect to time. Due to the fiber being the sensing element the fiber-optic cable has the ability to be implemented in vary harsh environments such as wells that exhibit high temperatures. The primary application when using fiber-optic sensing elements in wellbores is to determine reservoir temperature, strain on the near wellbore formation and acoustic data analysis. The two most common fiber optic measuring technologies is the distributed temperature sensor (DTS), figure (2-6) and the distributed acoustic sensor (DAS), figure (2-7), (Warpinski, 2019). The advantage of using DFOS is that only the measurement cable is subject to potentially hostile downhole conditions making the fiber-optic systems suitable for operations in high-temperature environments (Reinsch and Henninges, 2010; Reinsch et al., 2013).

DTS has been employed to measure the temperature along the wellbore in real-time, as well as finding applications in the understanding of stimulation diagnostics in both vertical and horizontal wells that provide insight into fracture genesis near the wellbore (Huckabee, 2009). DTS systems mostly use the temperature-sensitive Raman scattering (Dakin et al., 1985) and due to cooling during the stimulation process and the warming from fracture closure one can approximate fracture conditions by analyzing the scattering characteristics of the Stokes and Anti-Stokes Raman bands, where Stokes is weakly temperature dependent, and anti-Stokes is strongly temperature sensitive, one can compute the temperature along the length of the fiber optic cable (James and Alex, 2003).

DAS is used to acquire dynamic axial-strain changes caused by propagating elastic waves along the wellbore structure (Raab et al., 2019; Shatalin et al., 1998). DAS systems are often dependent on the detection of phase changes of Rayleigh backscattered light (Hartog, 2017). The signals are recorded by a permanently installed fiber-optic cable and are studied for the possibility of real-time well-integrity monitoring through the fiber undergoing vibration. A change in the phase difference of light scattered by two separate points along the fiber is linearly proportional to a change in fiber length separating the points (Masoudi et al., 2013). Determining these phase changes for consecutive fiber intervals and over time can therefore be used to record the dynamic strain progression of a fiber-optic cable induced by a seismic signal. Applications of DAS have been in vertical seismic profiling (Daley et al., 2013; Götz et al., 2018), flow profiling (Bukhamsin and Horne, 2016), near-surface geophysics (Dou et al., 2017), and seismology (Jousset et al., 2018). Measured strain changes are influenced by the coupling between the optical fiber and the medium in which the cable is installed (Daley et al., 2013; Reinsch et al., 2017).

DFOS is a powerful tool used in understanding or gaining approximate information at near wellbore conditions. The only drawback to this technology is due to the fact it can only give information a short distance from the wellbore. However, due to the fiber optic glass crystals along the fiber makes DFOS ideal to be able to understand well conditions in real-time and allow for near wellbore fracture quantification analysis.

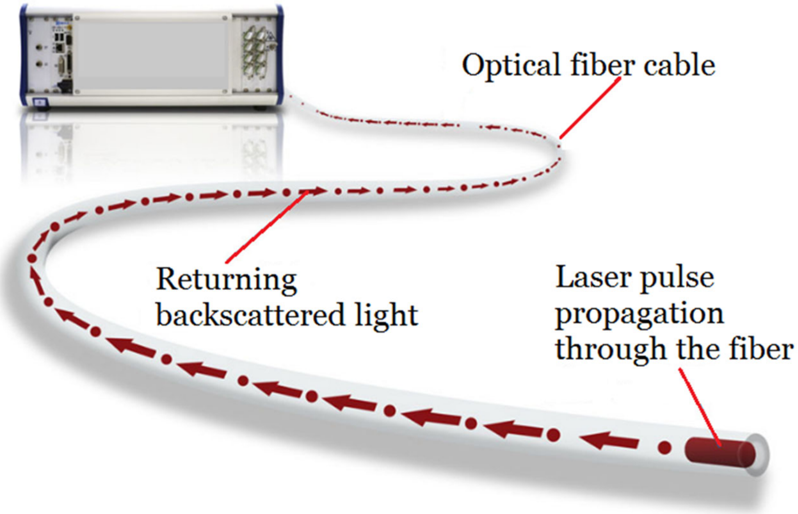

Figure 2 - 6: Illustration of a distributed temperature sensor fiber-optic wire distribution cable (fibergratings.com, accessed on 6/16/2020).

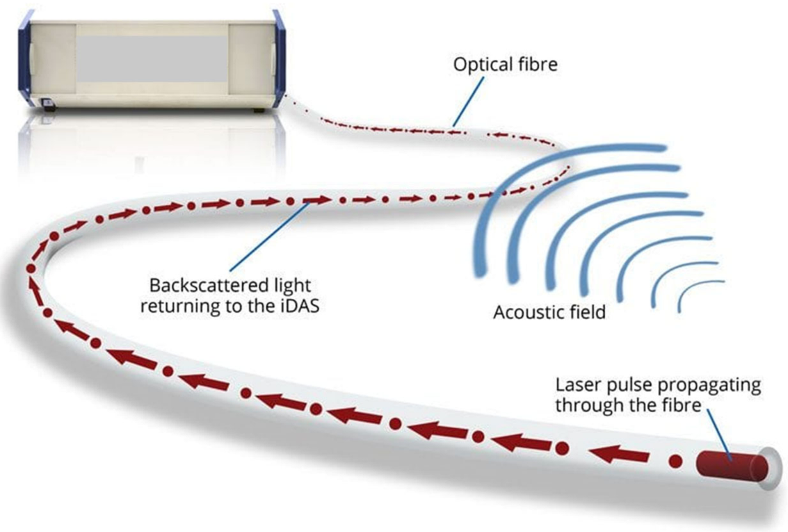

Figure 2 - 7: Illustration of a distributed acoustic sensor fiber-optic wire distribution cable (silixa.com, accessed on 6/16/2020).

Wellbore imaging is a data processing method used to produce quantitative information regarding the borehole with interest in understanding the stimulation effects on the wall of the wellbore. The purpose of wellbore imaging is for analyzing small-scale rock formation characteristics, identifying breakouts, irregularities in the borehole wall, understanding of the sedimentological features around the wellbore, and aide in fracture quantification (PetroWiki, 2020). Imaging the wellbore utilizes various logging tools that help in describing the wellbore through visual, sonic, and electrical logging applications. The equipment used in imaging the wellbore are video cameras, acoustic televiewer, advanced sonic logs, and resistivity imaging logs. The main disadvantage of using some of these imaging tools is that there needs to be an open hole segment of the wellbore to conduct imaging studies (Warpinski, 2019).

Optical Imaging, video downhole cameras, is an optical device that allows for a visual image of the wellbore in both pre and post fracture applications, illustration of a typical optical imaging device can be found in figure (2-8). The main disadvantage is that the downhole camera must be placed in a transparent fluid to provide quality resolution of the wellbore. In the early days of downhole camera applications another disadvantage is that the video camera would have to be retrieved from the wellbore to provide information. However, due to new advancements in imaging technology downhole cameras can be viewed in real-time or with slight delay in the video relaying the wellbore image in the subsurface. Applications of downhole cameras have been used evaluating casing integrity as well aiding in fracture diagnostic. Downhole cameras have been used in understanding fracture genesis in sandstones by Smith et al. (1982) and fracture genesis near the wellbore of coal seams by Palmer and Sparks (1991).

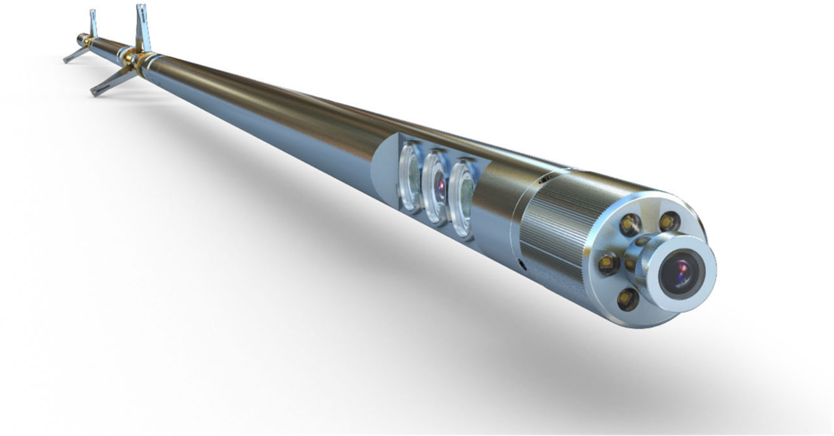

Figure 2 - 8: Illustration of a downhole optical imaging device used in evaluating wellbores (katwell.com.cn, accessed on 6/16/2020).

Acoustic imaging, which is also known as "acoustic televiewer", was developed by Zemanek et al. (1969); Zemanek et al. (1970) using pulse acoustic energy to image the wellbore wall through a non-translucent fluid media. Acoustic energy is supplied in small bursts by a transducer that is rotating in the wellbore housed inside a mandrel allowing for full coverage of the wellbore wall, see figure (2-9) for image. The time for which the acoustic energy travels is predicated on the distance between the borehole and the transducer as well as the drilling mud composition. As the acoustic energy pulses are reflected in the surrounding media the amplitude of these pulses allows for a wellbore image to be formed. If there are anomalies such as fractures, vugs, breakouts, the severity of the amplitude from the pulsed acoustic energy may skew acoustic imaging. Drilling mud weights and irregular borehole sizes also can impede amplitude allowing for poor acoustic imaging resolution. The best environments for the acoustic imaging to thrive is in smooth boreholes where high impendence in acoustic imaging is profound. The advantage of using acoustic imaging is that it can be applied in both closed and open hole applications; however, it cannot be applied in gas wellbore environments. The main application that acoustic imaging is used for in fracture diagnosis is in understanding where the fractures have occurred from a stimulation treatment near the wellbore wall and identifying potential breakouts. Some applications of acoustic imaging is in ultrasonic tools to access borehole stability (Hayman et al., 1994) and other studies regarding fracture identification, stratigraphic interpretation, and thin-bed analysis (Faraguna et al., 1989; Seller et al., 1990).

Figure 2 - 9: Illustration of an acoustic imaging device used in wellbore evaluations (mountsopris.com, accessed on 6/16/2020).

Electrical imaging is a microresistivity imaging tool, see figure (2-10), comprised of flaps and pads that contain a collection of electrode buttons set at a constant potential and spaced azimuthally on the electrical imaging tool and functioning as a dipmeter (Boyeldieu and Jeffreys, 1988; Ekstrom et al., 1986; Seller et al., 1994). The voltage potential allows for alternating current to flow from each electrode pad into the formation along the wellbore. The current then propagates back to an electrode at the top end of the electrical imaging tool. The electrodes on the pad are sensitive to the current density, which is related to the formation resistivity near the wellbore. The only drawback with the electrical imaging tool is that it cannot provide an absolute measurement of the formation resistivity. The effectiveness of the electrical imaging tool is predicated on the button size and any feature that is the same size as the button can be determined; however, smaller features may be obscured. Advantages to the use of the electrical imaging tools is that it is capable of determining characteristics of sedimentology and natural fractures in the formation along the wellbore. Conventional electrical imaging tools required a conductive mud to operate correctly; however, recent advancements in synthetic drilling mud applications can allow the electrical imaging tool to be run into the well without changing out fluid for the conductance needed to operate the electrical imaging tool effectively (Cheung et al., 2001; Dumont et al., 1987; Laastad et al., 2000).

Figure 2 - 10: Illustration of an electrical imaging device used in wellbore evaluations (slb.com, accessed on 6/16/2020).

Production logging is an array of logging tools such that are used to evaluate wellbore characteristics to gain insight into how the wellbore and how the well will operate during either production or injection operations. The main function of production logging is to understand formation cross flow, channeling, coning effects, casing leaks, corrosion, perforation impedance and understanding how fractures are produced (Houze et al., 2016). The logging tools that are available are: resistivity, spontaneous potential, gamma ray, photoelectric, neutron, density, sonic, dipmeter (electrical imaging), caliper and temperature logging device with both caliper and temperature logging devices used to aide in fracture diagnostics (Evenick, 2018). Any of the beforementioned logs can be applied at any stage of the life in the reservoir.

Caliper logs are used in assessing the diameter of the wellbore; however, can be used to ascertain lithological features to help in understanding how the fracture is generated near the wellbore (Satter and Iqbal, 2016). Temperature logs are used in cataloguing temperatures in the reservoir in real-time. The deeper one traverse into the wellbore the temperature will increase with respect to depth. Monitoring temperature and studying its effects may provide valuable insight in understanding fracture genesis; however, one needs to be cognizant that temperature may vary from basin to basin at similar depths and may require additional tools to quantify a fracture system. According to Evenick (2018) characteristic of a fracture system confined to a localized area would be an indication of a temperature decrease that may be due to fluid or gas emanating from a fracture system. Some recent applications utilizing temperature logging is understanding the heat transfer effects during fracture propagation that aides in understanding the effectiveness of multistage fracture treatments (Cui et al., 2016; Zhu et al., 2018). Since temperature logs are run using fiber optics, the temperature logging tool can be run downhole in harsh environments regardless of the operational condition of the well and aid in understanding fracture treatment.

2.2.3 Fracture Diagnostic Methods Direct Far-Field

Direct far-field methods are primarily used to analyze the far reaching effects of a fracture treatment. Ideally these methods are used to map hydraulic fractures as they propagate into the target formation. Far-field methods principally use applications of tiltmeter-fracture-mapping, which can be either through surface tiltmeters or downhole tiltmeters, and microsesmic-fracture-mapping. Both far-field diagnostic methods require sophisticated instrumentation embedded at the surface or downhole near the well that will undergo fracture treatment. In the case of microsesmic mapping, a receiver array that is comprised of accelerometers or geophones are used to detect the location of microearthquakes that are induced by shear slippage in natural fractures surrounding the hydraulic fracture. The sensitive receiver array instrumentation allows for noise detection caused by the shear slippage that can be analyzed, recorded, and mapped for diagnostic studies. When hydraulic fracture treatment is initiated, fracture expansion causes the earth around the fracture to deform and these deformations can be analyzed through microsesmic mapping around the well that is undergoing treatment. Tiltmeters are employed to measure the rock deformation and to allow for computation that can assess direction and size of the induced fractures. Surface tiltmeters find their application at the surface near the wellbore or in shallow holes surrounding the well. Downhole tiltmeters are placed in vertical wells at depths near the target zone to be fracture treated. Both surface tiltmeters and downhole tiltmeters are used to approximate fracture orientation and dimension of the induced fractures. Some of the common limitations of the far-filed methods is that these methods will lose accuracy the further away from the fracture and may not give good estimates on how the fracture grows nor any details regarding fracture conductivity (Cipolla and Wright, 2000c).

Tiltmeters are devices that can detect slight rotational movements due to the deformation of the earth at a precise location. During hydraulic stimulation, the formation parts creating a conductive flow path and causing shearing along the fracture surfaces resulting in the deformation of the rock formation. The small rotational movements induced by the stimulation fluid can be detected by the tiltmeter located at the surface or can be placed in the wellbore near the stimulation zone or in an offset well. Tiltmeters are primarily used in fracture mapping and to give a broad view of the fracture network and help aide in the understanding of how fractures propagate (Warpinski, 1996; Wright et al., 1998), see figure (2-11) for tiltmeter illustration. The tiltmeter is a precession bubble sensor that can detect changes in the angular position. In essence, a tiltmeter can be looked at as a leveling device commonly used in home building applications that measures height relative to a specified datum. The tilt gradient displacement is orthogonal to the displacement direction and can be used in detecting how the rock formation is distorting (Warpinski, 2019). Tiltmeters are also subject to external disturbance, noise that can corrupt the data collected from the tiltmeters and may skew the data of the actual fracture (Pandurangan et al., 2018). Primarily surface tiltmeters are used to ascertain fracture azimuth, dip, and complexity whereas downhole tiltmeters are used to obtain fracture dimensions (Bhatnagar, 2016). Furthermore, using the results from fracture mapping, over a specified time interval, one can generate a deformation map outlining how the fracture network is formed and couple the results with a specified forward model that will allow for the approximation regarding the orientation of the fracture, the fracture volume, and the potential understanding of the fracture geometry by an inversion process (Lecampion and Gunning, 2007). One item to note is that inverse problems can be ill-posed where multiple solutions can be obtained, and it can be difficult to determine fracture properties such as width and shape if the tiltmeters are placed far away from the fracture plane

(Lecampion et al., 2005). The mathematical geophysical inversion model is predicated on finding the minimized error difference between the predictions in the forward model and that of the measured data regarding fracture mapping. The residual error from the minimization error analysis allows for an approximation of secondary fractures (Wright et al., 1998), which play an invaluable role in fracture diagnostics.

Moreover, to overcome some of the inversion challenges Astakhov et al. (2012) introduced a new approach for tilt based SRV estimation for defining the growth of the fracture network and determine the areal extent of the fracture network. Zhou et al. (2015) studied the fracture network growth during synchronous fracturing through multiple wells on a cluster of horizontal wells observed using tiltmeters. Research conducted by Wang et al. (2013) described a new method for determining fracture complexity using surface tiltmeters and defined additional parameters to gain insight in characterizing sandstones, coalbeds, and shales. Additional applications of tiltmeters have been in studying reorientation refracturing that helps assess the direction of the maximum principal stress and how it is altered such that fracture growth may occur in a direction oriented differently than the original fracture (Siebrits et al., 2000; Wolhart et al., 2007; Yao et al., 2007). Additional applications for tiltmeters has been used to estimate the effectiveness of propped treatments downhole (Mayerhofer et al., 2006; Wright et al., 1998).

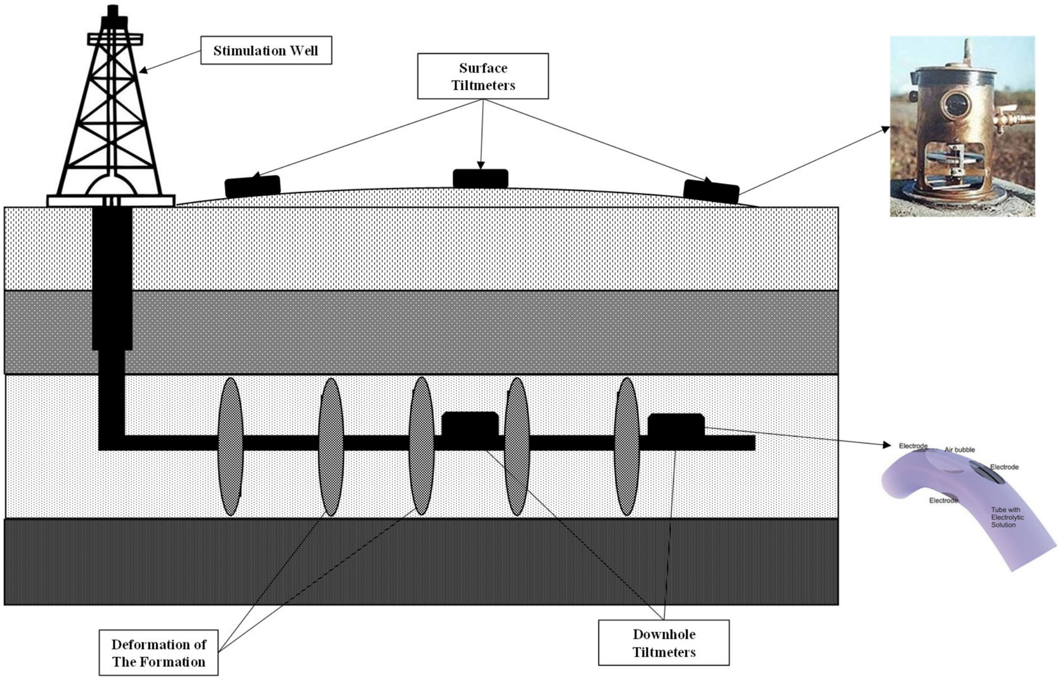

Figure 2 - 11: Illustration of the concept of both surface tiltmeters and downhole tiltmeters. Tiltmeter is a precession bubble sensor that can detect changes in the angular position and can measure small rotational changes incurred by the deformation of the rock during hydraulic stimulation (Tiltmeter images from wikipedia.org/wiki/tiltmeter, accessed 6/19/2020).

Microseismic monitoring is an application that is well founded for monitoring hydraulic fractures (Warpinski, 2009). The data provided from microseismic analysis aide in the monitoring and characterization of hydraulic fracturing treatment. During stimulation, the formation rock undergoes mechanical failure, which creates sudden releases of energy, due to changes in stress and pressure that propagates away from the event via elastic waves that are characteristic to a seismic event. Through the application of geophones, located in offset wells from the event, see figure (2-12) for illustration, the data collected from the geophones can be used to ascertain the seismic event location and severity. Over a specified time interval when monitoring seismic events, microsesmic data can be used to develop a three dimensional image of the fracture event of the wellbore that can aide in the understanding of rock properties, fracture characterization and stimulated reservoir volume, see figure (2-13) for three dimensional microsesmic map (Cipolla et al., 2010; King et al., 2008). Microseismic modeling is not without challenges and geophone placement, monitoring array, is critical in the location selection of the monitoring array, how one can handle noise, and determine the appropriate velocity structure (Eisner et al., 2010; Eisner et al., 2011). The seismic signal received by geophones are typically very weak and exhibit a low signal and noise ratio, introducing significant uncertainty about the location of the events, which is typically calculated by time separation of the P (primary)-wave and S (secondary)-wave and these wave signals can also aide in rock formation identification (Peyret et al., 2012). The spatial distribution, see figure (2-13), of microseismicity discloses information regarding fracture geometry and fracture development; however, it does not provide detailed information about the fracturing process, other than what is ascertained from the locations of the microsesmic event. (Warpinski et al., 2012).

Furthermore, microseismic data is primarily used for visually understanding how fractures are distributed in a target formation and help in quantifying geometric properties that may not allow for insight in which fractures are conductive or nonconductive. From King et al. (2008) understanding fracture networks and growth allows for more efficient conductive flow path to allow for hydrocarbons to flow to the wellbore. Moreover, tight formation reservoirs that have extremely low permeabilities will not be economical to recover, which is why understanding fracture propagation is paramount to economic success (Sutton et al., 2010).

Applications regarding microseismic technology have been used by Fisher and Warpinski (2012) to understand how fractures are not a threat to propagate into aquifers through the study of thousands of monitored fractured treatments and demonstrate that fractures will not propagate thousands of feet vertically and intersect potable water sources. Microsesmic technology identified, and helped build confidence in conclusions relative to, the fracture geometry and orientation, as well as confirming a completion problem (O'Brien et al., 2011). Through microseismic modeling Wesson and Nicholson (1987) documented minor earthquakes that were likely induced by local injection operations. Microseismic modeling has been used extensively in geothermal applications to monitor induced seismicity (Fehler, 1989; Majer et al., 2005; Smith et al., 2000).

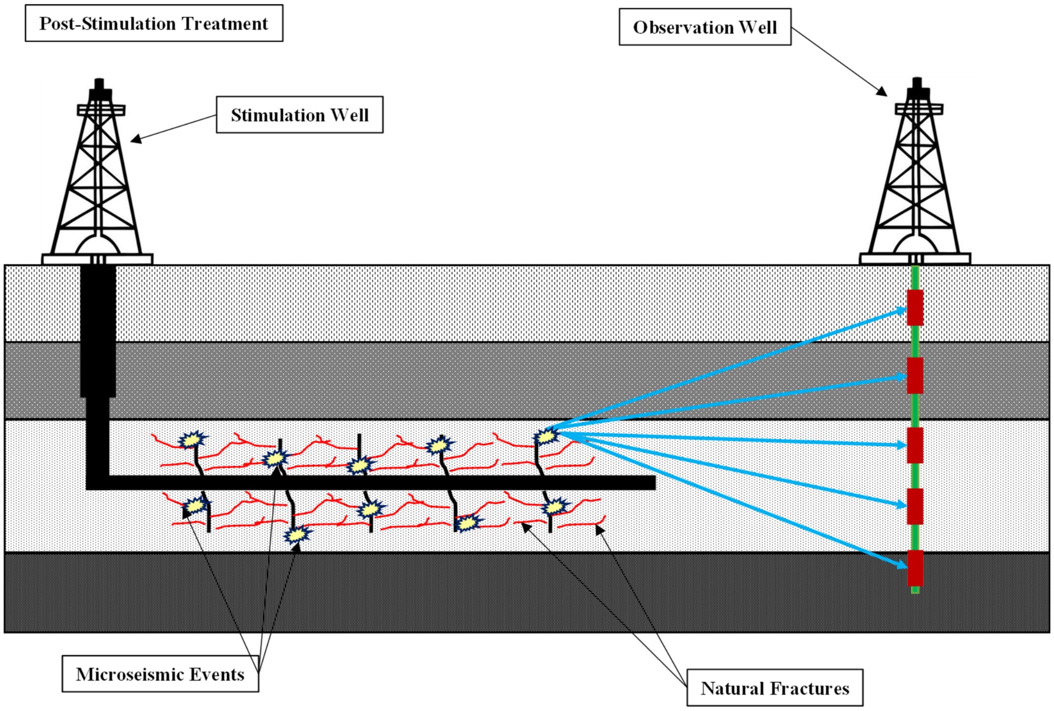

Figure 2 - 12: Illustration of a well that is undergoing hydraulic stimulation treatment. Observation wells are used to monitor seismic events from the stimulation treatment by placing geophones at various locations in the offset wellbore. As a seismic event occurs due to the hydraulic fracture treatment, the energy release will propagate away from the event and can be detected by the geophones in the offset well.

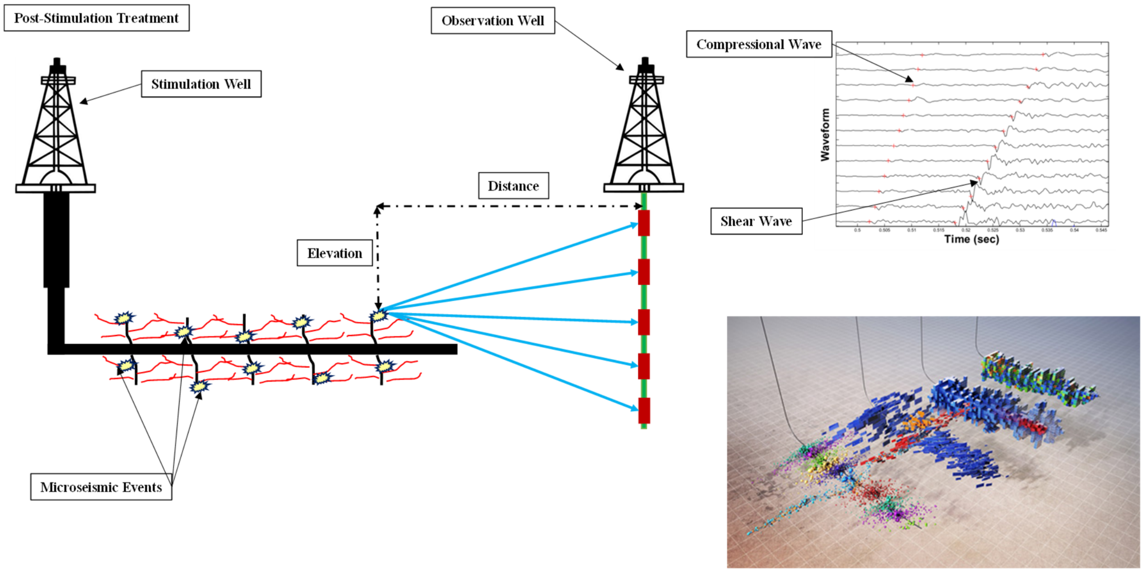

Figure 2 - 13: Example of microseismic modeling. The induced seismicity created by the stimulation treatment releases energy that is recorded by geophones in offset wells that allows for the detection of the event and determine the distance and elevation of the location of the seismic event of a well that is undergoing hydraulic stimulation treatment. The microsesmic model can be used to develop a three dimensional image of the stimulated area (3D Microseismic image, microseismic.com, accessed 06/19/2002).

Recent advances in complex fracture modeling via microseismic modeling have allowed for predictions of fracture propagation in unconventional reservoirs using sophisticated models (Cipolla et al., 2011; Rahman et al., 2002; Weng et al., 2011; Xu et al., 2010; Xu et al., 2009). Studies have also been conducted by Nagel et al. (2012) investigating fracture complexity through applications of higher viscosity fracture fluids, different proppant sizes, and natural fractures to address interaction between a single dominant vertical hydraulic fracture and pre-existing fracture networks. Microseismic modeling has aided in the understanding of fracture geometry and conductivity through flow and transport related data, with emphasis on tracer-test and production data applications that contain important information about matrix and fracture properties and can be used to update fracture properties, including fracture length and hydraulic conductivity (Elahi* and Jafarpour, 2015; Ghods and Zhang, 2012; King et al., 2008; Moreno et al., 2014).

2.2.4 Fracture Diagnostic Methods Indirect

Indirect methods use a variety of tools through the application of historical production. Tools that are used are reservoir simulation, fracture modeling and well test theory, rate transient analysis (RTA) and pressure transient analysis (PTA). Utilizing these tools one can achieve approximate information such as fracture dimensions, effective fracture length and fracture conductivity. Historical production is used to calibrate a history match between actual production and mathematical models. The underlying limitation of using these models is personal experience and some of the solutions may not be unique, which is why calibrating must be done between actual production data and the mathematical model of choice. However, the advantage of using indirect methods, especially that of well test theory, is that is relatively inexpensive, provided in-house expertise, and can lead to approximations of induced fracture dimensions that can be used in the development of optimized fracture models.

Reservoir simulation is by far one the most effective tools used in fracture design and its advantages and limitations have been discussed in the previous section. Reservoir simulation allows for what-if analysis that allows the engineer or scientist to run case studies of how the reservoir will respond to a set of conditions. However, one needs actual data to help allow for the calibration between simulated data and that of the actual data. Reservoir simulation software is readily available in the industry and can be employed to aid in fracture design as well as fracture diagnostics.

Fracture models are commonly used in the industry to understand the changes and complexities that reside in fracture genesis and help in aiding the engineer or scientist to execute a plethora of scenarios that honor the physic of the reservoir of interest (Weijers and De Pater, 2019). Fracture models look to understand elastic deformation, how fluids will leak off, viscous fluid effects, how proppant will be transported into the fracture and how the fracture will propagate into the target formation (Bellarby, 2009). The two most commonly used two dimensional models are the Perkins-Kern (PKN) (Perkins and Kern, 1961) and the Khristianovic-Gerrtsma-de Klerk (KGD) (Daneshy, 1973; Geertsma and De Klerk, 1969; Zheltov, 1955) and both are designed to combine physics with Darcy flow traversing between two parallel plates using the fracture deformation as a function of the pressure distribution via the Sneddon (1946) equation. The PKN model is applicable for deeply penetrating fractures and low permeability reservoirs, and the KGD model, is applicable with high-permeability, high fracture conductivity with short fracture penetration.

More recent advancements have led to parameterized three dimensional models. These models allow for the incorporation of the full coupling effects between the distribution of the pressure and fracture distribution in the entire fracture through nodal-analysis concepts and allow for incorporating the actual physics governing fracture genesis (Hsu et al., 2012). The main challenges regarding fracture modeling is that research is still trying to understand the mechanisms of how the fracture will actually grow, which is still an elusive phenomenon. Additional challenges are in the calibration process between the model and actual data and this challenge only further exasperates model predictions and will be an ongoing challenge into the future (Weijers and De Pater, 2019).

Well testing in regards to Rate Transient Analysis (RTA) is classified as the analysis of production data with flowing pressures to extract reservoir characteristics, hydraulic fracture properties, and ascertain fluids in place (Mattar and Anderson, 2003). RTA is equivalent to pressure transient analysis (PTA) and RTA models have been used in tight formation reservoir analysis and are continually evolving to divulge more unique characteristic in understanding how fractures are developed during hydraulic stimulation treatment (Clarkson, 2013a; Clarkson, 2013b; Clarkson and Williams-Kovacs, 2019; Deen et al., 2015; Ely and Herndon, 2019). When RTA is applied to real time production data, RTA can divulge beneficial information regarding not only the reservoir, but also gain some insight into hydraulic fracture characterization that is tied in well performance; however, similar to issues related to PTA regarding early time production, it is often difficult to ascertain early time information due to wellbore storage effects potentially masking the information. Detailed review of flowback studies have been analyzed by Williams-Kovacs (2017) and the workflow for conducting RTA during flowback has been emphasized by the work done by Clarkson (2013b). According to the research by Barree et al. (2019) RTA was applied to online production to quantify the effect of the hydraulic fracture length through the approximations using microcosmic mapped length, gross created length, propped length, flowing length and effective length, where the size of the effective hydraulic fracture length runs from largest to least respectively.

Moreover, RTA is a model inversion forecasting process that applies analytical and semi analytical methods. One disadvantage of using analytical models is that important ancillary information, such as reservoir physics, may be neglected that is critical in determining fracture creation. There is a surfeit of information in the literature that can aide in fracture diagnosis using indirect methods such as composition numerical simulation using multiple objective optimization algorithms to history match flow back and early time production in liquid-rich reservoirs (Kanfar and Clarkson, 2016). Well testing is an invaluable tool to understand how a fracture may generate if early wellbore storage effects can be interpreted.

2.2.5 Advances in Fracture Diagnostic Methods and Emerging Technologies

At the time of this writing, the advances that are henceforth have been in indirect methodologies in conjunction with classical fracture diagnostic tools. Current near-wellbore and far-field wellbore fracture quantification have allowed for better development of indirect methods to not only quantify fractures and how they are formed but assist in fine-tuning existing fracture models. Due to the heterogeneous anisotropic nature of the formation of interest and the range of geomechanical properties, one can observe in a target formation, the future of fracture diagnosis will be in a balance of developing more precise tools that can employ machine learning and big data via indirect methods to help sharpen the before-mentioned tools in this writing. Future research will be coupling reservoir simulation with data mining that is already becoming mainstream, such as works by (Esmaili and Mohaghegh, 2016) through the use of data mining, pattern recognition and machine learning algorithms to quantify in real-time a fracture stimulation program, which is a different approach than traditional stochastic methods (Mohaghegh, 2020). The use of discrete fracture modeling in reservoir simulation (Xu et al., 2017) is proposed for fracture quantification. Additional methods that use historical production through the connected reservoir storage model first introduced by (Childers and Wu, 2017) and later adapted for fracture quantification (Childers and Wu, 2020). A new fracture diagnostic concept that has shown promise is the Sealed Wellbore Pressure Monitoring (SWPM) technique. The application of the SWBP uses a sealed wellbore as a monitoring well that is applied with an external force that slightly deforms the casing of the monitoring well. This technique allows for real-time monitoring of fracture growth of the treatment well to understand how fractures will propagate by analyzing pressure data from the treatment well and that of the monitoring well (Haustveit et al., 2020). The limitation regarding this technique require a noncompleted well to be the monitoring well, which may be difficult depending on other completed wells in the area of interest (Jacobs, 2020).

2.2.6 Summary of Fracture Diagnostic Methods

The following figure (2-14) has been adapted from (Cipolla and Wright, 2000c) and is a synopsis of the different technologies that can aid in fracture diagnostic. This chart shows the different capabilities of each diagnostic technique along with their respective limitations.

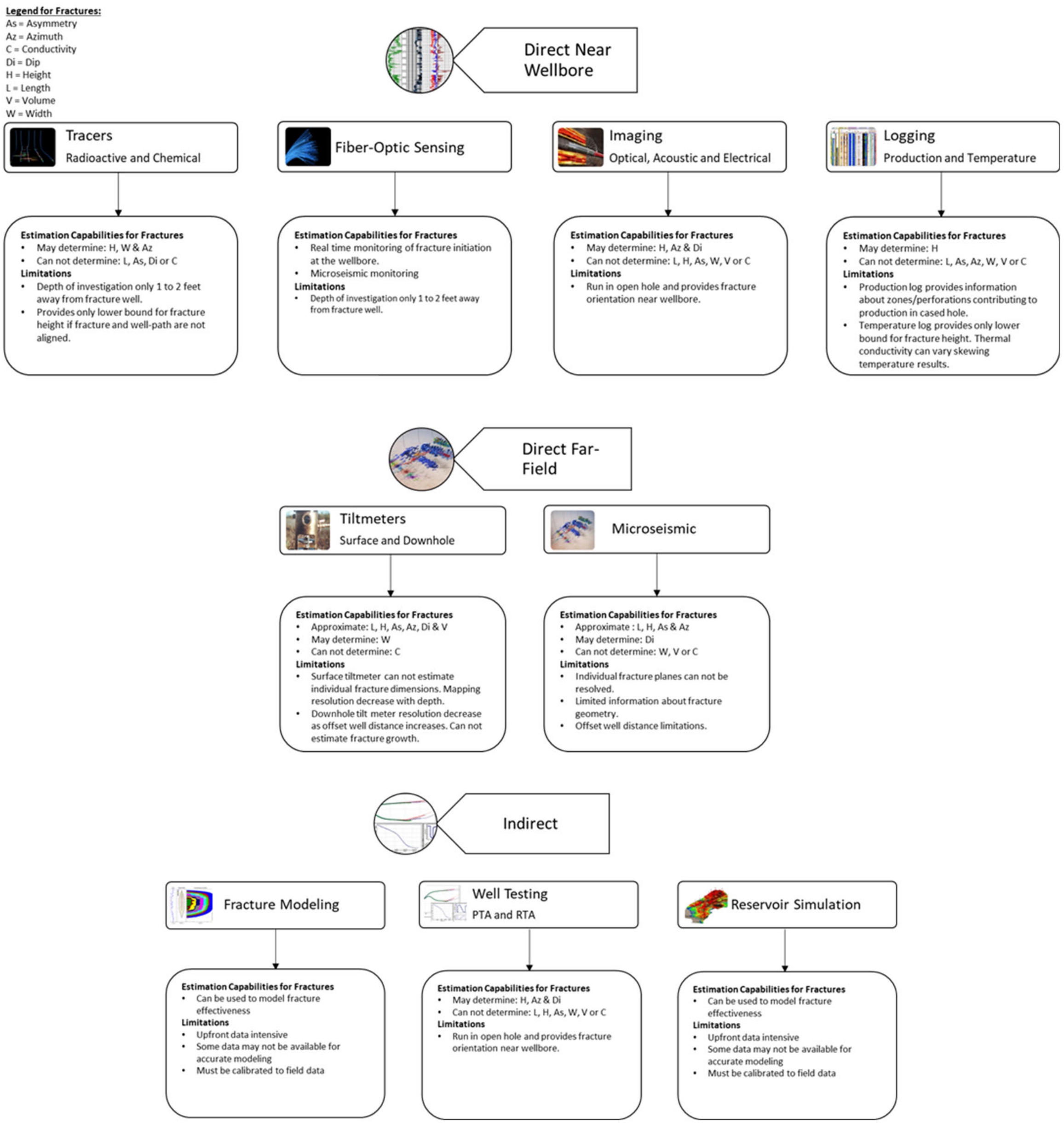

Figure 2 - 14: Diagram of fracture diagnostic methods demonstrating each method's ability to approximate fracture parameters along with the limitations of each technique. This diagram has been adapted and expanded (Cipolla and Wright, 2000b) to include a few modern diagnostic methods.

This section has presented a comprehensive review of fracture diagnostic methods used in the oil and gas industry, advantages, limitations, challenges, and possible solutions. Based on the above study and analysis, the following conclusions can be drawn. (1) fracture diagnostic analysis is an evolving science that allows for a greater understanding of how fractures form and understand the stress mechanisms to develop a stimulation program smartly. (2) fracture diagnostic techniques are multifaceted, meaning one fracture diagnostic technique is not enough to quantify fractures. Multiple techniques are required to understand the near wellbore effects along with the far-field effects. (3) indirect methods allow greater insight into fracture formation through historical production data that will yield information about the fracture to aid in developing new diagnostic methods or aid in advancing existing fracture diagnostic techniques.

Chapter 3: The Connected Reservoir Storage Model (CRSM)

In this chapter, the Connected Reservoir Storage Model will be presented from the fundamental material balance approach, and mathematical equations will be derived for this model related to gas reservoirs. This concept will then be validated through the development of synthetic models with varying permeabilities, porosities, and well geometries through the use of a reservoir simulation suite with known reservoir parameters along with the utilization of deconvolution techniques. Limitations involved with this method will be highlighted in the development procedures.

3.1 CRSM and the Governing Assumptions:

When an oil or gas well is initialized for production it begins to produce in the transient flow regime. The speed at which the pressure propagation occurs is determined through the diffusivity of the reservoir. When the propagation of the pressure reaches all boundaries of the reservoir, the well is in the pseudo steady state (PSS) which is also characterized as boundary dominated flow. Due to the pressure change in the finite volume, the energy contributing to the fluid flow in this volume includes the pore volume compressibility, fluid compressibility, and rock grain compressibility. The summation of pore compressibility and the saturation weighted average fluid compressibility is expressed as the total compressibility of the system and is represented by Eq. (3-1).

$$c_t = c_{PV} + \sum_{i=w,o,g} S_i c_i \tag{3-1}$$

The total compressibility quantifies the relationship between the variations in pore pressure on a body of a porous media, thus resulting in a change in its volume under a uniaxial compression. The total compressibility is defined by the following expression.

$$c_t = -\frac{1}{V}\frac{\Delta V}{\Delta P} \tag{3-2}$$

Where ΔP is the pressure change over an infinitely small volume and ΔV is the total volumetric change which is equal to the volume of fluids expelled from an infinitely small volume at the subsurface condition. When quantifying the cumulative production of the reservoir volume, one can determine this by the product of the total compressibility Eq. (3-3) and V_P which is the pore volume of an infinitely small volume and the pressure change over the same volume. The mathematical expression that relates the cumulative production of the reservoir volume is defined as the product of the total compressibility, pore volume, and the differential pressure change of the reservoir volume.

$$Q_{RV} = c_t V_P \Delta P \tag{3-3}$$

Here the concept of connected reservoir storage will be defined, and it is expressed as follows:

$$E(t) = c_t V_P(t) \tag{3-4}$$

Note that the Appendix (D) details the relationship of connected reservoir storage Eq. (3-4) as it relates to the radius of investigation (ROI) and time. The connected reservoir storage growth concept, from t_1 to t_2, is presented in Figure (3-1). If $t_1 = 0$, then Eq. (3-3) can be written as follows:

$$Q(t) = \int_0^{\tau} q(\tau) d\tau = E(t)\left[P_i - \overline{P}_r(t)\right] \qquad (3\text{-}5)$$

Where $Q(t)$ is defined as the cumulative fluid production at reservoir conditions with respect to time, $E(t)$ is defined as the connected reservoir storage (CRS) in the region of pressure propagation, and $\overline{P}_r(t)$ is defined as the average reservoir pressure at the time t.

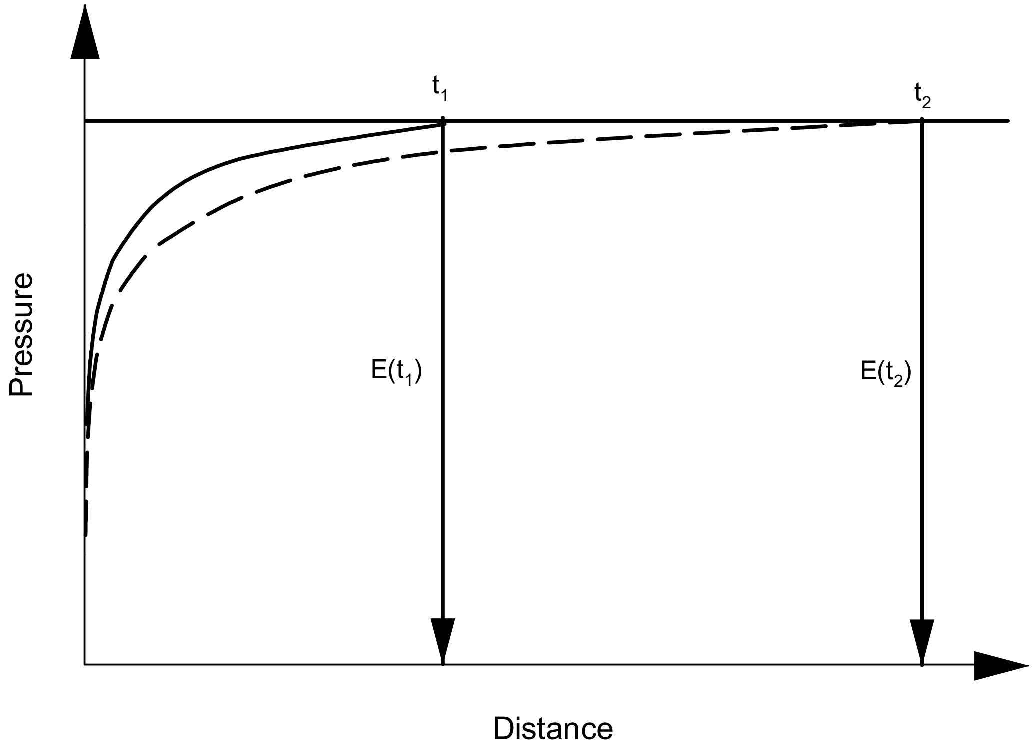

Figure 3 - 1: Diagram of the CRS changing from t_1 to t_2, the ordinate-axis displays the pressure and is the location of a producing well, whereas the abscissa axis represents the radius of investigation into the formation. As the well is initialized for production, the pressure response propagates into the formation, and the CRS can be determined at various times during well life.

The derivations of the CRSM can be found in appendix (A) and the connected reservoir storage can be modeled at any time for oil or gas reservoirs. The CRSM is not dependent on reservoir shape, heterogeneity, effective reservoir permeability or fluid properties. From Eq. (3-5), the average reservoir pressure can be written as follows:

$$\bar{P}_r(t) = P_i - \frac{Q(t)}{E(t)} \tag{3-6}$$

It should be noted that when evaluating actual production history, constant rate production is an unrealistic assumption since well production operations is a cyclical event with many service interruptions, such as well production shutdowns and startups, for various operational needs. To apply deconvolution to well production, one will need to normalize the production and cumulative production at any particular moment in time, t, for both oil and gas reservoirs as follows along with the governing assumptions of the CRSM, which are vertical well orientation, two-phase fluid is present either oil and water or gas and water media, constant production rate, radial flow in a circular reservoir of radius r_e, no mechanical skin effects exist, nor are there any effects of non-Darcy flow.

For liquid production:

$$q_N(t) = \frac{q_o(t)}{P_i - P_{wf}(t)} \tag{3-7}$$

$$Q_N(t) = \frac{Q_o(t)}{P_i - P_{wf}(t)} \tag{3-8}$$

where $q_N(t)$ and $Q_N(t)$ are the normalized production rate and normalized cumulative production values to the normalized derivation of the PSS solution to the radial diffusivity equation for liquid, and is expressed as follows:

$$1 = \varepsilon \ln[\sigma] q_N(t) + \frac{Q_N(t)}{E(t)} \tag{3-9}$$

where $\sigma = \dfrac{4E(t)}{C_A \gamma \phi h c_t r_w^2}$ and $\varepsilon = \dfrac{70.6\mu_o}{kh}$ (Childers and Wu, 2017)

For gas production:

$$q_{N_g}(t) = \frac{q_g(t)}{\delta_i - \delta_{wf}} \tag{3-10}$$

$$Q_{N_g}(t) = \frac{Q_g(t)}{\delta_i - \delta_{wf}} \tag{3-11}$$

where $q_{N_g}(t)$ and $Q_{N_g}(t)$ are the normalized production rate and normalized cumulative production values to the normalized derivation of the PSS solution to the radial diffusivity equation for gas, and is expressed as follows:

$$1 = \zeta \ln(\sigma) q_{N_g}(t) + \frac{Q_{N_g}(t)}{E(t)} \tag{3-12}$$

where $\zeta = \dfrac{70.6\mu_g}{kh}$, and $\sigma = \dfrac{4E(t)}{C_A \gamma \phi h c_t r_w^2}$ (Wu and Childers, 2020). For a detailed derivation of Eq. (3-7) – Eq. (3-12), liquid and gas production, the reader should consult appendix (A) of this dissertation. Therefore, t is the elapsed time in hours and $\left[P_i - P_{wf}\right]$ is the reservoir response curve with unit production rate for liquid production and $\left[\delta_i - \delta_{wf}\right]$ is for gas production. From the actual production rate, the relationship between time, t, and $\left[P_i - P_{wf}\right]$, liquid production, or $\left[\delta_i - \delta_{wf}\right]$ gas production, can be found using deconvolution techniques. Furthermore, from pressure transient analysis theory, the derivative function is defined as $\left[t\frac{d\left[P_i-P_{wf}\right]}{dt}\right]$ and $\left[t\frac{d\left[\delta_i-\delta_{wf}\right]}{dt}\right]$ for liquid and gas production, respectively, can be used to determine the reservoir boundaries. Once the normalized rate and normalized cumulative production have been determined, the connected reservoir storage can be readily ascertained. The connected reservoir storage can be calculated from the intersection of the tangent of the normalized decline curve with the normalized cumulative production axis as shown in Figure (3-2).

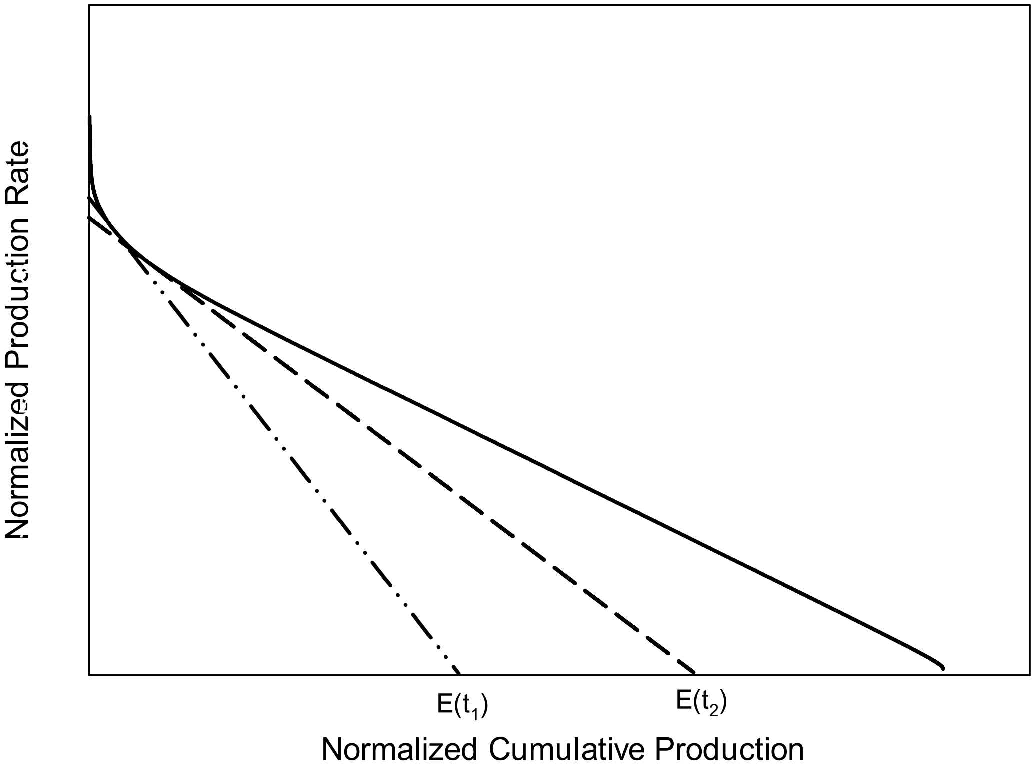

Figure 3 - 2: Determination of the connected reservoir storage at time t_1 and t_2.

The derivations above illustrate that the reservoir response to a unit production rate can be approximated with no prior knowledge of the reservoir formation characteristics or fluid properties, which makes for a very powerful tool when evaluating production behavior. The reservoir response curve can be used to calculate the production rate for a given pressure (or vice versa) using Duhamel's integral, which is given by equation Eq. (3-13).

$$P_{wf}(t) = P_i - \int_0^{\tau} q(\tau) \frac{dD_p(t-\tau)}{dt} d\tau \qquad (3\text{-}13)$$

The procedure to calculate the production rate for a given flowing bottom hole pressure has been outlined in the paper by Wu et al. (2012a)

Moreover, there are a few limitations when utilizing the connected reservoir storage model that need to be addressed. First, the original reservoir pressure should be uniform and constant. Second, the well being evaluated should be free of interference. If these assumptions are not adhered to then significant errors would occur in the analyzed results. Furthermore, it should be noted that the wellbore skin effect does not impede the application of this method as the skin does not affect the connected reservoir storage. If a well exhibits skin behavior, the calculated pressure response and its time derivative will encompass the skin effect already. An additional challenge as well is with the initial pressure being an unknown; however, the pressure rate deconvolution algorithm that was proposed by (Levitan, 2003; Levitan, 2005) and can be employed to reconstruct the pressure response and estimate the initial reservoir pressure.

3.2 CRSM Validation using Numerical Simulation Gas Reservoir:

Nine cases shown in Figure (3-3) through (3-5) were used to validate the above algorithm. These cases, with known reservoir geometries, along with variations in permeability and porosity are simulated to generate rate and pressure data. Table (3-1) gives other essential parameters for these nine cases that are used to develop bottomhole flowing pressure profiles utilizing reservoir simulation software.

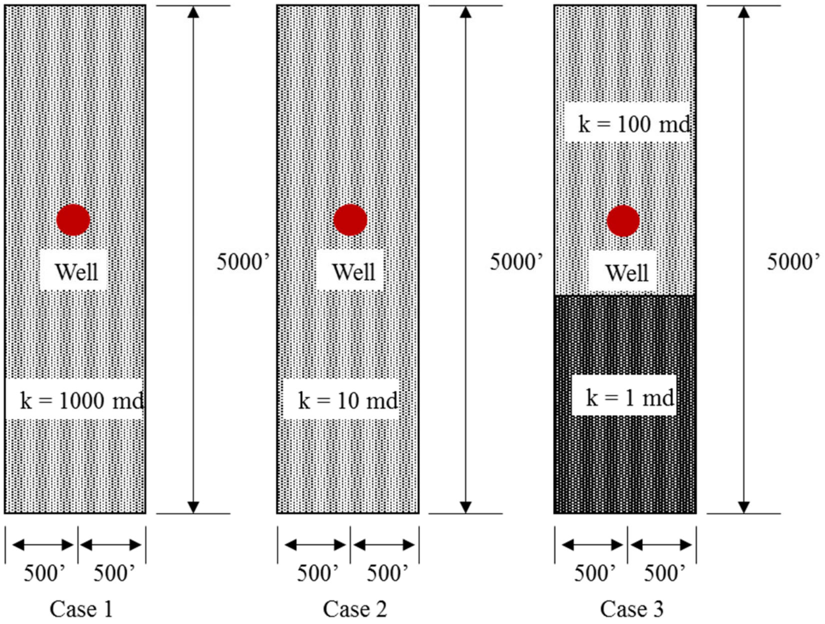

Figure 3 - 3: Rectangular reservoir models with varying permeability.

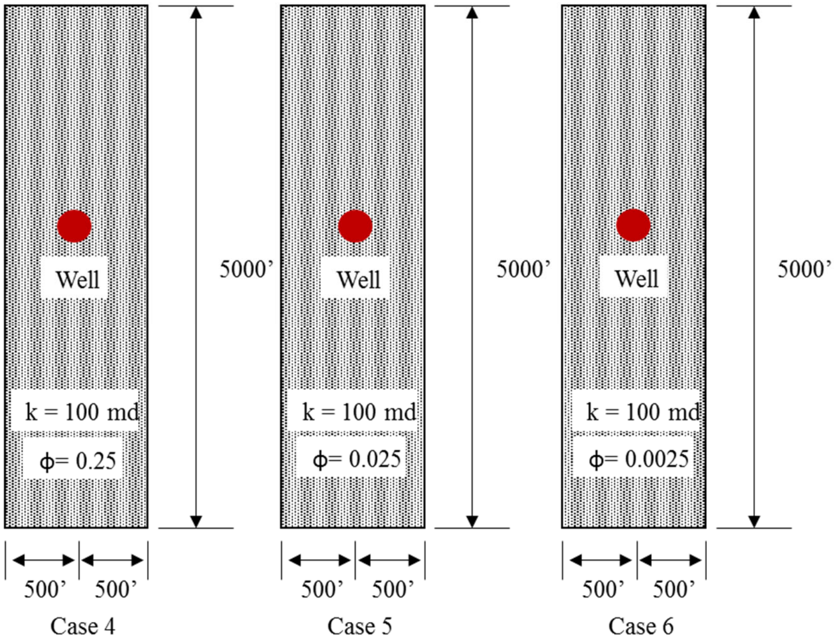

Figure 3 - 4 : Rectangular reservoir models with varying porosity.

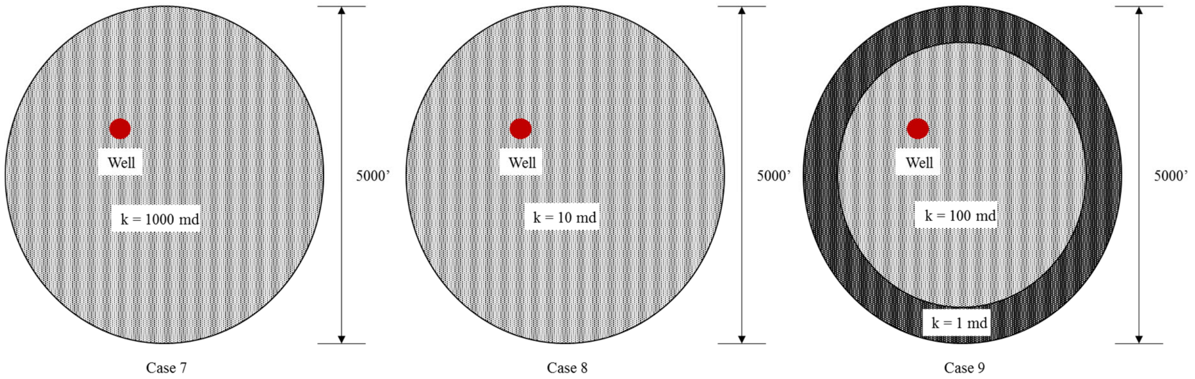

Figure 3 - 5: Radial reservoir models with varying permeability.

Table 3 - 1: Summarized input parameters for the rectangular and radial reservoir formation case studies at initial conditions.

Simulation Parameters			
Initial pressure , psia	5,000	Gas saturation, dimensionless	0.8
Formation temperature, F	212	Gas compressibility, 1/psi	1.33E-04
Pay thickness, ft	100	Rock compressibility, 1/psi	3.00E-07
Top of reservoir, ft	5,000	Total compressibility, 1/psi	1.07E-04
Skin dimensionless	0	Gas formation volume factor, cf/Mscf	3.82
Wellbore radius, ft	0.5	Gas viscosity, cP	2.49E-02
Gas deviation factor, dimensionless	1.01	Gas gravity, dimensionless	0.65
Water saturation, dimensionless	0.2	Gas flow rate, Mscfd	2,000
Water compressibility, 1/psi	3.39E-06	Porosity, dimensionless. Case studies (1,2,3,4,7,8,9) only	0.25

For a well that is testing at a constant production rate in all the above cases, the well bottomhole pressure can be calculated using well testing design based on the pressure response for laterally composite reservoirs (Kuchuk and Tarek, 1997). Figures (3-6), (3-9) and (3-12) shows the pressure profiles generated using reservoir simulation software for case studies one through nine along with the normalized production rate versus the normalized cumulative production and calculated connected reservoir storage at various times during well life. The tangent at any point on the normalized production rate versus the normalized cumulative production curve figures (3 - 7), (3-10) and (3-13) can be estimated using numerical differentiation to calculate the connected reservoir storage at any moment, which is the intersection of the tangent line with the normalized cumulative production axis (refer to Figure (3-2) for the general concept). After convergence of all case study models, the total connected reservoir storage model results are compared with the explicit connected reservoir storage solution which can be determined from Eq. (3-4).

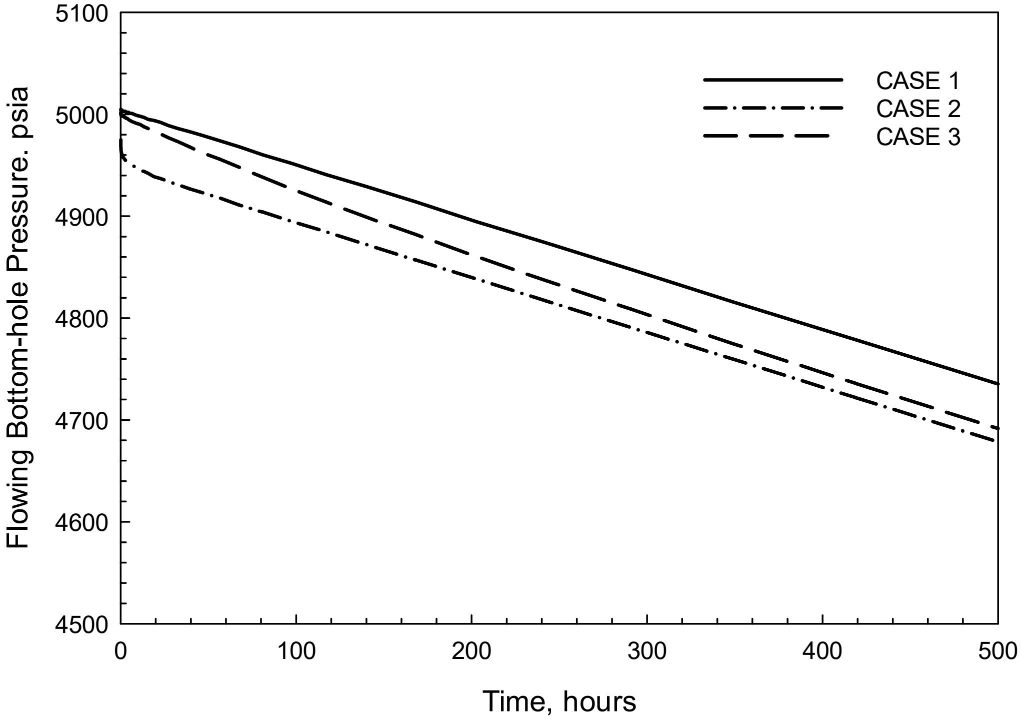

Figure 3 - 6: Simulated flowing bottomhole pressure for cases one through three, varying permeability.

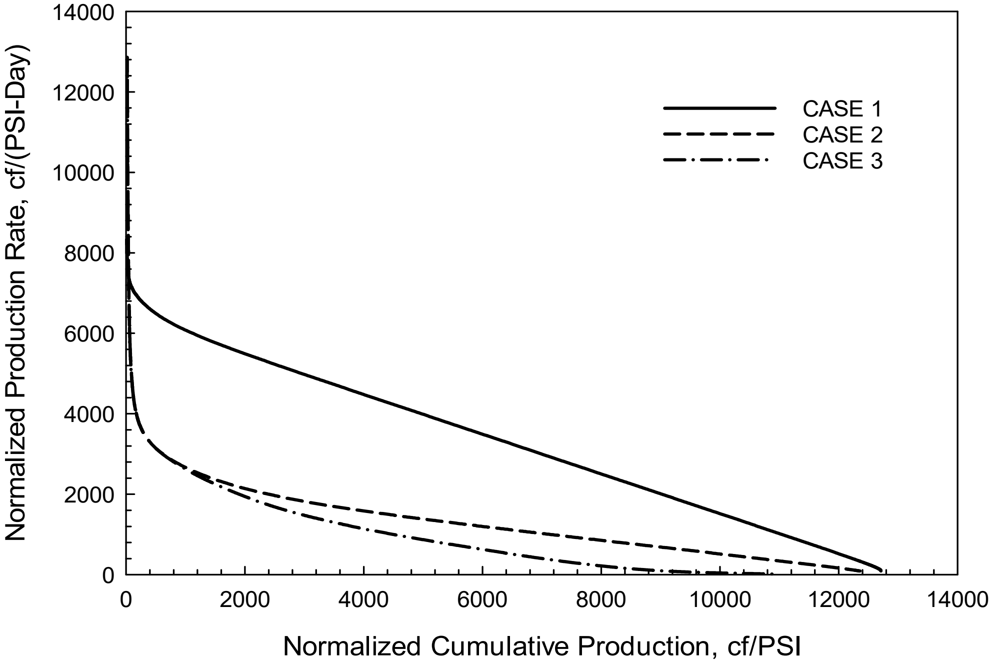

Figure 3 - 7: Normalized production rate and normalized cumulative production for cases one through three, varying permeability.

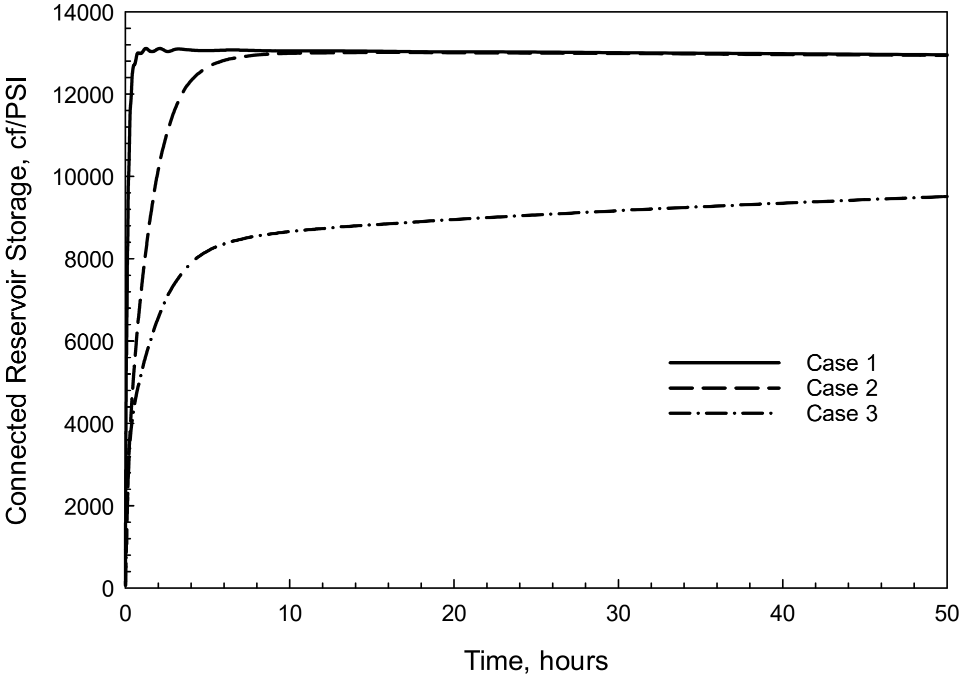

Figure 3 - 8: Calculated connected reservoir storage for cases one through three, varying permeability.

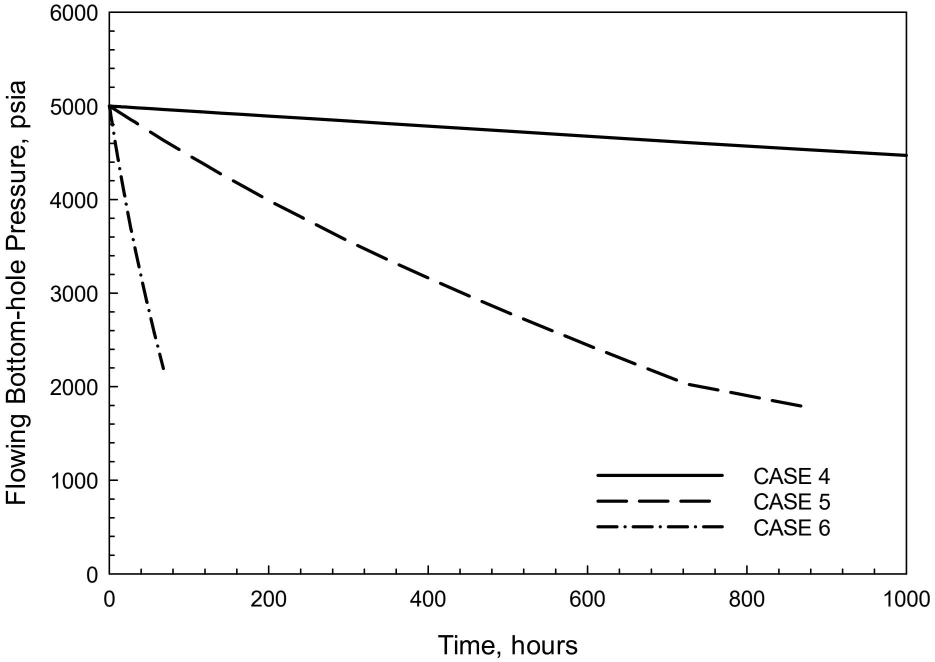

Figure 3 - 9: Simulated flowing bottomhole pressure for cases four through six, varying porosity.

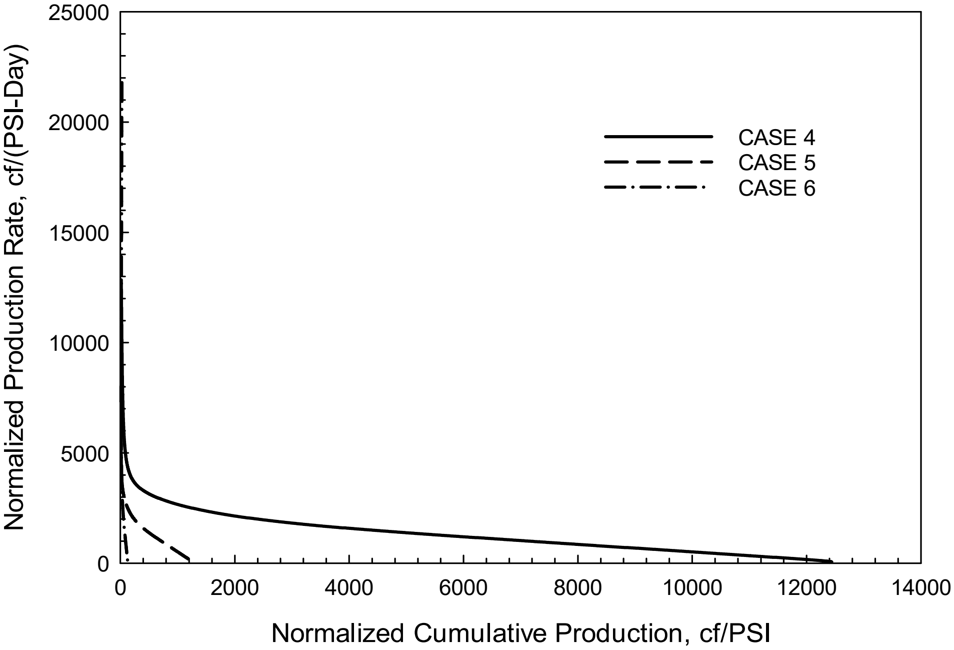

Figure 3 - 10: Normalized production rate and normalized cumulative production for cases four through six, varying porosity.

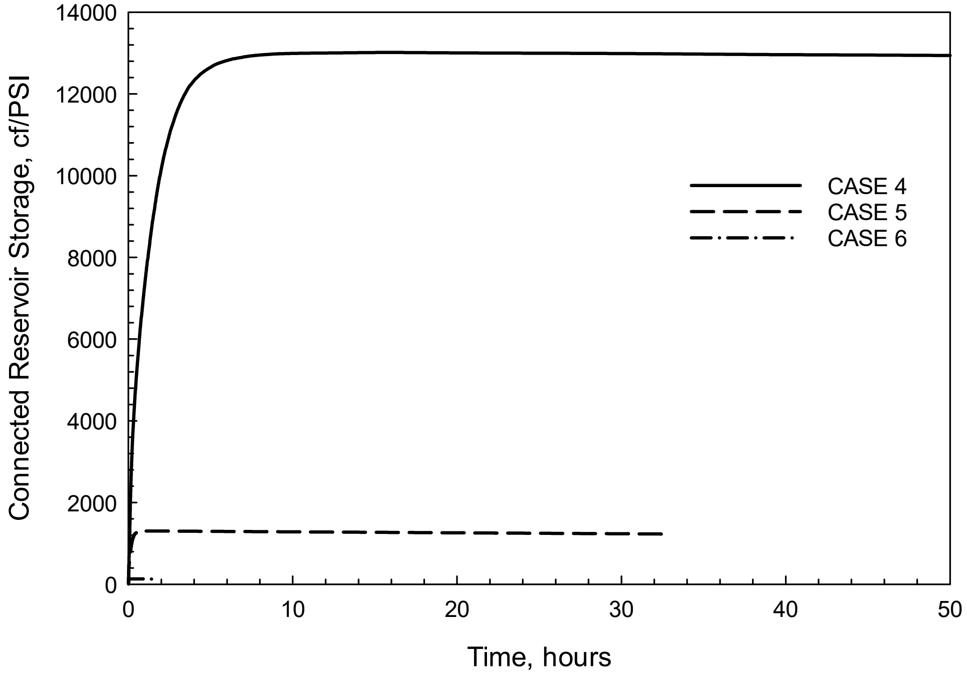

Figure 3 - 11: Calculated connected reservoir storage for cases four through six, varying porosity.

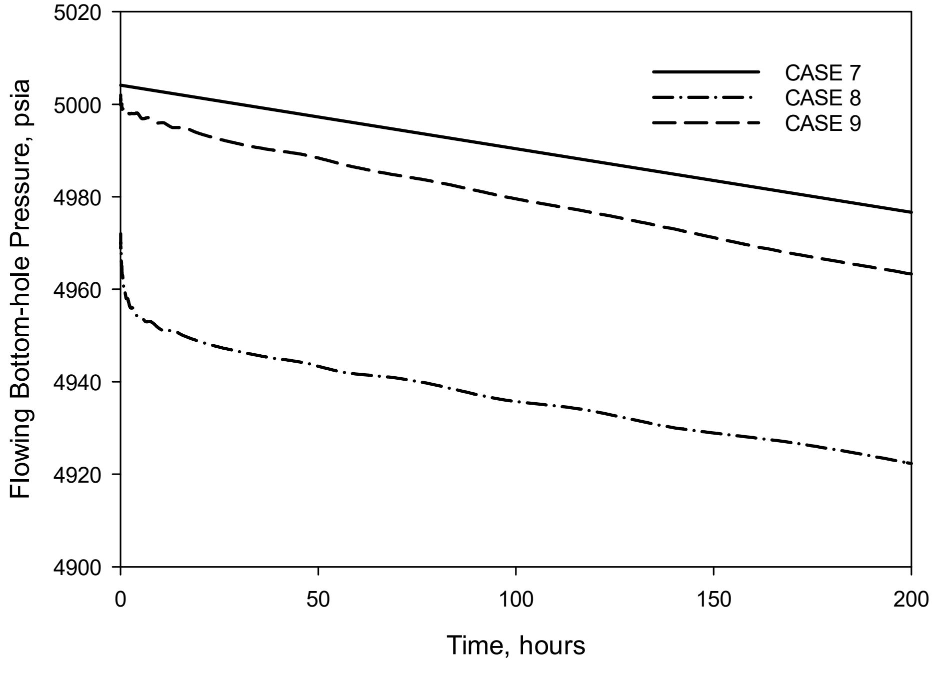

Figure 3 - 12: Simulated flowing bottomhole pressure for cases seven through nine, varying permeability.

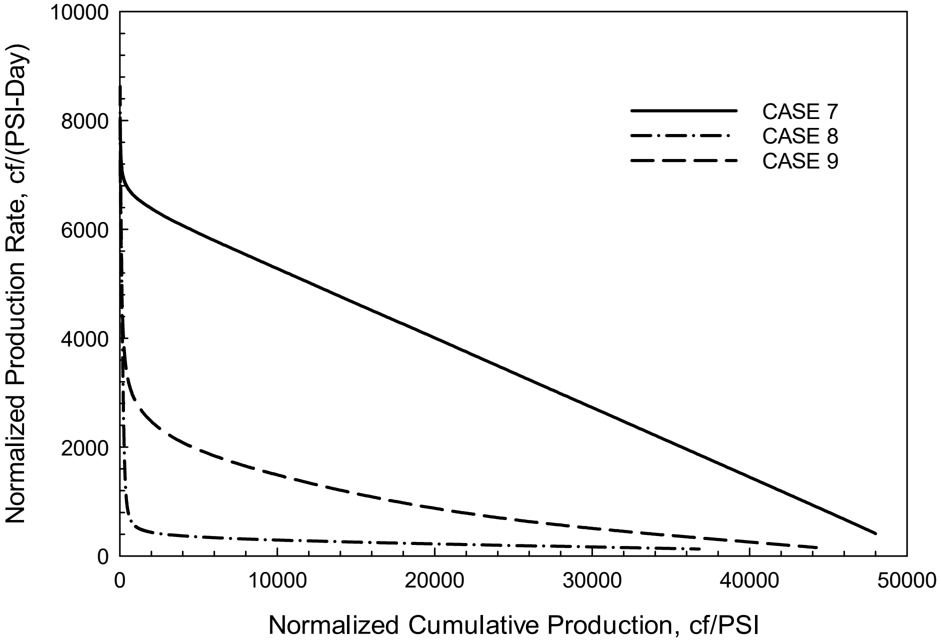

Figure 3 - 13: Normalized production rate and normalized cumulative production for cases seven through nine, varying permeability.

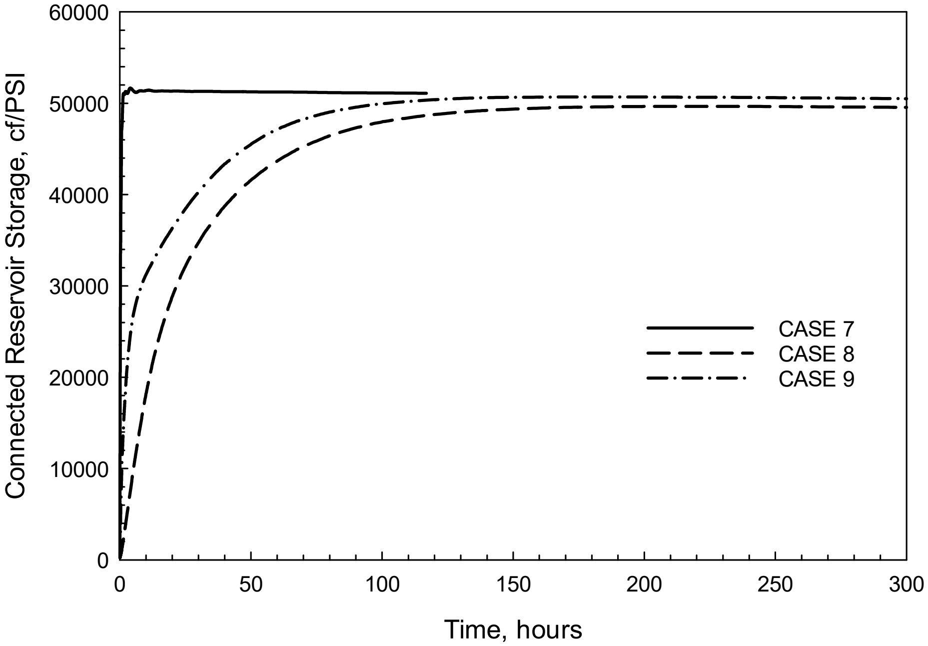

Figure 3 - 14: Calculated connected reservoir storage for cases seven through nine, varying permeability.

Table 3 - 2: Comparison of the calculated total connected reservoir storage explicit solution and the proposed algorithm connected reservoir storage model for cases one through nine.

Case Studies	Case 1	Case 2	Case 3
Pore volume, cf	125,000,000	125,000,000	125,000,000
Total storage (Explicit), cf/psi	13,375	13,375	13,375
Total storage (Model), cf/psi	13,111	13,017	11,735
Error =	1.97%	2.67%	12.36%
Case Studies	**Case 4**	**Case 5**	**Case 6**
Pore volume, cf	125,000,000	12,500,000	1,250,000
Total storage (Explicit), cf/psi	13,375	1,337	134
Total storage (Model), cf/psi	13,017	1,301	130
Error =	2.67%	2.71%	2.69%
Case Studies	**Case 7**	**Case 8**	**Case 9**
Pore volume, cf	490,873,852	490,873,852	490,873,852
Total storage (Explicit), cf/psi	52,522	52,522	52,522
Total storage (Model), cf/psi	51,587	49,652	50,694
Error =	1.78%	5.47%	3.48%

Using Figures (3-6), (3-9) and (3-12) and utilizing deconvolution techniques, the pressure response $\left[\delta_i - \delta_{wf}\right]$ (which describes the pressure drop for unit production rate) can be determined. The derivative of the pressure response $\left[t\frac{d\left[\delta_i - \delta_{wf}\right]}{dt}\right]$ describes the boundary conditions of the reservoir, and the calculating technique to determine the derivative has been discussed by Horne (Horne, 2000).

The results shown in Table (3-2) for case studies one through nine between the explicit solution and model solution agree very well with some degree of error. The error in the results come from the approximation error duration during the numerical calculation as well as error in the grid block calculations of the reservoir simulation. The absolute error ranges from approximately 2% to 12% with Case 3 exhibiting the highest absolute error value. The error in Case 3 is due to the two-zone linear composite model with one zone, 60% of the formation, having a permeability of 100 md and second zone having a permeability of 1 md making up 40% of the remainder of the formation. Moreover, the matching of the results would be acceptable once the error causing the difference between the explicit solution and the connected reservoir storage model is understood.

3.3 CRSM Implementation and Interrelated Curves:

The CRSM interrelated curves allow for reservoir diagnosis and can be used independently for multiple purposes of reservoir characterization and performance analysis. Figure (3 - 15) shows the various elements that govern the CRSM. The normalized decline curve (NDC), at the apex of figure (3 - 15), is found through the computation of Eq. (3-10) and Eq. (3-11). The next step is to find the connected reservoir storage curve (CRS), and reservoir response curve (RPC) which represent the pressure drop function at a different time at a unit production rate. The derivative function of RPC can be used independently or in conjunction with reservoir diagnosis. Moreover, to determine any of the interrelated curves, both the BHFP and production rate will be needed. The reservoir response curve also can be obtained from theoretical reservoir models such as image wells and pressure superposition, and numerical deconvolution of actual production data. The pressure drop curve can be used to predict production rates for complex reservoirs and zonal rate allocations by coupling this curve with Duhamel’s integral (Wu et al., 2012b). The pressure drop curve can be used to monitor the change in well productivity and skin history. The derivative curve can be utilized to state the boundary conditions and flow regimes for a given reservoir. Using the NDC, one can diagnose the well performance and flow region of a producing well. The CRS curve reveals the growth of the minimum pore volume contributing to the pressure behavior and production performance. With the knowledge of the minimum connected pore volume, the average reservoir pressure and volume can be estimated which is a required value needed when applying material balance analysis. The combination of these three curves is more useful in reservoir performance analysis and forecasting for complex reservoirs. For instance, a well with limited production history has a high probability to still be in the transient flow regime, especially if the reservoir is a tight formation. To forecast the production rate, many uncertainties associated with the reservoir volumes with different confidence intervals can be implemented in the CRSM. Integrating the CRSM with geological data, the overall CRS can be utilized in the development of probabilistic forecast models.

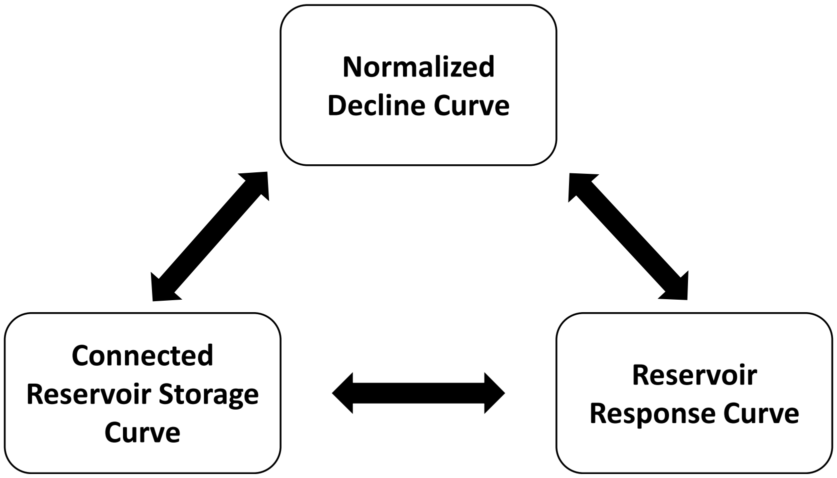

Figure 3 - 15: Connected Reservoir Storage Model flow chart process. Normalized Decline Curve (NDC) is determined from the normalized cumulative production and production rates. Connected Reservoir Storage (CRS) curve is determined from NDC. The reservoir response curve (RPC) is determined through the deconvolution of the normalized cumulative production and production rate history.

3.4 Summary:

This chapter has introduced a novel concept of the CRSM. The CRSM adds a needed bridge between production decline and the reservoir pressure response. Using the methodology presented in this chapter, it has been demonstrated that the CRS term can be calculated directly from production data without any prior knowledge of the reservoir geometric information, petro-physical data, or fluid properties. This in turn, significantly streamlines the pressure transient analysis and can be directly used to forecast production, pressure behavior, average reservoir pressure and original fluids in place. In addition, the CRS concept can also be related to the superficial radius of investigation as demonstrated in Appendix (D). The capabilities of decline curve analysis have been greatly expanded. With the concept of the connected reservoir storage model, decline curve analysis can now be applied to the transient flow regime which, in turn, will greatly enhance reservoir forecasting for wells that exhibit long life in the transient flow region.

Chapter 4: CRSM Applied to Simulated Liquid Well Performance

This chapter will demonstrate the ability of the CRSM to predict production performance and compare the result to two classical empirical techniques currently used in tight formation predictions, and the validation is done via numerical simulation. Based on the CRSM, this chapter will reveal the interrelated paradigms among well performance, increasing reservoir connected volume, and rate forecasts with uncertainties.

4.1 Applying the CRSM Oil Well Application:

To validate the performance of CRSM and to forecast well performance, a bi-wing synthetic reservoir model was used for a base and sensitivity case studies. Figure (4 - 1) is an illustration of the numerical model with known parameters summarized in Table (4 - 1). The model represents a half of fracturing cluster in a tight formation. Since the purpose of this exercise is to validate the CRSM, we must use existing flow mechanisms with known flow regions and reservoir properties. Permeability impact was studied by changing the matrix permeability to 0.1 md, and 0.01 md. Each synthetic reservoir simulation was simulated for 30 years and the data derived from the reservoir simulation was the BHFP, liquid rate production and cumulative liquid production, see figure (4 - 2), (4 - 3), and (4 - 4) respectively.

Table 4 - 1: Summarized input reservoir simulation parameters for the case studies at initial conditions. The parameters outlined in this table were utilized with bi-wing hydraulically fractured reservoir model, figure (4 - 1), to determine the BHFP, liquid production rate and liquid cumulative production for base and sensitivity case studies.

Simulation Parameters			
Bubble point pressure, psi	1,323	Oil formation volume factor, rb/STB	1.15
Formation temp., F	220	Pay thickness, ft	210
Fracture perm., md	10,000	Skin factor	0
Initial reservoir pressure, psia	8,000	Specific gas gravity, dimensionless	0.71
Matrix perm., md	1, 0.1, 0.01	Total vertical depth, ft	5,085
Matrix porosity, fraction	0.081	Wellbore radius, ft	.5
Minimum BHFP limit, psi	1,500	Oil compressibility, 1/psi	2.80E-06
Oil density, lbm/cf	55.3	Pore volume compressibility, 1/psi	2.80E-06
Oil flow rate, STB/D	750	Water compressibility, 1/psi	2.80E-09
Model Geometry			
Length, ft	1,000	Thickness, ft	210
Width, ft	1,000	Number of layers	1

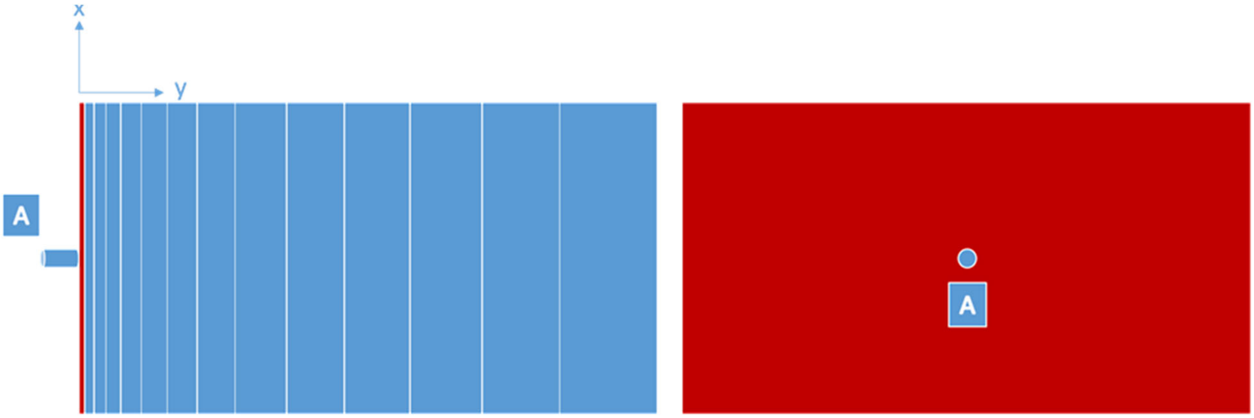

Figure 4 - 1: Bi-wing hydraulically fractured reservoir simulation model (half fractured system cluster) where point A is the location of the wellbore. The model was developed with a logarithmic single layer gird. The left picture is the top view looking down on the reservoir from the surface, where the red layer, first grid block represents the hydraulic fracture, and the blue grid block represents the matrix formation. The right view is looking into the formation from the left side.

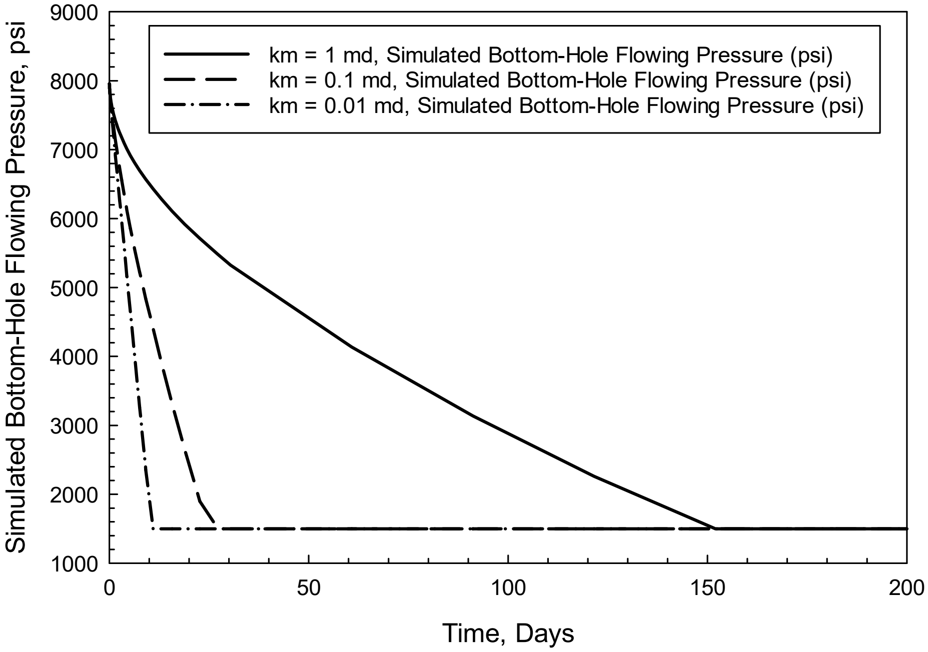

Figure 4 - 2: BHFP determined from the reservoir simulation. The BHFP were determined using the base case, 1 md and for the sensitivity case studies of 0.1 md and 0.01 md, respectively.

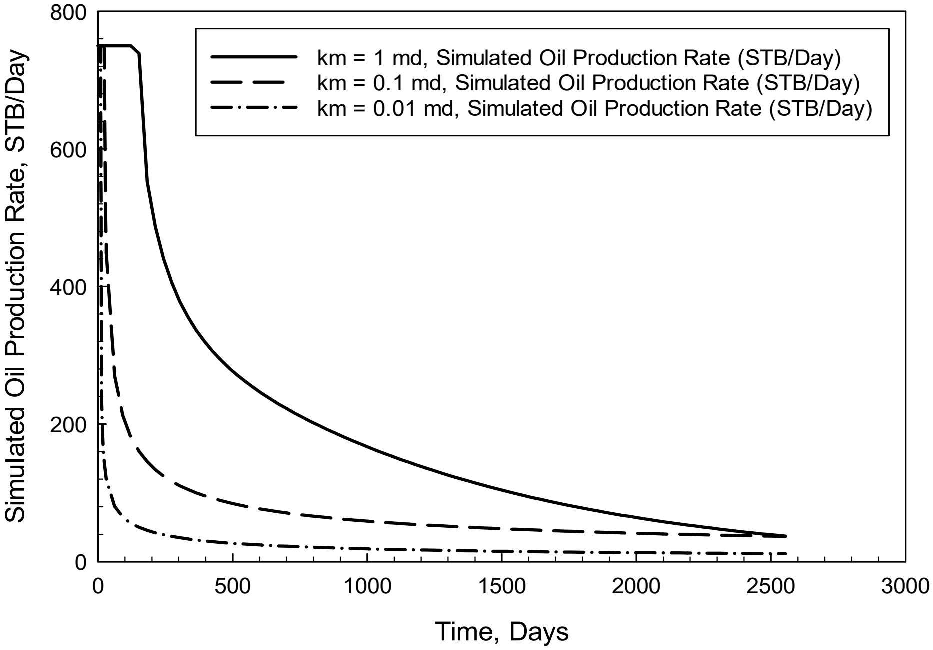

Figure 4 - 3: Simulated oil production rate from reservoir simulation. The oil production rate was determined using the base case study of 1 md and for the sensitivity case studies of 0.1 md and 0.01 md, respectively.

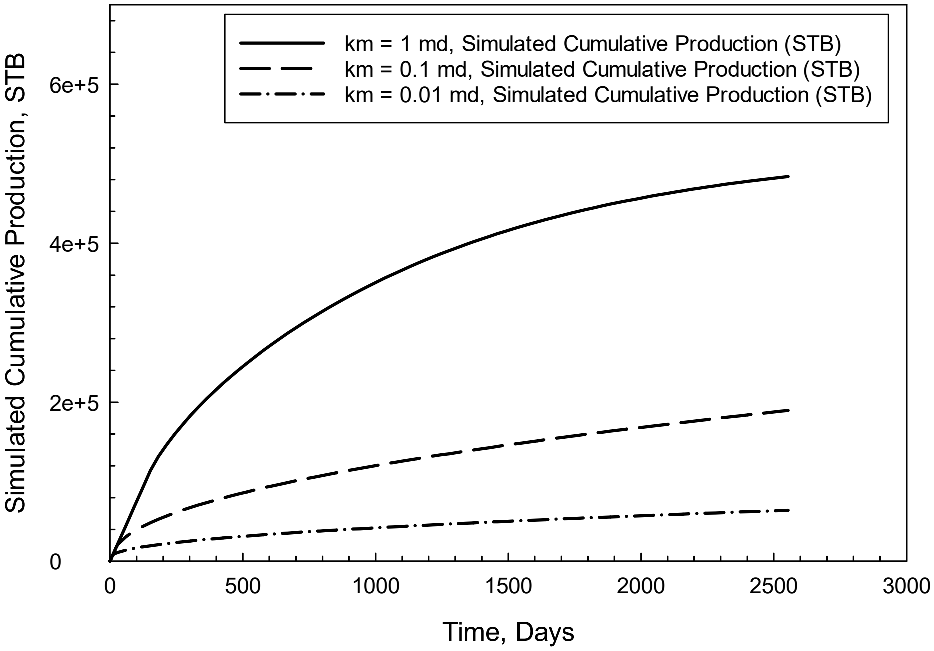

Figure 4 - 4: Cumulative production for the base case study, 1 md and the sensitivity case studies of 0.1 md and 0.01 md respectively. The cumulative production is used in the normalized cumulative production calculation of Eq. (3-8)

4.2 Production Forecasting using CRSM:

The base case with the matrix permeability of 1 md is used to demonstrate the implementation of the CRSM. The numerical simulator yields the well production history and BHFP with which the NDC can be obtained as shown in Figure (4-5) as the procedure outlines in appendix (C).

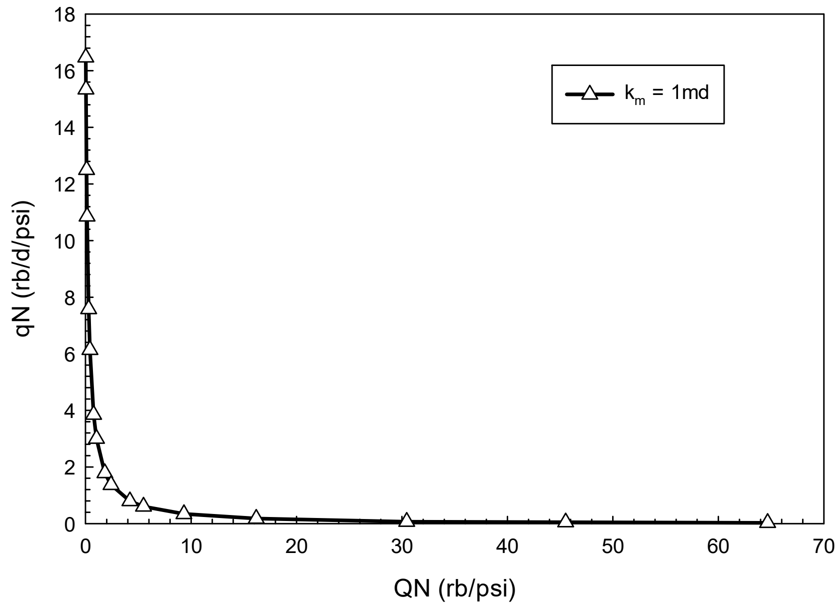

Figure 4 - 5: The determination of the normalized decline curve model for the base case k$_m$ = 1 md. This model was derived from the computations of Eq. (3-7) and Eq. (3-8).

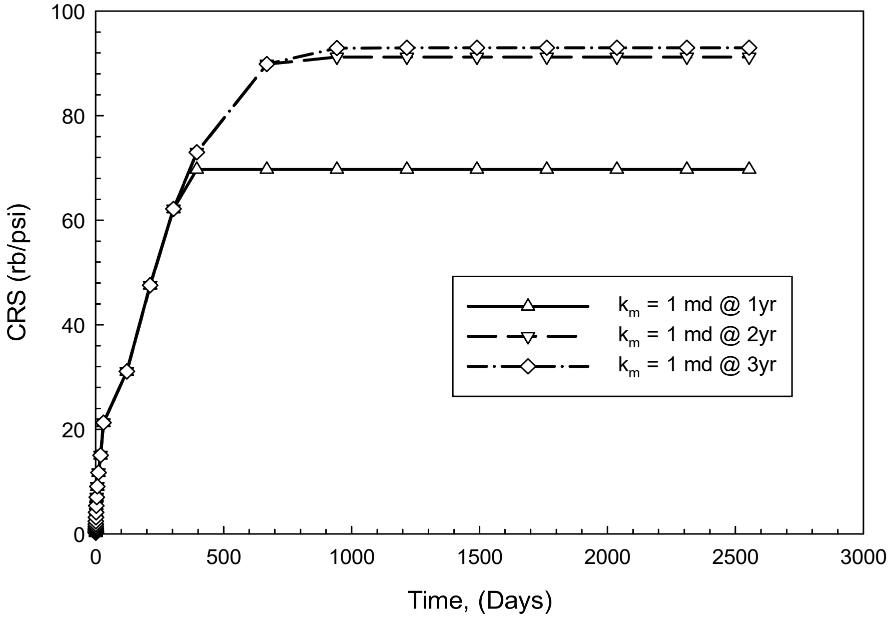

Figure 4 - 6: The connected reservoir storage determined for the base case of k$_m$ = 1 md. CRS was determined looking at historical production of one, two and three years, respectively. The CRS can be determined from A-(40)

Once the NDC has been determined, the next step is to determine the CRS curve by applying Eq. A-(40), to the data formulated from Eq. (3-7) and Eq. (3-8), see figure (4 - 6). Note that the CRS assumes that PSS flow has been reached at the end of one, two and three year production histories. This assumption allows for the projection of the unit pressure response since deconvolution will only be applied to the historical data set of interest. Once both the NDC and CRS curves have been determined, the unit pressure response will be determined by deconvolution, see figure (4-7). The unit pressure response forms the basis such that the CRSM can be implemented. Moreover, due to the numerical errors that arise from the normalization computations presented earlier as well as the deconvolution being ill-posed (Kuchuk et al., 2010a), there can be noise in the data that may require some data smoothing to reduce the amount of noise seen in the unit pressure response when applying the CRSM algorithm for production forecasting predictions illustrated in appendix (A).

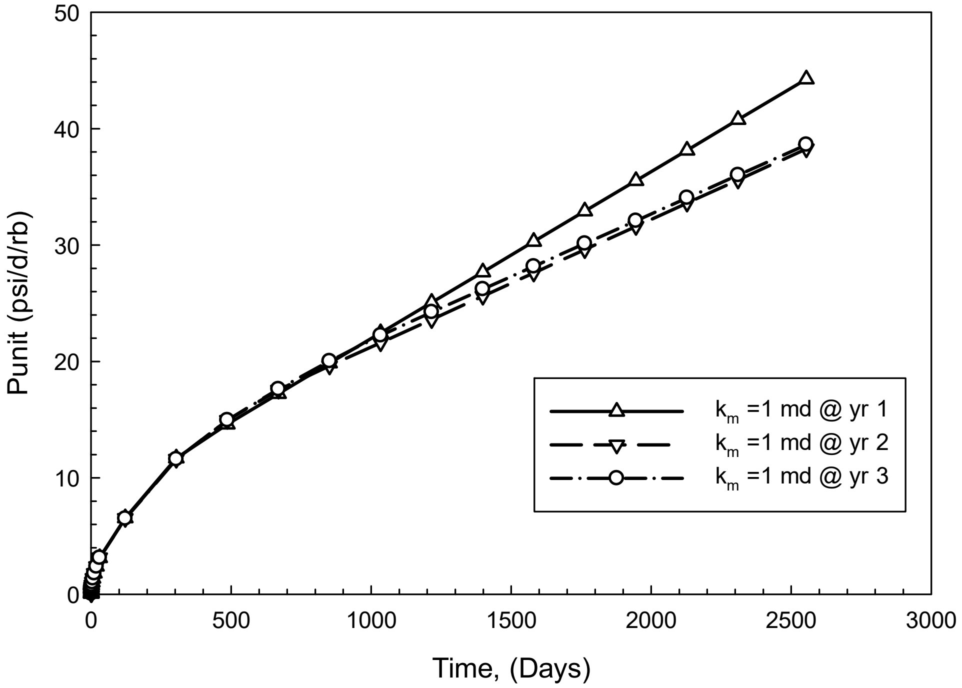

Figure 4 - 7: Determination of the unit pressure response for the base case model of k_m = 1 md. The unit pressure response was determined using deconvolution on the historical production of one, two and three years, respectively. The unit pressure response was projected into the future at a linearly increasing rate that assumes the reservoir has reached PSS flow.

Two empirical models will be used for comparison of the production forecasting models, which is the Arps' hyperbolic model Eq. (2-4) and Duong model Eq. (2-11). The traditional Arps' model and Duong parameters were determined using the procedures outlined (Arps, 1945) and (Duong, 2011) and can be found in table (4-2). It is important to note that for tight formation production analysis using the Arps' hyperbolic model, it is not uncommon to have Arps exponent values greater than unity (Poston and Poe, 2008). The results of table (4-2) will be used for both the Arps' and Duong empirical models to forecast future production performance and these parameters where determined using numerical regression to minimize the error between the simulation data and the empirical models. Figure (4 - 9) and (4 - 10) show the production performance between simulated production and empirical models.

Table 4 - 2: Tabulated parameters found for the Arps and Duong Model's base case study. The constraints for the Arps Model are with the Arps' exponent such that: b = 0 for exponential decline, 0 < b < 1 for hyperbolic decline and b = 1 for harmonic decline. The constraints for Duong Model are with the Duong intercept "a" and Duong slope "m" with constraints of 0 < a ≤ 2 and 1 ≤ m ≤ 2, respectively.

Empirical Model Parameters Summary		**Arps Parameters**			**Duong Parameters**		
Model Data	**Matrix Per, (md)**	**qi (rb/Day)**	**Di (1/Day)**	**b**	**qi (rb/Day)**	**a (1/Day)**	**m**
Year 1	1	862.5	8.69E-03	0.39	862.5	4.58	1.55
Year 2	1	862.5	4.27E-03	0.67	862.5	2.21	1.26
Year 3	1	862.5	3.74E-03	0.75	862.5	2.09	1.24

Figure (4 - 8) shows the production forecasting performance of the CRSM as shown in figure (4 - 7). Illustrated on Figure (4 - 8) are three coloring schemes to represent the production history that was used for the prediction models. The one year (Yr1) represents one year of historical production data, two years (Yr2) represent two years of historical production data and three years (Yr3) represent three years of historical production data, which were used for prediction model forecasting. The method in figure (4 - 8) was carried over to figures (4 - 9) through (4 - 10) and will not be repeated in the following figures.

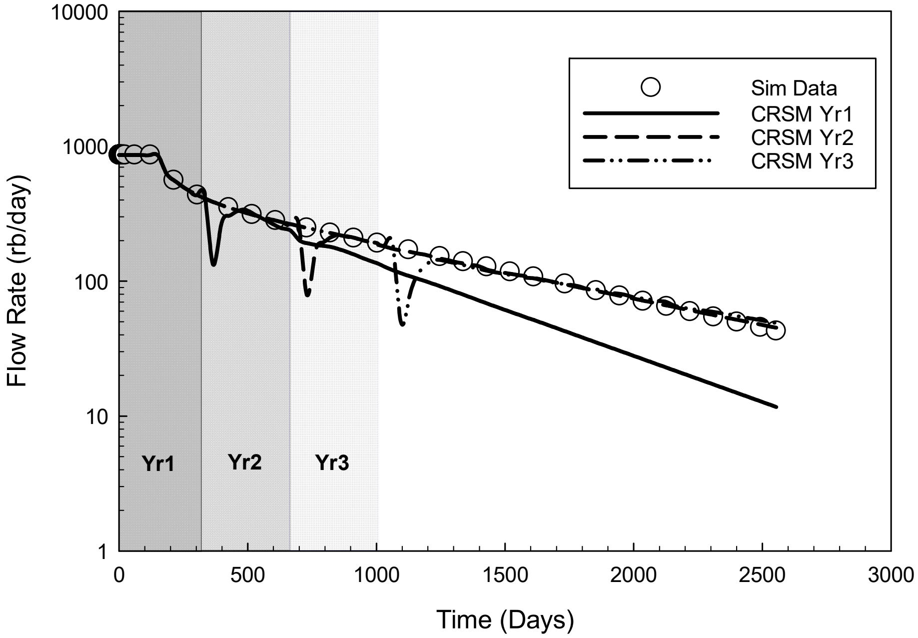

Figure 4 - 8: Flow rate prediction using the CRSM for the base case of $k_m = 1$ md. The CRSM used one, two- and three-year historical data utilizing Eq. B-(9).

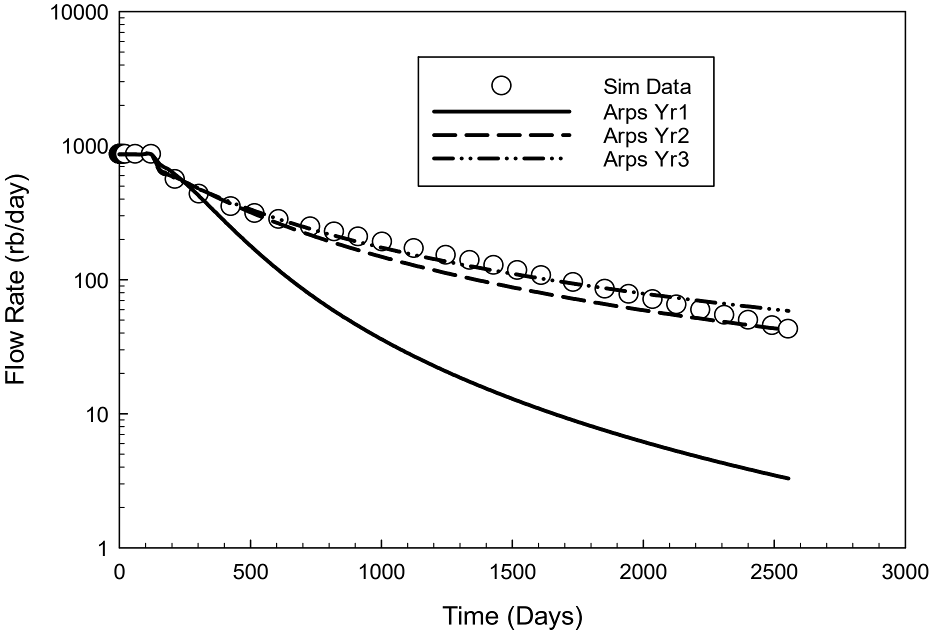

Figure 4 - 9: Flow rate prediction using the Arps' model Eq. (2-4) for the base case of $k_m = 1$ md. The Arps' model used one, two- and three-year historical data to determine the Arps' parameters using numerical regression.

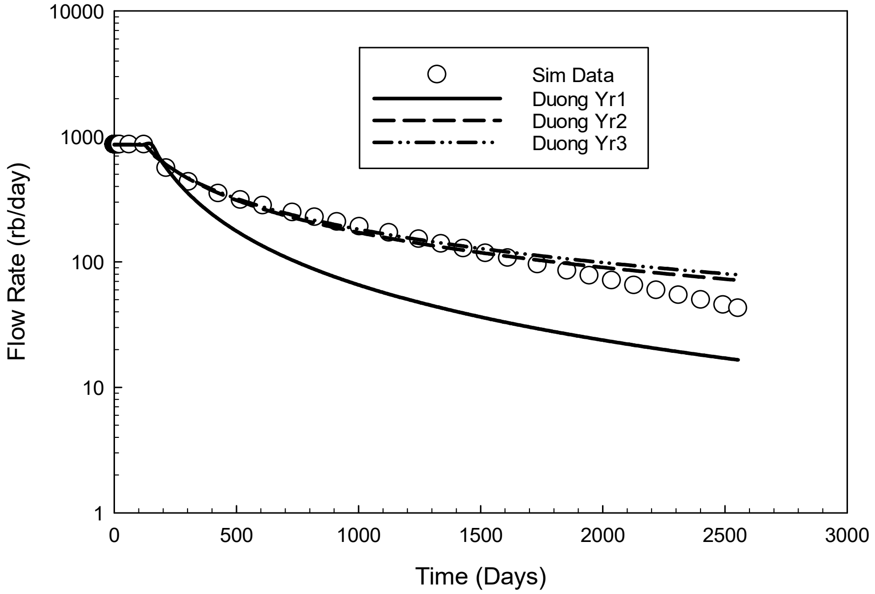

Figure 4 - 10: Flow rate prediction using the Duong's model for the base case of k_m = 1 md. The Duong's model Eq. (2-11) used one, two- and three-year historical data to determine the Duong's model parameters using numerical regression.

Using the same procedural steps as in the base case, the sensitivity cases of matrix permeability of 0.1 md and 0.01 md are conducted and the results compared to that of Arps' and Duong empirical models are shown in figures (4 - 11) - (4 - 16).

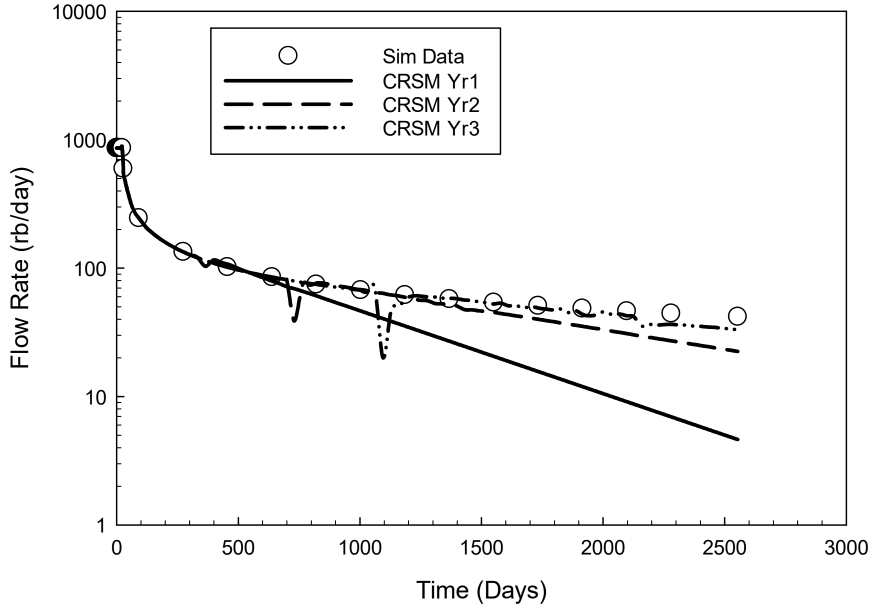

Figure 4 - 11: Flow rate prediction using the CRSM for the sensitivity case of k_m = 0.1 md. The CRSM used one, two- and three-year historical data utilizing Eq. B-(9).

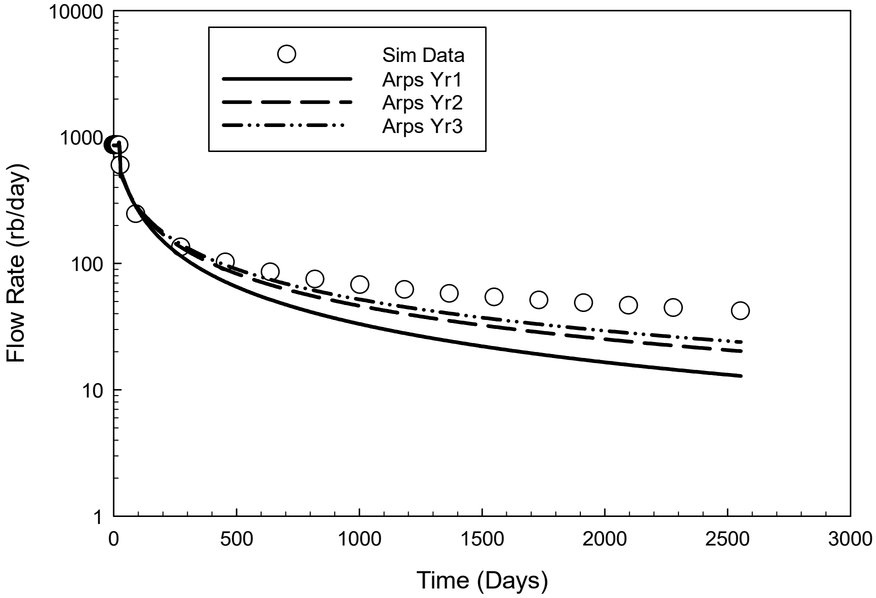

Figure 4 - 12: Flow rate prediction using the Arps' model Eq. (2-4) for the sensitivity case of k_m = 0.1 md. The Arps' model used one, two- and three-year historical data to determine the Arps' parameters using numerical regression.

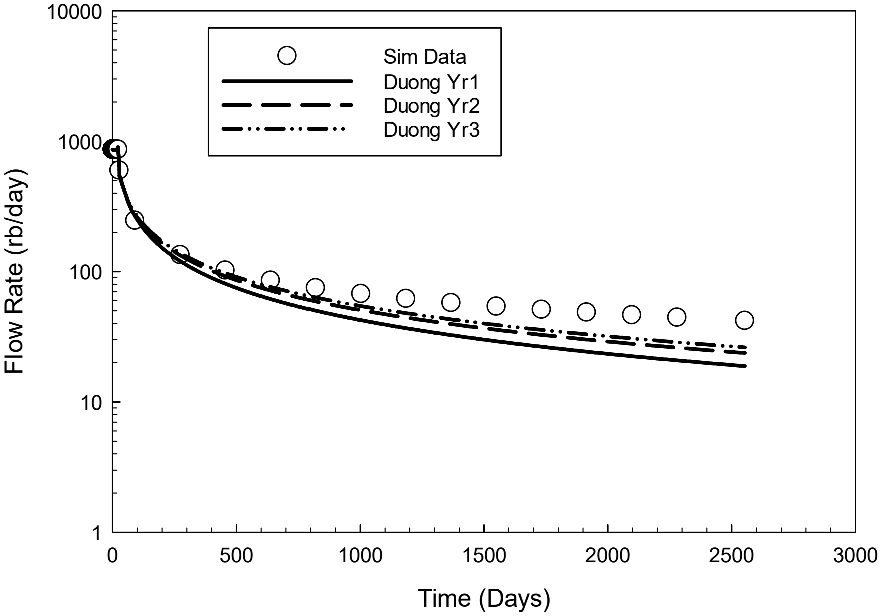

Figure 4 - 13: Flow rate prediction using the Duong's model for the sensitivity case of k_m = 0.1 md. The Duong's model Eq. B-(9) used one, two- and three-year historical data to determine the Duong's model parameters using numerical regression.

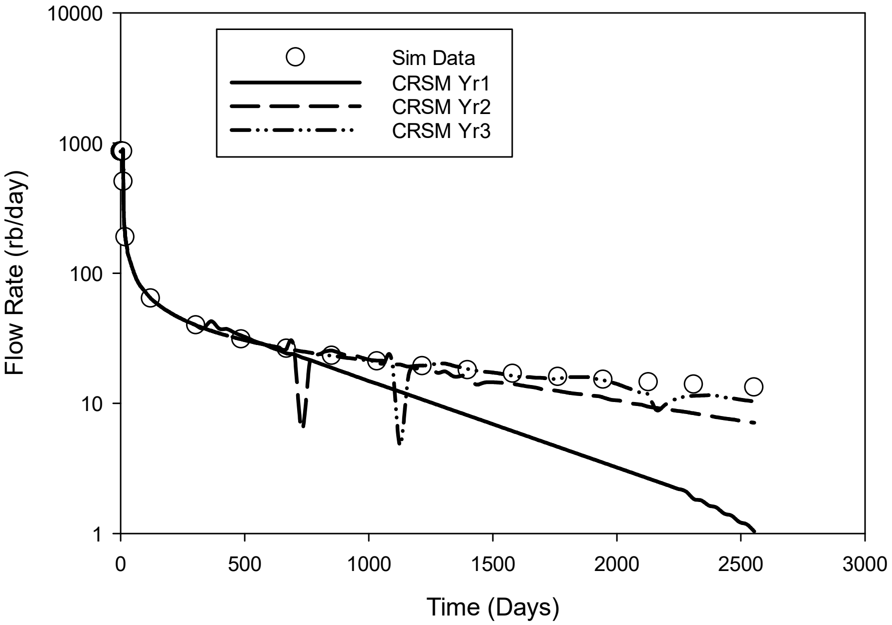

Figure 4 - 14: Flow rate prediction using the CRSM model for the sensitivity case of k_m = 0.01 md. The Duong's model Eq. B-(9) used one, two- and three-year historical data to determine the Duong's model parameters using numerical regression.

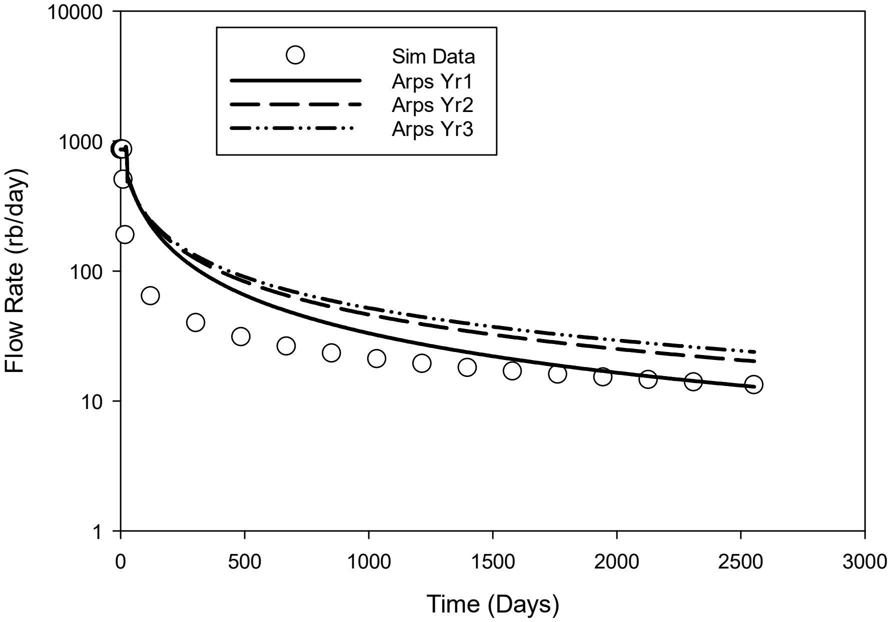

Figure 4 - 15: Flow rate prediction using the Arps' model Eq. (2-4) for the sensitivity case of k_m = 0.01 md. The Arps' model used one, two- and three-year historical data to determine the Arps' parameters using numerical regression.

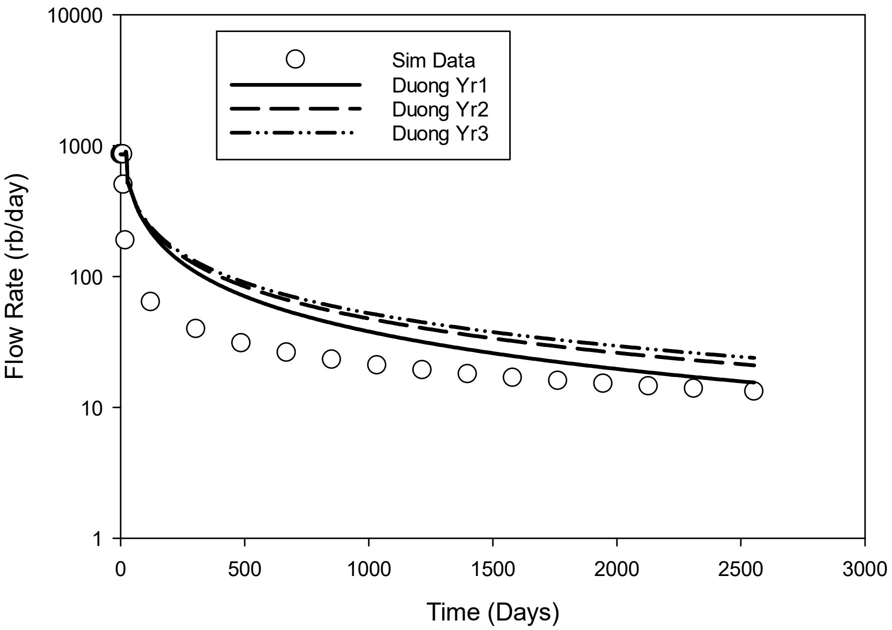

Figure 4 - 16: Flow rate prediction using the Duong's model for the sensitivity case of k_m = 0.01 md. The Duong's model Eq. (2-11) used one, two- and three-year historical data to determine the Duong's model parameters using numerical regression.

4.3 Discussion of the results:

Table (4-3) shows the tabulated data between Arps and Duong models for the sensitivity case studies. As one should expect, using numerical regression to fit the historical results will lead to different empirical coefficients depending on how much historical data is available.

Table 4 - 3: Tabulated parameters found for the Arps and Duong model's sensitivity case studies. The constraints for the Arps model are with the Arps' exponent such that: $b = 0$ for exponential decline, $0 < b < 1$ for hyperbolic decline and $b = 1$ for harmonic decline. The constraints for Duong Model are with the Duong intercept "a" and Duong slope "m" with constraints of $0 < a \le 2$ and $1 \le m \le 2$, respectively.

Model Parameters Summary		Arps Parameters			Duong Parameters		
Model Data	**Matrix Per, (md)**	**qi (rb/Day)**	**Di (1/Day)**	**b**	**qi (rb/Day)**	**a (1/Day)**	**m**
Year 1	0.1	862.5	2.32E-02	0.97	862.5	1.82	1.17
Year 1	0.01	862.5	2.32E-02	0.97	862.5	1.59	1.24
Year 2	0.1	862.5	2.12E-02	1.09	862.5	1.70	1.15
Year 2	0.01	862.5	2.12E-02	1.09	862.5	1.46	1.20
Year 3	0.1	862.5	2.07E-02	1.15	862.5	1.65	1.14
Year 3	0.01	862.5	2.07E-02	1.15	862.5	1.4	1.19

This study has compared the production forecast performance between Duong's model and Arps' hyperbolic decline methods and CRSM by using production histories of one, two and three-years from reservoir simulation results. Moreover, there are limiting boundaries for each of the coefficients such that the variables like the Arps' exponent "b" being greater than unity. The original work by Arps did not allow for the Arps' exponent to be greater than unity; however, there has been many tight reservoirs that have exhibited Arps' exponent's that are greater than unity to best fit the historical data. Moreover, if the Arps' exponent is greater than unity, the predicted cumulative productions could be unbounded for tight reservoirs in the transient flow regime (Valkó and Lee, 2010). It should be noted that the governing assumptions regarding the Arps' hyperbolic model were constant BHFP, constant drainage area, constant skin factor and constant boundary dominated flow or PSS. None of these assumptions are realistic or true in the production life of tight reservoirs. The Duong model is more applicable in tight reservoirs; however, it also has limitations when finding the empirical coefficients that govern the Duong model. Illustrated in the table (4-3), the Duong coefficients are shown for both Duong slope, "m", and Duong intercept, "a"; however, both coefficients are bounded by constraints outlined in tables (4-2) and (4-3) captions. Using unconstrained numerical regression for these parameters to best fit the historical data, the Duong parameters are satisfied for different periods except for the Duong intercept parameter for each time series of matrix permeabilities of 1 md, base case study. For this study, the constraints were left unbounded to illustrate the advantages of CRSM in lieu of empirical models, which does not require any parameters to undergo curve fitting optimization, or tuning, as in empirical methods.

Starting with the base case of matrix permeabilities of 1 md, figures (4 - 10), (4 - 11) and (4 - 12), the results show at one-year historical best-fit regressions of Arps' and Duong underestimate performance; however, comparing their performance at two and three year historical best fit analysis, shows a much better improvement comparing the model to the simulation data; however, both models still under-predict performance. The CRSM predicts production performance slightly better than both Arps' and Duong models at year one historical data. Moreover, it should be noted that there is a numerical error that is occurring at the very first-time step of the superpositions algorithm within the CRSM. This error is due to errors within the numerical simulation as well as numerical errors in the computations of Eq. (3-7) and Eq. (3-8). As the superposition moves forward with every time step this error is summed out resulting in a good fit of the CRSM, physical model, to that of the simulation data. Also, note that the accuracy of the CRSM improves, like Arps' and Duong models, based on the amount of historical production data that is used or is available. When comparing the overall error between the simulation data and the CRSM, Arps' and Duong models, the CRSM predicts slightly better than both the Arps' and Duong models. The error analysis used to compare all models was the Mean Relative Error (MRE), Eq. (4-1), between simulation production data to the CRSM, Arps and Duong forecasting models and is illustrated with a bar chart, figure (4 - 17).

$$MRE = \frac{1}{n}\sum_{i=1}^{n}\left|\frac{q_H - q_P}{q_H}\right| \tag{4-1}$$

Moreover, evaluating the sensitivity cases of 0.1 md and 0.01 md, as the matrix permeabilities decrease, figure (4 - 11) – (4 - 16), the empirical models, Arps and Duong, still underestimate performance in the early stage of well life; however, improve overall performance, later in well life when best fitting the data through numerical regression. Comparing both Arps' and Duong models to the CRSM, the CRSM estimates production performance slightly better than both Arps and Duong for the historical time steps, except for year one prediction beyond 1500 days. As previously stated, the prediction performance improves the more historical production data that is available and the CRSM estimates historical production better than both Arps' and Duong models when evaluating both two- and three-year historical production history. Figure (4 - 11) – (4 - 16) shows that for a matrix permeability of 0.01 md both Arps' and Duong models over predict performance, whereas, the CRSM provides a better overall estimate for year one, two- and three-year historical projections especially in the early stages of well life where transient flow is observed.

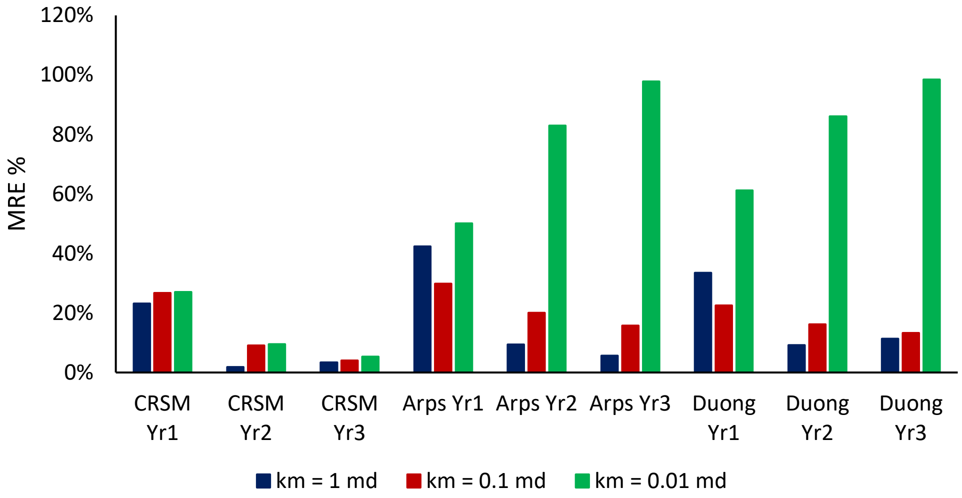

Figure 4 - 17: Error Analysis between Prediction Models. Comparing the average percent error found between the simulated data to that of the prediction model for one, two- and three-year historical production trends using the MRE calculation Eq. (4-1).

4.4 Summary and Conclusion:

This study has demonstrated the application of the CRSM using a numerical simulation of a tight oil reservoir with a bi-wing hydraulically fractured reservoir with low permeable matrix. The CRSM was developed utilizing the BHFP and production rate. Several major advantages of using the CRSM over curve fitting based models include:

(1) CRSM is physics-based with a rigorous mathematical foundation without the knowledge of reservoir geometry or properties.

(2) CRSM can be used in scenarios with variable production operations which is more realistic than the assumption of constant flowing bottom hole pressure used in classical empirical models.

(3) CRSM can be used to bypass the ambiguous results found when using empirical models when encountering multiphase flow phenomena experienced during well life.

One limitation of the CRSM is that the deconvolution of the normalized cumulative production and normalized production rate history can induce noise in the CRSM prediction. Therefore, when determining the unit pressure response, data smoothing may be required when dealing with matrix permeabilities of micro and nano-Darcy scale.

Chapter 5: CRSM Applied to Shale Gas Well Performance

This study uses the operational history of a shale gas well to demonstrate the CRSM's capability in rate prediction under variable operating conditions with uncertainties. This chapter will also feature the CRSM's applicability in well diagnostics to aide in the understanding of production performance via triangular distribution with Monte Carlo simulations.

5.1 Brief discussion regarding flow regimes of a shale gas reservoirs:

Before applying the CRSM to shale gas production performance it is important to discuss the various flow regimes that comprise a shale gas well. Figure (5-1) will be used to describe the flow phenomena during the production life of a shale gas well. After the hydraulic fracture stimulation treatment, and the commissioning of a shale gas well, the first flow regime that will occur will be fracture linear flow illustrated by point A of figure (5-1). At this stage, fluid flowback will take place in the hydraulically induced fractures and the fracture linear flow regime may not be visible at early times due to wellbore storage effects. The next flow regime that will be encountered is the bilinear flow regime illustrated by point B on figure (5-1). The bilinear flow regime is characterized by fluid flowing through the hydraulic fracture and the natural fractures in the formation. After bilinear flow, formation linear flow regime will appear point C on figure (5-1), which is demonstrated by fluids being produced from the stimulated reservoir volume (SRV). Point D on figure (5-1) is the transition from the linear flow periods in the early stages of production to radial flow regimes at later stages of well life, which exhibits an elliptical flow regime. The last phase encountered in the production life of a shale gas well is the pseudo radial flow, point E of figure (5-1), and at this stage, all boundaries have been reached and the reservoir is producing primarily from the formation matrix.

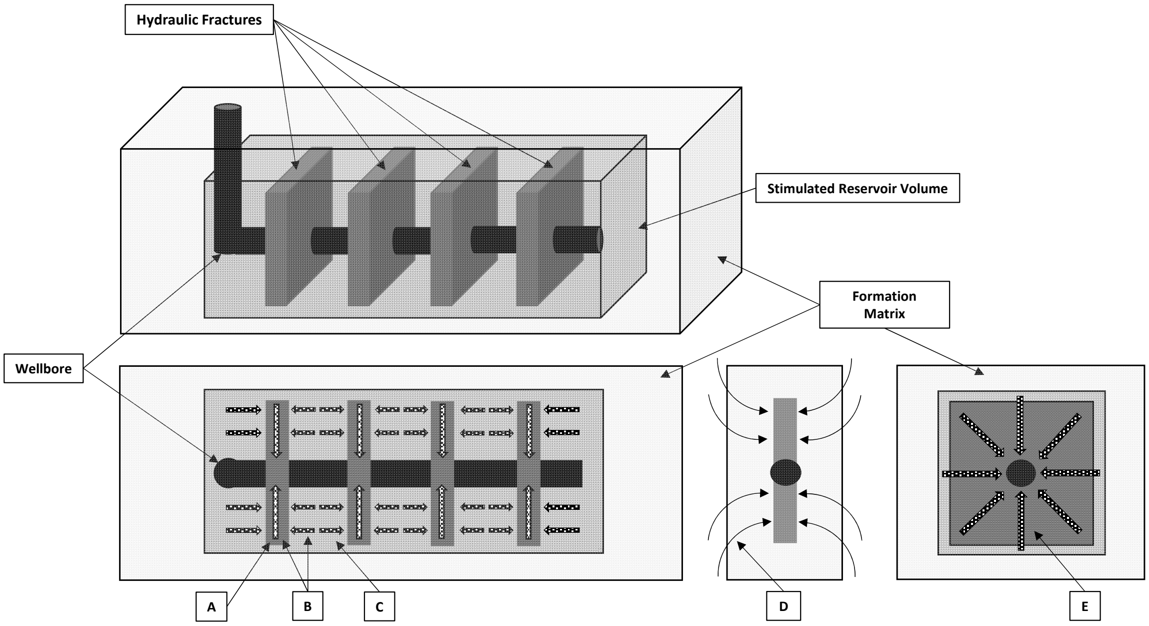

Figure 5 - 1: Schematic representing the flow regime phenomena encountered during shale gas production. Point A represents fracture linear flow, point B represents bilinear flow, point C represents formation linear flow, point D represents the transition from linear to a radial flow regime, and point E represents pseudo-radial flow.

5.2 Applying the CRSM to Shale Production Well Field Example:

The well selected for this case study is a hydraulically fractured shale gas well located in Chongqing, China, and will be referred throughout this study as well A. The shale play is intermediated between the middle-upper Longmaxi formation and the overlain upper Ordovician tight limestone with a thickness of 38-45 meters (125 – 148 ft) organic-rich section with a maturity range 2.2-3.0% Ro (Guo, 2015). The original reservoir pressure was about 5400 psi, and reservoir temperature was 206°F. The shale gas has more than 98% methane with a specific gravity of 0.61. The original pressure gradient is approximately 0.67 psi/ft. A typical wellbore structure of well A is provided below in figure (5-2). For the shale gas well, the tubing head pressure was recorded daily, and this pressure was converted to bottomhole pressure at the end of the tubing string to reduce pressure noise induced from wellbore uplifting performance. The daily production data of the shale gas well was recorded and plotted together with the converted downhole pressure as shown in figure (5-3). From the production data, figure (5-4), one can see the rate variations are caused by pressure depletion and well intervention over production life.

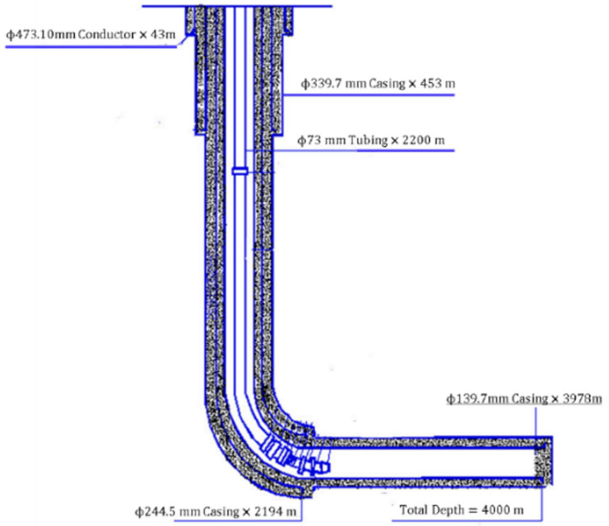

Figure 5 - 2: Wellbore diagram for the horizontal well A, illustrating the tubing and open hole section of the gas well. This well has been fractured with multiple stages along the horizontal segment, and is located in Chongqing, China.

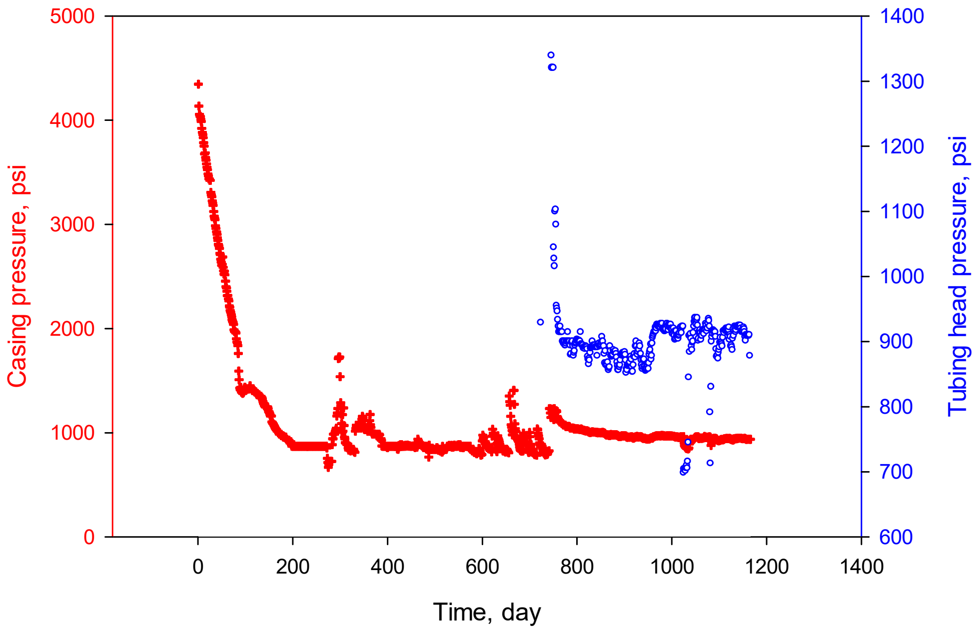

Figure 5 - 3: Casing and tubing head pressure after well A was put on production. This chart illustrates the bottomhole flowing pressure and the tubing head pressure over time.

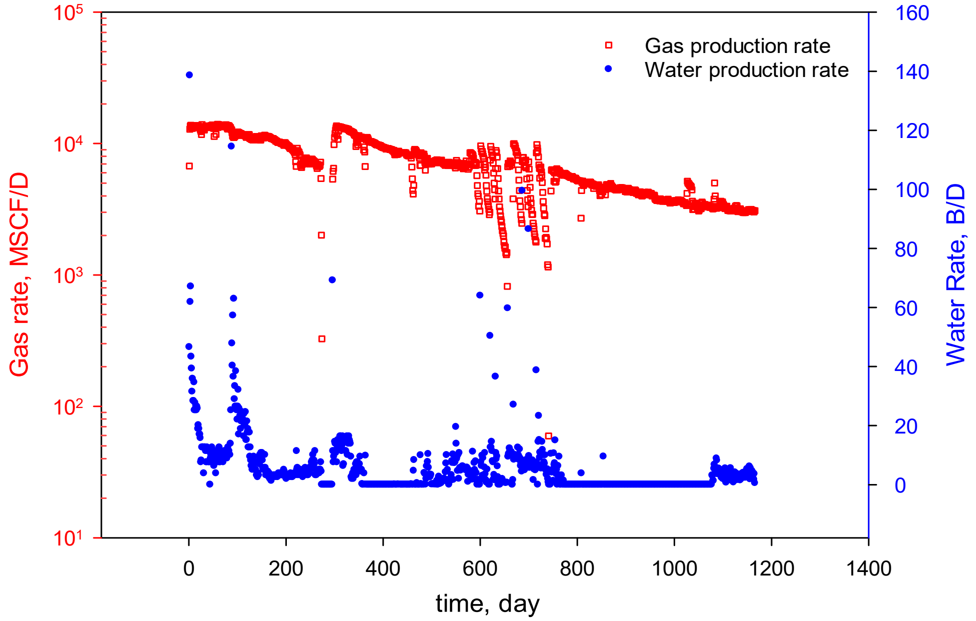

Figure 5 - 4: Gas and Water production rate after well A was put online. This chart illustrates the gas and water production at standard conditions over time.

The CRSM was applied to well A and only the first 200 days of the historical production data were used to forecast its performance to an economic limit of 10 Mscf/d, which will be used in predicting the EUR. A true EUR is predicated on many economic factors such as commodity price, severance, and taxes. During the life of well A there are several instances where the well experienced interruptible service during production operations, start-up, and shut-in periods, which caused some instances of flush production at various times when well A was brought back online. The purpose of this study is to demonstrate the gas production prediction potential of the CRSM and the beforementioned factors that go into determining EUR can be added to any future prediction analysis. The 200 days illustrated in figure (5-5) are represented by the red data set and will be used to generate the unit pressure response for three linear relationships for the approximations of gas production performance. The three linear projections will be used to develop a triangular distribution using Monte Carlo approximation to determine the best probable outcome based on the three linear projection assumptions, which will lead to a fourth linear projection of the unit pressure response. Figure (5-10) displays the four linear projection models on the unit pressure response curve. A step-by-step implementation is demonstrated using well A.

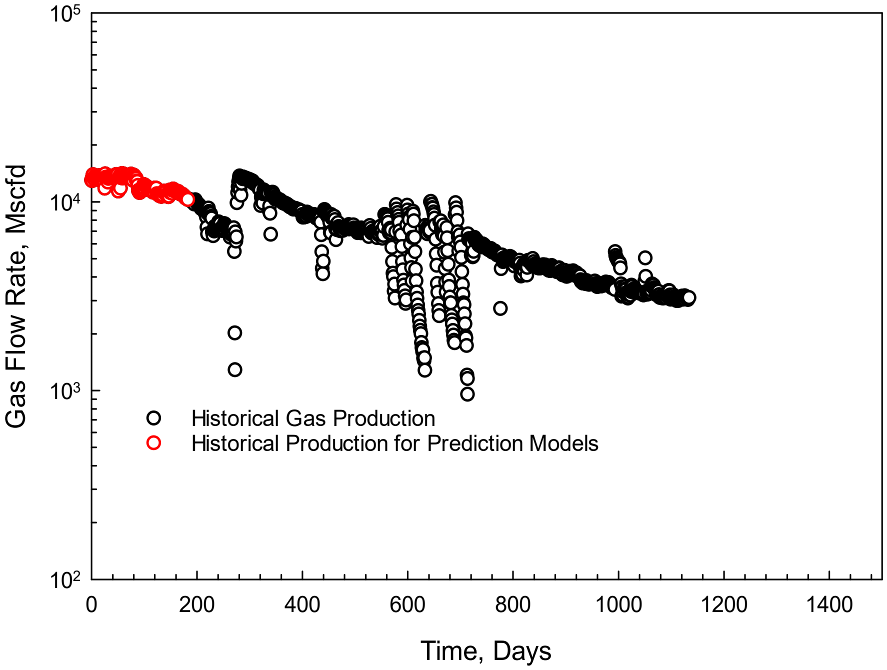

Figure 5 - 5: Semi-log plot of the gas production rate history of well A. The black data points are the production history corresponding to approximately three years of historical production for well A. The red data points will be used in the CRSM gas production prediction models.

The first step is to covert the well head pressure to the bottom-hole flowing pressures from figures (5-3) and (5-4). Using the historical production of well A, both the normalized production rate and normalized cumulative production for gas can be computed, Eq. (3-10) and Eq. (3-11) and is shown in figure (5-6). The flush production was omitted from the NDC analysis as it does not represent the actual decline of the well during production. It should be noted that during the early life of shale gas production the rate of decrease on the NDC is caused by fracturing fluid flow back and the gas rate data must be omitted from the analysis. After data cleaning the production data from well A is shown on the NDC figure (5-7). The connected reservoir storage curve (CRS) can also be used to illustrate the transitions of the transient regime to that of the PSS regime, figure (5-8). The red points in figure (5-8) represents the filtered data from the NDC and the black data points are the actual CRS values over the entire three-year history of well A. Note that for the gas production forecast prediction models, the CRS assumes that PSS flow has been reached at the end of 200 days. This assumption allows for the projection of the unit pressure response linearly overtime. The filtered NDC data is represented by the red data points of figure (5-7). Once both the NDC and CRS curves have been determined the unit pressure response will be determined by deconvolution, see figure (5-9). The unit pressure response forms the basis such that the CRSM can be implemented. Moreover, due to the computational nature of the normalized equation computations presented early as well as the deconvolution being ill-posed (Kuchuk et al., 2010b), there can be noise in the data that may require some data smoothing to reduce the amount of noise seen in the unit pressure response when applying the CRSM algorithm for production forecasting predictions illustrated in appendix (A). Therefore, figure (5-9) shows three important aspects regarding the information associated with well A. First the red data, is the historical data that will be used for linear projections of the unit pressure response. Second, the green data set represents the bottom-hole flowing pressure of well A to help further illustrate the transient and PSS regimes. The black data set is the unit pressure response of the filtered data set over the three years of historical production, figure (5-9).

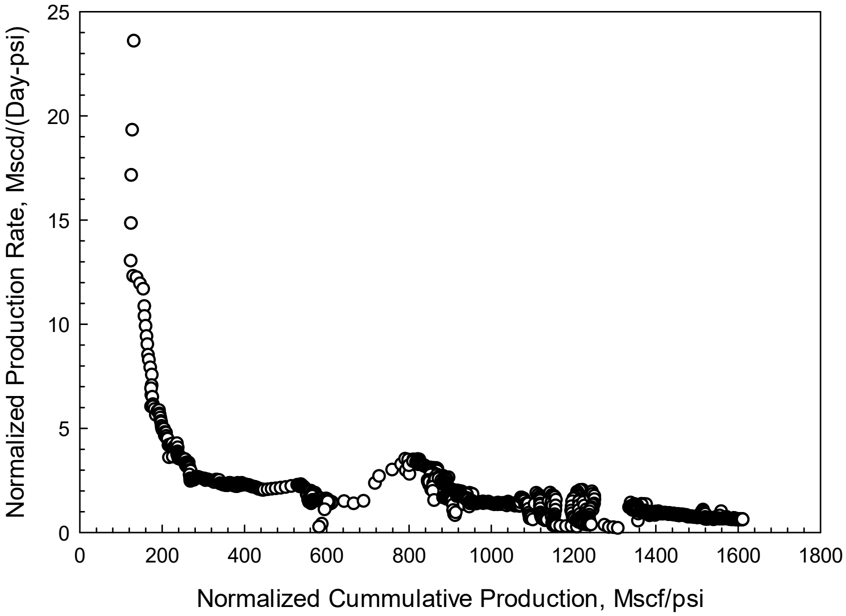

Figure 5 - 6: Normalized Decline Curve of well A. The abscissa axis is the normalized cumulative production, and the ordinate axis is the normalized rate production. The NDC is shown over the entire historical production of well A and will need to be filtered to utilize the NDC for the CRSM analysis.

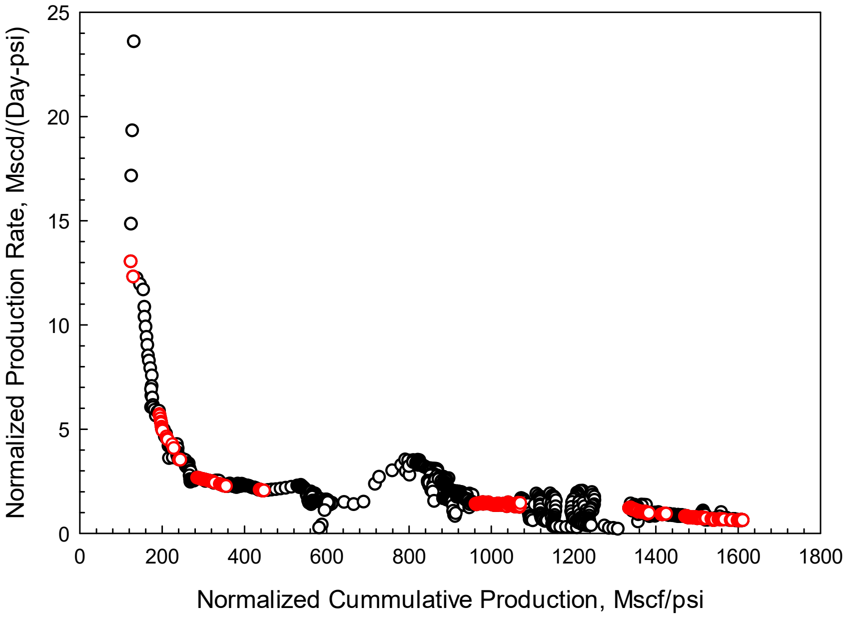

Figure 5 - 7: Filtered Normalized Decline Curve of well A. The red data points have been superimposed onto figure (5 - 6) indicating the data set that will be used to employ the CRSM analysis to well A for the first 200 days of production.

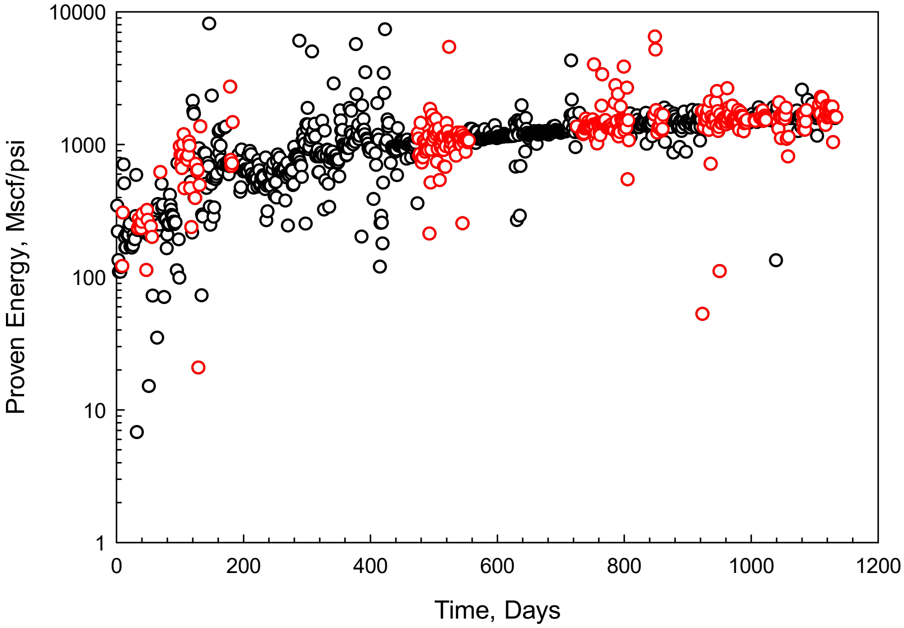

Figure 5 - 8: Connected Reservoir Storage (CRS) curve also known as the proven energy of the reservoir. This curve demonstrates the amount of energy at any given time in the reservoir's life. As the well is initiated for production the energy of the reservoir will increase at a decreasing rate until the transition from transient flow regime to pseudo-steady state (PSS) flow regime has been reached, which will run parallel to the abscissa axis.

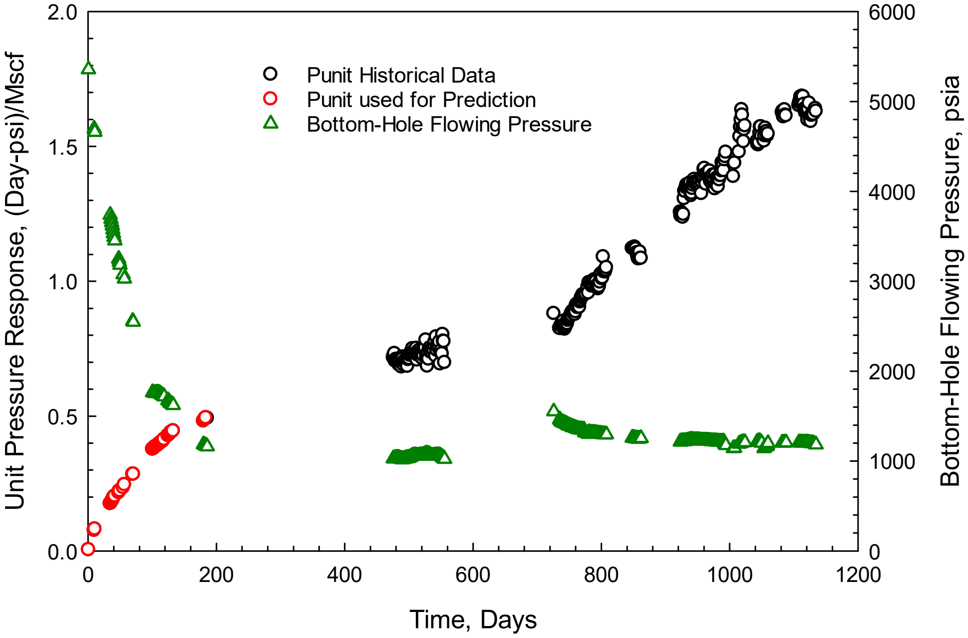

Figure 5 - 9: The unit pressure response curve shows the change in pressure drop for one unit of gas production (1 Mscf/d). The unit pressure response curve can be used for well behavior diagnostics. The unit pressure response prediction models were developed using 200 days of well A data illustrated by the red data points. The bottom-hole flowing pressure is shown on the secondary axis to illustrate the transient and PSS transitions.

Some important observations regarding the unit pressure response curve, figure (5-9). Using deconvolution to determine the unit pressure response, the filtered data set shows some interesting trends. First, if the unit pressure response is parallel to the ordinate axis, it indicates the well is in steady-state, which is usually not the case for shale reservoirs. The unit pressure response will increase linearly once PSS has either been assumed, for forecast prediction purposes, or naturally based on reservoir physics. One key concept to take from figure (5-9) is that the red data set is all that is used for the prediction models, which is approximately 200 days. Furthermore, between 400 to 600 days of well life the unit pressure response appears to be increasing linearly; however, once 700 days of production has been reached it should be noted that the unit pressure response increases dramatically. This rapid increase in unit pressure response behavior can be due to multiple factors playing in tandem. For example, as the unit pressure response increases rapidly from 700 days to the 1200 days of historical production, this may be contributed by skin change taking place near fracture channels or the wellbore. Likewise, the net stress occurring in the formation is increasing relative to production, which would yield a decrease in fracture conductivity. Both the increase in the net stress and a decrease in fracture conductivity will lead to an increase in the unit pressure response behavior. Moreover, as water accumulation takes place in the wellbore, the gas production would subsequently decrease as the water droplets become entrained in the near-wellbore in two-phase flow regimes. Therefore, the gas production is inversely proportional to the unit pressure response and this will be illustrated in the prediction models.

The next step will be to use unit pressure response projections to determine shale gas production prediction models. Using the 400 to 700 days as a starting point, a linear projection will be placed above the historical data of 400 to 700 days, blue line illustrated in figure (5-10).

Similarly, another linear projection will be placed below the 400 to 700 days of historical production, illustrated by the grey line figure (5-10). Lastly, the mean of the upper and lower projection will be illustrated by the dark green line of figure (5-10). The upper, lower and mean linear projections will be used with a triangular distribution to determine the Monte Carlo representation of both the slope and intercept of the unit pressure response linear projection of the most probable outcome for the unit pressure response projection, which is illustrated by the red line of figure (5-10). Figures (5-11) and (5-12) represent the Monte Carlo simulation to determine the most probable slope and intercept from the slope and intercepts of the upper, lower and mean linear unit pressure response projections. From figure (5-11) and (5-12) convergence for both the slope and intercept appear to occur at approximately 800 iterations in both cases; however, over 1500 iterations were used to minimize any deviations in the random variables that are used in determining the most probable outcome of the slope and intercept of the unit pressure response.

Now that the unit pressure response has been determined for four cases, all cases will be used to develop the gas production forecast predictions to illustrate the power of using the CRSM. It should be noted that the CRSM can be viewed as a model that will update in real-time. Since this analysis uses only 200 days of historical production data for prediction purposes, the more data that becomes available, the CRSM will update in real-time providing for a better approximation of unit pressure response behavior, which lends itself to easy implementation as it does not require any variables to be tuned as in empirical models that use nonlinear regression methods.

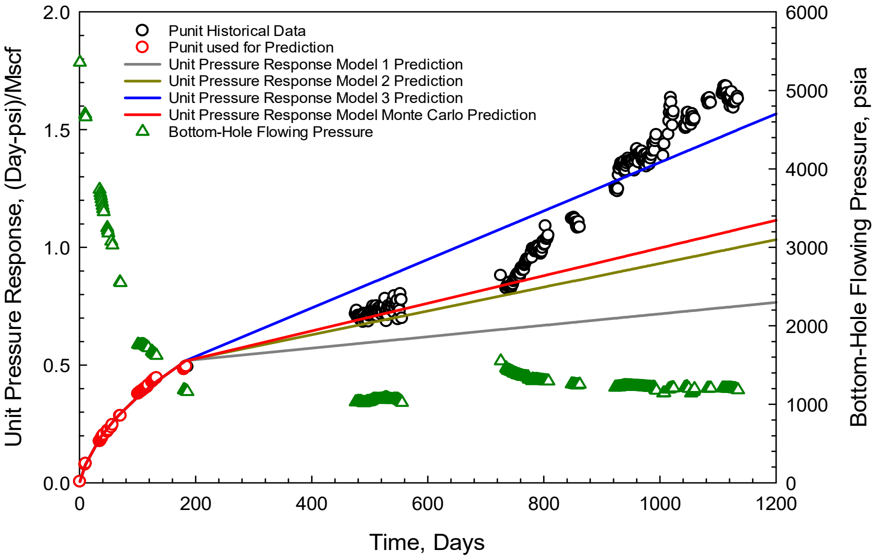

Figure 5 - 10: Unit pressure response from the filtered NDC of well A. The red data was used for shale gas forecast projections. Each unit pressure response projection was projected at the end of 200 days of the historical data of well A. The black data points are the unit pressure response determined over the filtered NDC data set up to the current history of the production of well A. The green triangular data set represents the calculated bottom-hole flowing pressure represented by the secondary axis, which demonstrates the early transient regime and transition to PSS regime.

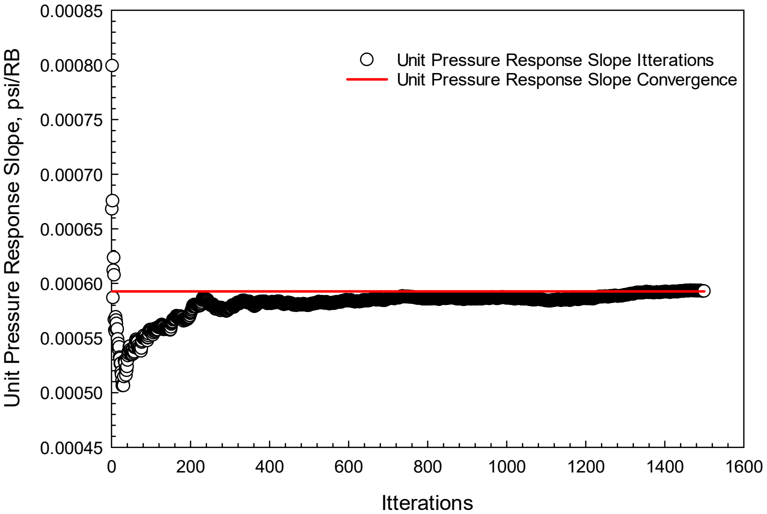

Figure 5 - 11: The slope of the unit pressure response projections of the upper, lower, and mean linear projections. Monte Carlo simulations were conducted for 1500 iterations until convergence has been reached on the most plausible outcome to represent the slope of the linear unit pressure response projections.

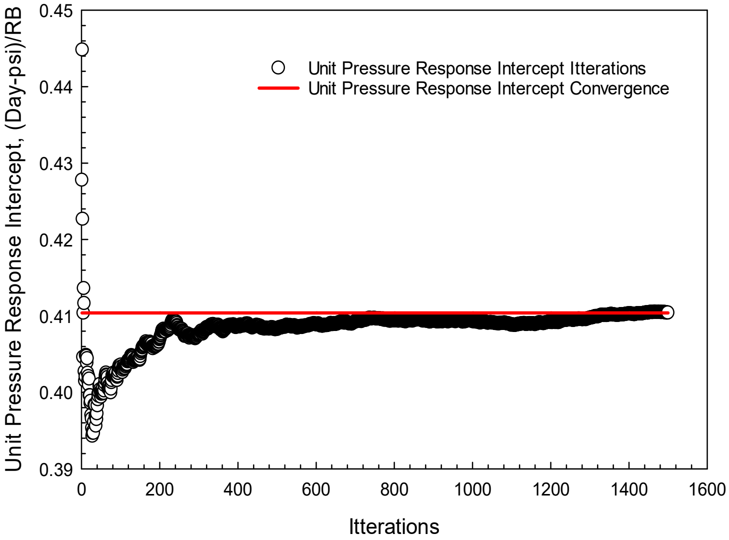

Figure 5 - 12: The intercept of the unit pressure response projections of the upper, lower, and mean linear projections. Monte Carlo simulations were conducted for 1500 iterations until convergence has been reached on the most plausible outcome to represent the intercept of the linear unit pressure response projections.

5.3 Shale Gas Production Performance CRSM Predictions:

The next phase of the CRSM analysis will be to predict gas production performance using the results found in figures (5-6) - (5-12) for gas production projections, and using rate prediction model based on the unit pressure response and superposition Eq. B-(9). The four-unit pressure response projections were conducted using only 200 days of historical data. With the assumption that all unit pressure responses have reached PSS and utilizing the various slopes and intercepts of the unit pressure response, the gas production performance can be approximated for each of the four case studies, figure (5-13).

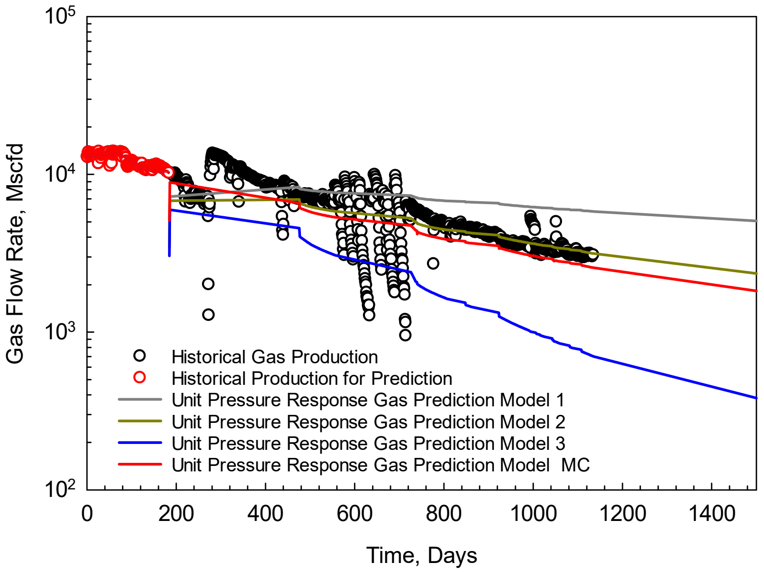

Figure 5 - 13: Shale gas production predictions for well A. The blue line represents the unit pressure response resulting in the upper limit approximation of well performance, due to the skin factor and liquid loading, which results in an under prediction of production to historical data. The grey line represents the lower limit of the unit pressure response analysis and results in an overestimate of historical data. The red and green prediction models represent the mean and Monte Carlo predictions and yield a more approximate performance prediction to historical data.

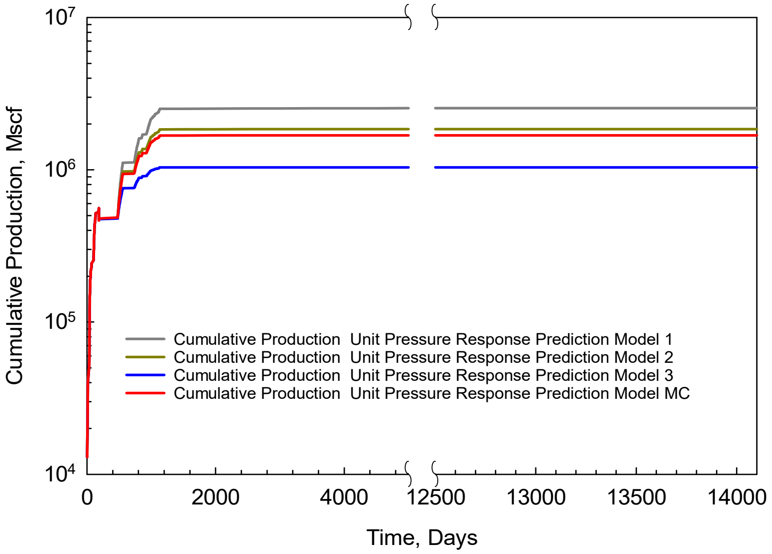

Figure 5 - 14: Cumulative production predictions for all four case studies. As should be expected the unit pressure response associated with the blue line is the upper limit of the unit pressure response from figure (5 - 10) and yields a lower EUR. The grey line represents the lower limit of the unit pressure response and will yield the most conservative EUR. The green and the grey line represents the mean and the Monte Carlo prediction and yield the average and the most probable outcome for EUR, respectively.

The first gas production projection was for the minimum assumed slope and intercept of the unit pressure response curve, grey line, which shows that for lower assumed unit pressure response would correlate to an overestimate of gas production performance. The production trend from the minimum assumed slope and intercept of the unit pressure response correlates with a relatively low skin effect that would allow for greater production flow from the shale gas reservoir. The next gas production projection uses the maximum assumed slope and intercept of the unit pressure response, blue line, which shows that if the unit pressure response prediction is relatively high there will be an inverse relationship with production rate or underestimate shale gas production due to the increase in the skin factor as well as other contributing factors that would impede gas production, such as liquid loading in the wellbore. The mean unit pressure response, green curve, was used as an arithmetic average between the maximum and minimum slope and intercept values found for the unit pressure response predictions. Using the mean unit pressure response yields a good approximation to the actual shale gas production projections. Furthermore, using both the maximum, minimum and mean unit pressure response slope’s and intercept’s a triangular distribution with Monte Carlo simulation was done to generate multiple realizations of shale gas production prediction based on the assumed maximum and minimum values of the parameters of the unit pressure response. The red line, displayed in figure (5-13), shows that there is a slight under-prediction of the historical shale gas production performance. The results of the shale gas prediction performance between the four-prediction models and the historical shale gas performance are displayed in the table (5 - 1). The Mean Relative Error (MRE) was used to compare errors between each model prediction and is also shown in table (5 - 1). Furthermore, using the four prediction models, the estimated ultimate recoveries (EUR) of each prediction model were also determined to an economic limit of 10 Mscf/d. The result of the EUR is displayed in figure (5-14) for each of the four shale gas prediction models. As previously stated, the EUR for this analysis does not incorporate any economic metrics and is purely a volumetric number only. The results of the EUR's for all four prediction models are also given in table (5-1).

Table 5 - 1: Comparative analysis between all four prediction models relative to actual historical data by comparing the EUR of the historical data to the model prediction of 1200 days. Further EUR's are shown for each of the prediction models to and economic limit of 10 Mscfd. Please note that the EUR computation is a purely driven volumetric number that does not incorporate any economic metrics. MRE, Eq (4-1) is also documented showing the error between actual historical data and prediction models.

Models	Estimated Ultimate Recovery (Mscf)	Mean Relative Error
Unit pressure response gas prediction model 1	2,540,913	44.8%
Unit pressure response gas prediction model 2	1,848,378	10.8%
Unit pressure response gas prediction model 3	1,038,368	58.4%
Unit pressure response gas prediction model MC	1,685,005	18.4%

Moreover, one important factor when utilizing the CRSM is that the model will self-update as new data become available, which lends itself to a very robust prediction performance model. The more data that is available the more accurate the model will become as the CRSM was designed to be a physics-based model that incorporates reservoir physics and updates in real-time as more production data comes in. Assumptions regarding this model are how to predict unit pressure response performance. Furthermore, it should be noted that there is a numerical error that is occurring at the very first-time step of the superpositions algorithm within the CRSM, which is seen as a dip, very first iteration, in figure (5-13). This error is due to errors in the forward differentiation computations of Eq. (3-10) and Eq. (3-11). As the superposition moves forward with every time step this error is summed out resulting in a good fit of the CRSM, physical model, to that of the historical data.

5.4 Summary and Conclusions:

This chapter has demonstrated the capabilities of the CRSM for shale gas production forecasting predictions using the production history of a shale gas well. The CRSM was developed utilizing the BHFP and production rate. This chapter has demonstrated how to use CRSM to handle uncertainties of production scheme and changing well conditions such as increasing skin factor using stochastic methods. From this study the following conclusion can be drawn. (1) When CRSM is used in rate forecast of a shale gas well, it is very critical to analyze the production rate history. (2) Shale gas production rates are affected by multiple factors and its forecast has a large uncertainty. The shale gas well early history can be affected by flow back water production, and at the late time, the rate history can be affected by many mechanisms leading to increasing skin factor. The CRSM model reveals the dynamics of flow mechanisms through a deconvoluted unit pressure response. (3) The complex constraints of shale gas production render the long term rate forecast with large uncertainties and failures of curve-fitting based models. Coupled with stochastic analysis, CRSM can capture these constraints and make a reasonable range of production forecasts even with short production history.

Chapter 6: CRSM in Fracture Diagnostics of a Shale Gas Well

This chapter proposes the utilization of the CRSM in lieu of SRV for multiple stage fracture characterization. CRSM directly characterizes the stimulation performance, only utilizing actual production which is free of subsurface uncertainties and can be used efficiently in characterizing the flow regimes and reservoir boundaries. The CRSM allows for the estimation of the efficiency of a stimulation program through production decline and reservoir pressure response from production data and is strongly physics-based. A real field shale gas production case will be used.

6.1 Gas Well Field Example :

Using figure (5-2) to ascertain volumetric properties of the tubing and open-hole segments of well A in conjunction with the reservoir properties for well A are given in tables (6-1) and (6-2) at initial conditions respectively. Both tables (6-1) and (6-2) will be used for characterizing the hydraulic fracture treatment.

Table 6 - 1: Volumetric properties of the tubing and open-hole segments of well A.

From Fig (5 - 2)	Dia. (in)	Length (ft)	Volume (bbls)
Tubing dimensions	2.88	7218	58.2
Open-hole dimensions	5.50	5926	173.9

Table 6 - 2: Reservoir properties of well A at initial conditions.

Gas specific gravity, fraction	0.61
Bottom-hole temperature, F	206
Initial reservoir pressure (psi)	5,400
Gas viscosity, cP	0.025
Gas compressibility, dimensionless	1.068

The CRSM will be applied to the production history of well A to characterize the effectiveness of the fracture program through the deconvolved pressure derivative curve. Applying the CRSM procedure outlined in Appendix (C), a diagnostic analysis can show the production potential of well A during the transient and pseudo-steady state (PSS) flow regimes. The normalized decline curve (NDC) was generated using equations Eq. (3-10) and Eq. (3-11). During the life of well A there where several instances where the well experienced interruptible service during production operations, start-up, and shut-in periods, which caused some instances of flush production at various times when well A was brought back online. The flush production was omitted from the NDC analysis as it does not represent the actual decline of the well during production. Figure (6-1), which is an adaptation of figure (5 - 7), represents the NDC during well life. It should be noted that during the early life of shale production the rate of decrease on the NDC is very short lived and this represents the transient portion of the reservoir that will be used to quantify fracture stimulation effectiveness.

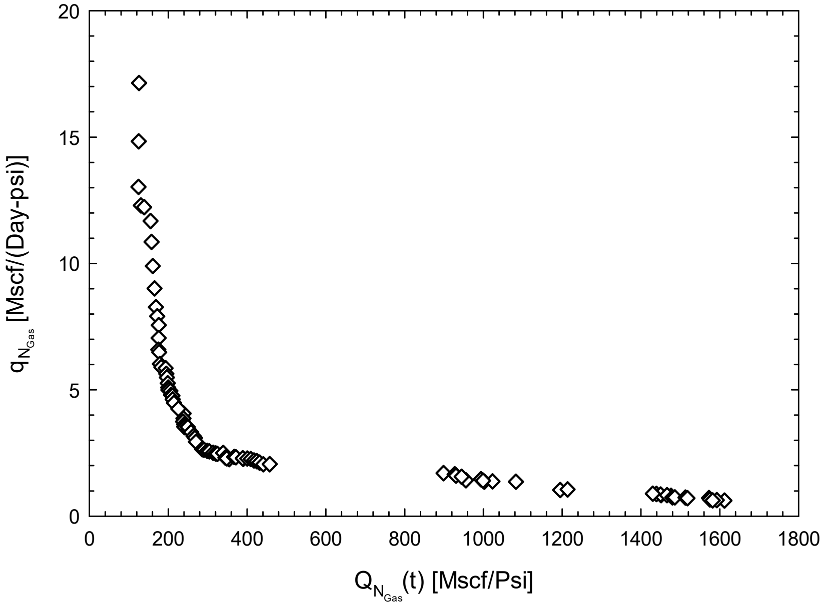

Figure 6 - 1: The normalized decline curve (NDC) of well A. This curve was generated using a filtered data set of the historical production.

Using deconvolution methods, the deconvolved dimensionless pressure and pressure derivative can be determined. The deconvolved dimensionless pressure derivative curve is used to predict the production rate for complex reservoirs and zonal rate allocations. The dimensionless pressure drop curve can be further used to monitor well productivity change and skin history. The dimensionless pressure derivative curve shows the boundary conditions and flow regimes in the reservoir Figure (6-2).

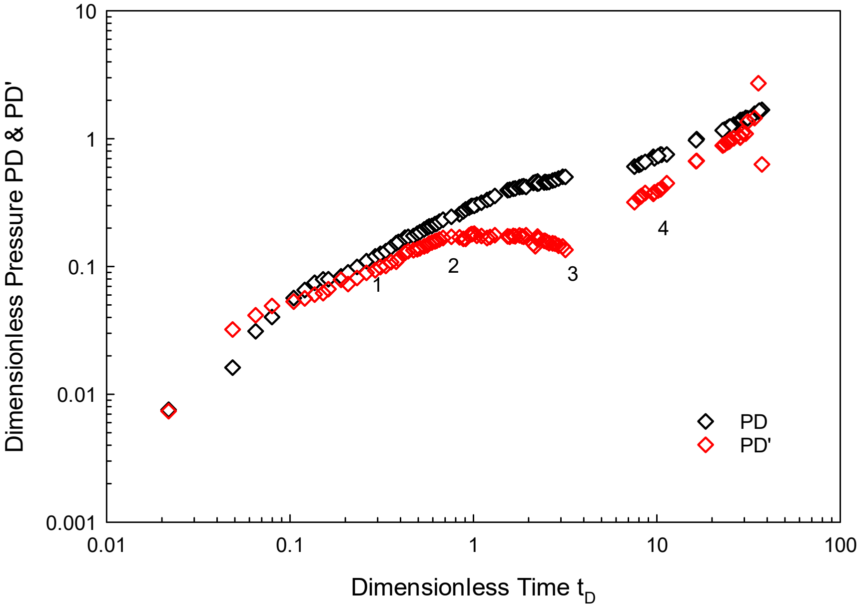

Figure 6 - 2: Deconvolved dimensionless pressure derivative curve of well A. The deconvolved dimensionless pressured derivative curve is derived from the unit pressure response from the deconvolution of the normalized decline curve model.

From figure (6-2), it can be seen that the deconvolved dimensionless pressure derivative shows characteristics of a flow regime as seen in dual-porosity systems with a transient matrix flow - a common phenomenon seen in shale gas reservoirs (Jahanbani and Aguilera, 2008). As illustrated in figure (6-2), the dual porosity phenomenon can be seen in the deconvolved dimensionless pressure derivative curve. Points 1 to 2, on the deconvolved dimensionless pressure derivative curve, gas flow is occurring only from the fractures in the reservoirs near the wellbore. Points 2 to 3, gas begins to produce from the matrix and gas begins to flow from the matrix into the natural fractures of the reservoir. During points 2 and 3 both the matrix storativity and interporosity parameters can be ascertained. The details in regards to the determination of both the matrix storativity and interporosity parameter from the deconvolved dimensionless pressure derivative curve have been discussed in detail by Horne (Horne, 1995). Points 3 to 4, the pressure in the matrix and the natural fractures will reach an equilibrium state. Although it is not seen in figure (6-2), the transition point beyond point 4 will experience various flow regime transitions until PSS is reached (Kim and Lee, 2015). Moreover, if figure (6-1) is utilized the CRS profile - the time at which PSS flow occurs - can be approximated and has been illustrated (Childers and Wu, 2017) and will not be repeated here. Using the early time information from figure (6-2). The dimensionless wellbore storage can be found on the deconvolved pressure derivative curve, figure (6-3) at any time along the unit slope, illustrated by the blue line on figure (6 - 3).

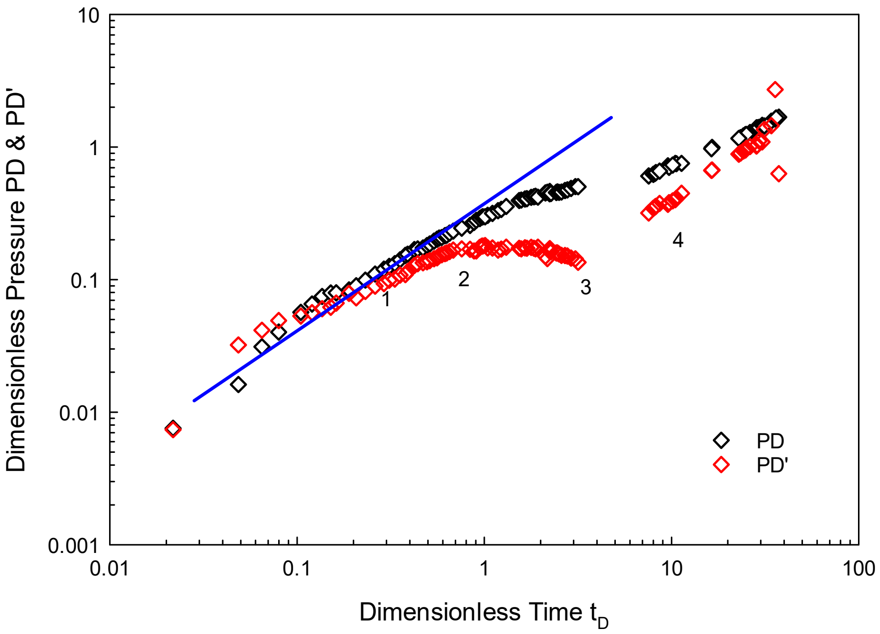

Figure 6 - 3: Deconvolved dimensionless pressure derivative curve of well A. Unit slope is illustrated by the blue line on the deconvolved dimensionless pressure derivative curve.

The dimensionless wellbore storage will be used to approximate the effective fracture treatment using the definition of wellbore storage given by Eq. (6-1) and Eq. (6-2) and the volume of the tubing and open-hole section of the wellbore outlined in table (6-1). From the definition of the wellbore storage for gas the approximate volume after treatment can be determined from Eq. (6-1).

$$C = c_{wb} V_{wb} \tag{6-1}$$

$$C = \frac{2.36 q_g T}{\mu_g} \left[\frac{t}{\Delta \delta} \right] \tag{6-2}$$

where Eq. (6-2) the wellbore storage is determined from normalized pseudopressure. By introducing the unit pressure response found from the deconvolved dimensionless pressure derivative curve figure (6-3); therefore, Eq. (6-2) can be rewritten as a function of the unit pressure response from Eq. A-(38) from appendix (A) and takes the form of Eq. (6-3).

$$C_{gas} = \frac{2.36 T}{\mu_g} \left[\frac{t}{P_{Unit}} \right] \tag{6-3}$$

The units of Eq. (6-3) are in cf/psi and the units of Eq. (6-1) are in bbls/psi. Using the dimensionless wellbore storage found from the unit slope of figure (6-3), the gas wellbore storage from Eq. (6-3) was found to be 328.8 cf/psi. Converting the units of Eq. (6-3) to bbls/psi the wellbore storage is 58.6 bbls/psi. Evaluating the gas compressibility at the initial tubing pressure, the volume of the wellbore from Eq.(6-3) was found to be 83,697 bbls with a gas compressibility 7.0×10^{-4} 1/psi. The tubing pressure was used due in part that pressure drawdown of the tubing pressure relative to the bottomhole flowing pressure is very small at the early stages of well life. Using the volume calculated from the tubing string and the open-hole section of the wellbore the stimulated fracture volume was found to be approximately 83,500 bbls, see tabulated results table (6-3) below. From this result one can see the effectiveness of the fracture treatment and if the geometry of the fracture is known one can estimate if the initial fracture design was successful based on the assumed fracture geometry and comparing the hydraulic stimulation design phase to actuals through the fracture volume.

Table 6 - 3: The approximated hydraulic fracture volume at the beginning of well life determined from the dimensionless pressure derivative curve and the unit pressure response of the wellbore storage Eq.(6-3)

Hydraulic Fracture Volume Approximation	
Wellbore storage, cf/psi	328.82
Wellbore storage, bbl/psi	58.56
Gas compressibility, 1/psi	7.00E-04
Wellbore volume, bbls	83,697.67
Volume of the tubing section, bbls	58.16
Volume of the open-hole section, bbls	173.86
Hydraulic fracture volume, bbls	83,465.66

Further analysis was done to compare model results from commercial well testing software. Using results found from commercial well testing software regarding the storativity and interporosity table (6-4), the CRSM predicted results similar to the commercial well test software. Figure (6-4) shows a comparison of the results of both the commercial well testing software and to that of the CRSM.

Table 6 - 4: Commercial Rate Transient Analysis Software used to determine duel porosity model parameters based on the historical production of well A at initial conditions.

From Commercial RTA Software			
Storativity	0.179	Skin	0.125
Interporosity	9.38E-10	kh, md-ft	2.17
Dimensionless radius of investigation	1,746		

Using the dual-porosity model parameters found in table (6-4), the dual porosity model was converted to dimensionless time and pressure and superimposed on the dimensionless pressure and time data found through the deconvolution of the normalized rate and cumulative production, figure (6-4).

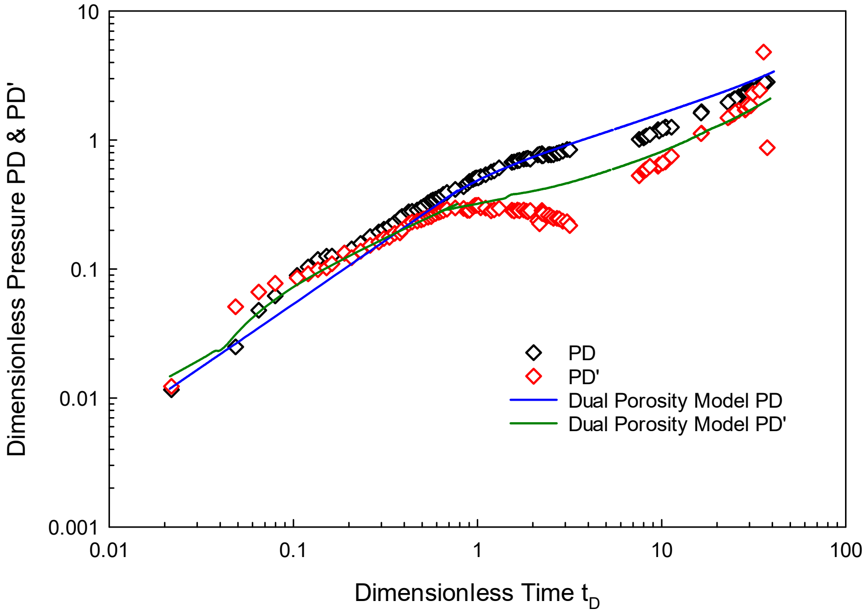

Figure 6 - 4: Deconvolved dimensionless pressure and pressure derivative curve with the dual porosity model of well A.

From the figure (6-4), a satisfactory match was found between the dual porosity model and the results found through deconvolution techniques.

6.2 Summary and Conclusions :

This chapter has demonstrated the application of the CRSM using a shale gas well example to characterize hydraulic fracture treatment. Utilizing actual production data, regardless of production interruptions, the CRSM can be used in forecasting production performance relying only on reservoir physics, through production rate and bottom hole flowing pressure data. The shale gas example illustrated in this study allows for the characterization of fracture effectiveness while honoring the physics of the reservoir.

Chapter 7: Conclusions

7.1 Summary and Conclusion:

This research has demonstrated that the Connected Reservoir Storage Model (CRSM) is a physics-based, mathematically robust, and easy to implement algorithm for reservoir characterization, production forecasting, and fracture volume quantification. The CRSM uses historical production history, production rate and bottom-hole flowing pressure (BHFP), for reservoir characterization and rate forecast with variable operating conditions. CRSM's predictive performance is mainly governed by how much the reservoir pore volume has been "contacted" by the production performance. Reservoir geometries, petro-physical properties, and fluid properties are not required when implementing the CRSM algorithm; however, they can be inferred.

Below is a synopsis of the research findings:

1. The CRSM was validated comparing the CRSM model to that of the explicit definition of the CRS through the BHFP and production rate response that contain the physics of the reservoir.
2. This research further demonstrates how versatile the CRSM is through the application of a simulated bi-wing fractured reservoir system and how this algorithm is more advantageous in lieu of tested curve-fitting models in rate forecasting accuracy, where more extended production history is usually required to yield a more accurate estimation on rate forecast for empirical models whereas the CRSM can be employed with minimal production history.
3. The CRSM was applied to an actual shale gas production well where gas production rates are affected by multiple factors and its forecast has a large uncertainty. Its early history can be affected by flow back water production, and at late time, the rate history can be affected by many mechanisms leading to increasing skin factor. The CRSM

model reveals the dynamics of flow mechanisms through a deconvoluted unit pressure response. The complex constraints of shale gas production render the long-term rate forecast with large uncertainties and failures of curve-fitting based models. Coupled with stochastic analysis, CRSM can capture these constraints and make a reasonable range of production forecasts even with short production history.

4. The CRSM can be used to analyze fracture effectiveness via stimulation treatment through the applications of NDC and CRS curve to help understand the flow behaviors in the early stages of well life. Coupling this information with the ability to forecast production performance without the use of empirical methods through nonlinear regression analysis makes the CRSM a dynamic tool for a full gambit of well diagnostics applications.

Moreover, the CRSM can be used as a diagnostic tool to provide a better estimation of a well's production performance during the transient flow regime and illustrates flow regime transition to ensure steady production operations with minimal downtime. Furthermore, it can be further demonstrated through applications of the CRSM that one can determine a variety of reservoir parameters for all reservoir types.

7.2 Recommendations and Future Research Endeavors:

Future research will extend the CRSM to multiple wells from similar areas to better quantify the unit pressure response as further studies need to be done to understand the boundaries encountered by this method. Using this method for unit pressure response prediction, assumptions were made such that one can get an understanding of the upper and lower limits of the unit pressure response. However, more production samples are needed such that a compare and contrast analysis can be done on the unit pressure response taking into account the basin, geological structures, reservoir properties, drilling, completion, and operational practices by producers to better quantify the unit pressure response for more robust forecast predictions.

Future research will extend the CRSM to all types of reservoir formations and apply the CRSM to illustrate its ability to handle flow rate interruptions and to be used to determine pressure behavior, average reservoir pressure as well as ascertain original fluids in place for all formation types. Additional research utilizing the CRSM will be to compare and contrast through numerical simulation, the quantification of the hydraulic fracture volume from the production history via hydraulicly fractured reservoir simulation.

Nomenclature

A = Reservoir Surface Area, L^2,ft^2
a = Duong Intercept, 1/t, 1/Day
B_o = Oil Formation Volume Factor,L^3/L^3, RB/STB
B_g = Gas Formation Volume Factor,L^3/L^3,ft^3/Mscf or RB/Mscf
C_A = Dietz Shape Factor, dimensionless
c_t = Total compressiblity, Lt^2/m,1/psia
CRS = Connected Reservoir Storage, L^2t^2/m, RB/psi
E(t) = Connected Reservoir Storage, L^2t^2/m, RB/psi
h = Formation thickness, L, ft
k = Permeability, L^2, md
MRE = Mean Relative Error, fraction
m(P) = Pseudo Pressure, m/Lt^3, psi^2/cP
$\underline{P}$ = Pressure, m/Lt^2, psia
P_{Norm_r} = Average Normalized Pressure, m/Lt^2, psia
$P_D(t)$ = Dimensionless pressure
$P_D(t\text{-}t_j)$ = Dimensionless pressure at j^{th} time step
P_i = Initial Reservoir Pressure, m/Lt^2, psia
$P_{Norm} = \delta$ = Normalized pressure, m/Lt^2, psia
PrE = Proven Energy, L^3/t, rb/Day
$\underline{Pr}$V = Proven Volume, L^3, rb
P_r = Average Reservoir Pressure Proven Volume, m/Lt^2, psia
$P_{Unit}(t)$ = Unit pressure response, m/L^2t, Day-psi/RB
P_{wf} = Bottomhole Flowing Pressure, m/Lt^2, psia
$\Delta P(t) = P_i - P_{wf}$ Differential pressure, m/Lt^2, psi
δ_i = Inital Normalized pressure, m/Lt^2, psia
δ_r = Reservoir Normalized pressure, m/Lt^2, psia
$\underline{\delta}_{wf}$ = Normalized Bottomhole Flowing Pressure, m/Lt^2, psia
δ_r = Average Normalized Reservoir Pressure Proven Volume, m/Lt^2, psia
$Q_o(t)$ = Cumulative Production of the Oil, L^3, ft^3
$Q_g(t)$ = Cumulative Production of the Gas, L^3, Mscf
$Q_{N_g}(t)$ = Normalized Cumulative Production, L^2t^2/m, RB/psi
Q_N = Normalized Cumulative Production, L^2t^2/m, RB/psi
q_N = N^{th} Step Production Rate, L^2t/m, RB/Day-psi
$q_N(t)_{int}$ = Normalized Production Rate Intercept, L^2t/m, RB/Day-psi
q_{N-1} = N^{th} - 1Step Production Rate, L^2t/m, RB/Day
$q_{N_s}(t)$= N^{th} Step Production Rate, L^2t/m, RB/Day-psi
$q_o(t)$ = Production Rate of the Oil, L^4t/m, RB/Day
$q_g(t)$= Production Rate of the Gas, L^4t/m, cf/Day
$q_{N_g}(t)$ = Normalized Production Rate, L^2t/m, cf/psi
q_H = Historical Gas Production Rate Data at actual conditions, L^4t/m, RB/Day
q_P = Predicted Gas Production Rate Data at actual conditions, L^4t/m, RB/Day
$q_j - q_{j-1}$ = j^{th} Step Production Rate, L^2t/m, RB/Day
r_e = External drainage radius, L, ft
r_w = Wellbore radius, L, ft
γ = Euler constant, γ =1.78
μ_g = Gas Viscosity, cP
μ_o = Oil Viscosity, cP
φ= Porosity, fraction
t = Production time, Days
$V_P(t)$=Pore Volume at actual conditions,L^3, ft^3
z = Gas Deviation Factor, fraction

Subscripts
i = i^{th} index
o = Oil
w = Water
g = Gas

References

Aanonsen, S.I., Nævdal, G., Oliver, D.S., Reynolds, A.C. and Vallès, B., 2009. The Ensemble Kalman Filter in Reservoir Engineering--a Review. SPE Journal, 14(03): 393-412 doi:https://doi.org/10.2118/117274-PA

Agarwal, R.G., Gardner, D.C., Kleinsteiber, S.W. and Fussell, D.D., 1999. Analyzing well production data using combined type curve and decline curve analysis concepts, SPE Annual Technical Conference and Exhibition. Society of Petroleum Engineers, New Orleans, Louisiana doi:https://dx.doi.org/10.2118/49222-MS

Ahmad, S., BinAkresh, S. and Anisur Rahman, N., 2016. Application of a Deconvolution Technique in PTA for Enhanced Reservoir Characterization, SPE Kingdom of Saudi Arabia Annual Technical Symposium and Exhibition. SPE-182765-MS, Saudi Arabia doi:https://dx.doi.org/10.2118/182765-MS

Akbarnejad-Nesheli, B., Valko, P. and Lee, J.W., 2012. Relating fracture network characteristics to shale gas reserve estimation. Society of Petroleum Engineers

API, 2020. HYDRAULIC FRACTURING

Arps, J.J., 1945. Analysis of decline curves. Transactions of the AIME, 160(01): 228-247 doi:https://dx.doi.org/10.2118/945228-G

Astakhov, D., Roadarmel, W. and Nanayakkara, A., 2012. A New Method of Characterizing the Stimulated Reservoir Volume Using Tiltmeter-Based Surface Microdeformation Measurements, SPE Hydraulic Fracturing Technology Conference. Society of Petroleum Engineers, The Woodlands, Texas, USA, pp. 15 doi:https://dx.doi.org/10.2118/151017-MS

Barree, R.D., Duenckel, R.J. and Hlidek, B.T., 2019. The Limits of Fluid Flow in Propped Fractures- the Disparity Between Effective Flowing and Created Fracture Lengths, SPE Hydraulic Fracturing Technology Conference and Exhibition. Society of Petroleum Engineers, The Woodlands, Texas, USA, pp. 27 doi:https://dx.doi.org/10.2118/194355-MS

Barree, R.D., Fisher, M.K. and Woodroof, R.A., 2002. A Practical Guide to Hydraulic Fracture Diagnostic Technologies, SPE Annual Technical Conference and Exhibition. Society of Petroleum Engineers, San Antonio, Texas, pp. 12 doi:https://dx.doi.org/10.2118/77442-MS

Barree, R.D. and Mukherjee, H., 1995. Engineering Criteria for Fracture Flowback Procedures, Low Permeability Reservoirs Symposium. Society of Petroleum Engineers, Denver, Colorado, pp. 14 doi:https://dx.doi.org/10.2118/29600-MS

Bellarby, J., 2009. Well completion design, 56. Elsevier.

Bhatnagar, A., 2016. Overcoming Challenges in Fracture Stimulation through Advanced Fracture Diagnostics, SPE Asia Pacific Hydraulic Fracturing Conference. Society of Petroleum Engineers, Beijing, China, pp. 15 doi:https://dx.doi.org/10.2118/181802-MS

Boyeldieu, C. and Jeffreys, P., 1988. Formation MicroScanner: new developments

Bukhamsin, A. and Horne, R., 2016. Cointerpretation of Distributed Acoustic and Temperature Sensing for Improved Smart Well Inflow Profiling, SPE Western Regional Meeting. Society of Petroleum Engineers, Anchorage, Alaska, USA, pp. 17 doi:https://dx.doi.org/10.2118/180465-MS

Bybee, K., 2011. Optimization of completions in unconventional reservoirs. Journal of Petroleum Technology, 63(07): 102-104 doi:https://doi.org/10.2118/0711-0102-JPT

Cheung, R. et al., 2001. Field Test Results Of A New Oil-Base Mud Formation Imager Tool, SPWLA 42nd Annual Logging Symposium. Society of Petrophysicists and Well-Log Analysts, Houston, Texas, pp. 14

Childers, D. and Callard, J., 2015. Forecasting Reserves in the Bakken Reservoir Incorporating Flow Regime Changes, SPE Production and Operations Symposium. Society of Petroleum Engineers doi:https://dx.doi.org/10.2118/173622-MS

Childers, D. and Wu, X., 2017. Analyzing Gas Well Production Data through the Application of the Connected Reservoir Storage Model, SPE Annual Technical Conference and Exhibition. Society of Petroleum Engineers doi:https://dx.doi.org/10.2118/187334-MS

Childers, D. and Wu, X., 2020. Characterize Hydraulic Fracturing Treatment Directly from Production Data using Connected Reservoir Storage Model, American Rock Mechanics Association. ARMA, Golden, Colorado, USA, pp. 9 doi:in press

Cipolla, C. and Wallace, J., 2014. Stimulated Reservoir Volume: A Misapplied Concept?, SPE Hydraulic Fracturing Technology Conference. Society of Petroleum Engineers

Cipolla, C. and Wright, C., 2000a. State-of-the-art in hydraulic fracture diagnostics, SPE Asia Pacific Oil and Gas Conference and Exhibition. Society of Petroleum Engineers

Cipolla, C.L. et al., 2011. Integrating Microseismic Mapping and Complex Fracture Modeling to Characterize Hydraulic Fracture Complexity, SPE Hydraulic Fracturing Technology Conference. Society of Petroleum Engineers, The Woodlands, Texas, USA, pp. 22 doi:https://dx.doi.org/10.2118/140185-MS

Cipolla, C.L., Williams, M.J., Weng, X., Mack, M.G. and Maxwell, S.C., 2010. Hydraulic Fracture Monitoring to Reservoir Simulation: Maximizing Value, SPE Annual Technical

Conference and Exhibition. Society of Petroleum Engineers, Florence, Italy, pp. 26 doi:https://dx.doi.org/10.2118/133877-MS

Cipolla, C.L. and Wright, C.A., 2000b. Diagnostic Techniques to Understand Hydraulic Fracturing: What? Why? and How?, SPE/CERI Gas Technology Symposium. Society of Petroleum Engineers, Calgary, Alberta, Canada, pp. 13 doi:https://dx.doi.org/10.2118/59735-MS

Cipolla, C.L. and Wright, C.A., 2000c. State-of-the-Art in Hydraulic Fracture Diagnostics, SPE Asia Pacific Oil and Gas Conference and Exhibition. Society of Petroleum Engineers, Brisbane, Australia, pp. 15 doi:https://dx.doi.org/10.2118/64434-MS

Clark, A.J., Lake, L.W. and Patzek, T.W., 2011a. Production Forecasting with Logistic Growth Models, SPE Annual Technical Conference and Exhibition. Society of Petroleum Engineers, Denver, Colorado, USA, pp. 11 doi:http://dx.doi.org/10.2118/144790-MS

Clark, A.J., Lake, L.W. and Patzek, T.W., 2011b. Production forecasting with logistic growth models, SPE annual technical conference and exhibition. Society of Petroleum Engineers doi:https://dx.doi.org/10.2118/144790-MS

Clarkson, C.R., 2013a. Production data analysis of unconventional gas wells: Review of theory and best practices. International Journal of Coal Geology, 109: 101-146 doi:https://doi.org/10.1016/j.coal.2013.01.002

Clarkson, C.R., 2013b. Production data analysis of unconventional gas wells: Workflow. International Journal of Coal Geology, 109: 147-157

Clarkson, C.R. and Williams-Kovacs, J. (Editors), 2019. Flowback and Early-Time Production Data Analysis. Monograph Series, 1. Society of Petroleum Engineers, Richardson, Texas, 524 pp.

Crestani, E., 2013. Tracer Test Data Assimilation for the Assessment of Local Hydraulic Properties in Heterogeneous Aquifers

Crockett, A.R., Willis, R.M., Jr. and Cleary, M.P., 1989. Improvement of Hydraulic Fracture Predictions by Real-Time History Matching on Observed Pressures. SPE-15264-PA, 4(04): 408-416 doi:https://dx.doi.org/10.2118/15264-PA

Cui, J., Yang, C., Zhu, D. and Datta-Gupta, A., 2016. Fracture Diagnosis in Multiple-Stage-Stimulated Horizontal Well by Temperature Measurements With Fast Marching Method. SPE Journal, 21(06): 2289-2300 doi:https://doi-org.ezproxy.lib.ou.edu/10.2118/174880-PA

Dakin, J.P., Pratt, D.J., Bibby, G.W. and Ross, J.N., 1985. Distributed antistokes ratio thermometry. Optical Society of America, pp. PDS3 doi:https://doi.org/10.1364/OFS.1985.PDS3

Daley, T.M. et al., 2013. Field testing of fiber-optic distributed acoustic sensing (DAS) for subsurface seismic monitoring. The Leading Edge, 32(6): 699-706 doi:https://doi.org/10.1190/tle32060699.1

Daneshy, A.A., 1973. On the Design of Vertical Hydraulic Fractures. Journal of Petroleum Technology, 25(01): 83-97 doi:http://dx.doi.org/10.2118/3654-PA

Dastkhan, Z., Zolalemin, A., Razminia, K. and Parvizi, H., 2015. Minimization and Removal of Wellbore Storage Effect by Direct Deconvolution of Well Test Data, SPE Reservoir Characterisation and Simulation Conference and Exhibition. Society of Petroleum Engineers doi:https://dx.doi.org/10.2118/175595-MS

Deen, T., Daal, J. and Tucker, J., 2015. Maximizing Well Deliverability in the Eagle Ford Shale Through Flowback Operations, SPE Annual Technical Conference and Exhibition. Society of Petroleum Engineers, Houston, Texas, USA, pp. 13 doi:https://doi-org.ezproxy.lib.ou.edu/10.2118/174831-MS

Descant, F., Blackwell, R., Pope, G.A. and Sepehrnoori, K., 1989. The Use Of Single Well Tracer Testing To Estimate Heterogeneity. Society of Petroleum Engineers, pp. 26

Dou, S. et al., 2017. Distributed acoustic sensing for seismic monitoring of the near surface: A traffic-noise interferometry case study. Scientific reports, 7(1): 1-12 doi:https://doi.org/10.1038/s41598-017-11986-4

Dugstad, Ø., 2007. Well-to-Well Tracer Tests, Chapter 6 (pp. 651–683), Petroleum Engineering Handbook, Vol. 5-Reservoir Engineering and Petrophysics by Edward D. Holstein (Ed.) SPE, Richardson, Texas

Dumont, A., Kubacsi, M. and Chardac, J.L., 1987. The Oil-Based Mud Dipmeter Tool, SPWLA 28th Annual Logging Symposium. Society of Petrophysicists and Well-Log Analysts, London, England, pp. 15

Duong, A.N., 2011. Rate-decline analysis for fracture-dominated shale reservoirs. SPE Reservoir Evaluation & Engineering, 14(03): 377-387 doi:https://dx.doi.org/10.2118/137748-PA

Earlougher, R.C., 1977. Advances in well test analysis, 5. Henry L. Doherty Memorial Fund of AIME New York.

Economides, M.J., Hill, A.D., Ehlig-Economides, C. and Zhu, D., 2013. Petroleum production systems. Pearson Education.

Eisner, L. et al., 2010. Comparison of surface and borehole locations of induced seismicity. Geophysical Prospecting, 58(5): 809-820 doi:https://doi.org/10.1111/j.1365-2478.2010.00867.x

Eisner, L., Thornton, M. and Griffin, J., 2011. Challenges For Microseismic Monitoring, 2011 SEG Annual Meeting. Society of Exploration Geophysicists, San Antonio, Texas, pp. 5 doi:https://doi.org/10.1190/1.3627491

Ekstrom, M.P., Dahan, C.A., Chen, M.-Y., Lloyd, P.M. and Rossi, D.J., 1986. Formation Imaging With Microelectrical Scanning Arrays, SPWLA 27th Annual Logging Symposium. Society of Petrophysicists and Well-Log Analysts, Houston, Texas, pp. 21

Elahi*, S.H. and Jafarpour, B., 2015. Characterization of Fracture Length and Conductivity From Tracer Test and Production Data With Ensemble Kalman Filter, Unconventional Resources Technology Conference. Unconventional Resources Technology Conference, San Antonio, Texas, USA, pp. 12 doi:https://dx.doi.org/10.15530/URTEC-2015-2174307

Ely, J.W. and Herndon, R.A. (Editors), 2019. Fracturing Fluids and Additives. Hydraulic Fracturing Fundamentals and Advancements, Volume 1. Society of Petroleum Engineers, Richardson, Texas, 166-197 pp.

Ertekin, T., Sun, Q. and Zhang, J., 2019. Reservior Simulation: Problems and Solutions, 1. Society of Petroleum Engineers, Richardson, Tx, 599 pp.

Esmaili, S. and Mohaghegh, S.D., 2016. Full field reservoir modeling of shale assets using advanced data-driven analytics. Geoscience Frontiers, 7(1): 11-20 doi:https://doi.org/10.1016/j.gsf.2014.12.006

Evenick, J., 2018. Introduction to well logs and subsurface maps. PennWell Books.

Evensen, G. and Van Leeuwen, P.J., 1996. Assimilation of Geosat altimeter data for the Agulhas current using the ensemble Kalman filter with a quasigeostrophic model. Monthly Weather Review, 124(1): 85-96 doi:https://doi.org/10.1175/1520-0493(1996)124%3C0085:AOGADF%3E2.0.CO;2

Faraguna, J.K., Chance, D.M. and Schmidt, M.G., 1989. An Improved Borehole Televiewer System: Image Acquisition, Analysis And Integration, SPWLA 30th Annual Logging Symposium. Society of Petrophysicists and Well-Log Analysts, Denver, Colorado, pp. 11

Fehler, M.C., 1989. Stress control of seismicity patterns observed during hydraulic fracturing experiments at the Fenton Hill hot dry rock geothermal energy site, New Mexico. Elsevier, pp. 211-219 doi:https://doi.org/10.1016/0148-9062(89)91971-2

Ferreira, L.E.A., Descant, F.J., Delshad, M., Pope, G.A. and Sepehrnoori, K., 1992. A Single-Well Tracer Test To Estimate Wettability, SPE/DOE Enhanced Oil Recovery Symposium. Society of Petroleum Engineers, Tulsa, Oklahoma, pp. 11 doi:https://dx.doi.org/10.2118/24136-MS

Fetkovich, M.J., 1980a. Decline curve analysis using type curves. Journal of Petroleum Technology, 32(06): 1,065-1,077

Fetkovich, M.J., 1980b. Decline Curve Analysis Using Type Curves. Journal of Petroleum Technology, 32(06): 1065-1077 doi:http://dx.doi.org/10.2118/4629-PA

Fisher, M.K. and Warpinski, N.R., 2012. Hydraulic-Fracture-Height Growth: Real Data. SPE Production & Operations, 27(01): 8-19 doi:https://dx.doi.org/10.2118/145949-PA

Förster, A., Schrötter, J., Merriam, D.F. and Blackwell, D.D., 1997. Application of optical-fiber temperature logging; an example in a sedimentary environment. Geophysics, 62(4): 1107-1113 doi:https://doi.org/10.1190/1.1444211

Freeborn, R. and Russell, B., 2012. How To Apply Stretched Exponential Equations to Reserve Evaluation, SPE Hydrocarbon Economics and Evaluation Symposium. Society of Petroleum Engineers doi:https://dx.doi.org/10.2118/162631-MS

Fulford, D. and Blasingame, T., 2013. Evaluation of time-rate performance of shale wells using the transient hyperbolic relation, SPE Unconventional Resources Conference Canada. Society of Petroleum Engineers

Gardien, C.J., Pope, G.A. and Hill, A.D., 1996. Hydraulic Fracture Diagnosis Using Chemical Tracers, SPE Annual Technical Conference and Exhibition. Society of Petroleum Engineers, Denver, Colorado, pp. 8 doi:https://dx.doi.org/10.2118/36675-MS

Geertsma, J. and De Klerk, F., 1969. A Rapid Method of Predicting Width and Extent of Hydraulically Induced Fractures. Journal of Petroleum Technology, 21(12): 1571-1581 doi:http://dx.doi.org/10.2118/2458-PA

Ghods, P. and Zhang, D., 2012. Automatic Estimation of Fracture Properties in Multistage Fractured Shale Gas Horizontal Wells for Reservoir Modeling, SPE Western Regional Meeting. Society of Petroleum Engineers, Bakersfield, California, USA, pp. 19 doi:https://dx.doi.org/10.2118/153913-MS

Götz, J., Lüth, S., Henninges, J. and Reinsch, T., 2018. Vertical seismic profiling using a daisy-chained deployment of fibre-optic cables in four wells simultaneously–Case study at the Ketzin carbon dioxide storage site. Geophysical Prospecting, 66(6): 1201-1214 doi:https://doi.org/10.1111/1365-2478.12638

Guo, T., 2015. The Fuling Shale Gas Field—A highly productive Silurian gas shale with high thermal maturity and complex evolution history, southeastern Sichuan Basin, China. Interpretation, 3(2): SJ25-SJ34

Gupta, I., Rai, C., Sondergeld, C. and Devegowda, D., 2018. Variable Exponential Decline-Modified Arps to Characterize Unconventional Shale Production Performance, Unconventional Resources Technology Conference, Houston, Texas, 23-25 July 2018.

Society of Exploration Geophysicists, American Association of Petroleum …, pp. 3552-3568 doi:https://dx.doi.org/10.15530/URTEC-2018-2902794

Hartog, A., 1983. A distributed temperature sensor based on liquid-core optical fibers. Journal of Lightwave Technology, 1(3): 498-509 doi:https://dx.doi.org/10.1109/JLT.1983.1072146

Hartog, A.H., 2017. An introduction to distributed optical fibre sensors. CRC press.

Hartog, A.H., Leach, A.P. and Gold, M.P., 1985. Distributed temperature sensing in solid-core fibres. Electronics letters, 21(23): 1061-1062 doi:https://dx.doi.org/10.1049/el:19850752

Haustveit, K. et al., 2020. Monitoring the Pulse of a Well Through Sealed Wellbore Pressure Monitoring, a Breakthrough Diagnostic With a Multi-Basin Case Study, SPE Hydraulic Fracturing Technology Conference and Exhibition. Society of Petroleum Engineers, The Woodlands, Texas, USA, pp. 42 doi:10.2118/199731-MS

Hayman, A.J., Parent, P., Cheung, P. and Verges, P., 1994. Improved Borehole Imaging by Ultrasonics, SPE Annual Technical Conference and Exhibition. Society of Petroleum Engineers, New Orleans, Louisiana, pp. 16 doi:https://dx.doi.org/10.2118/28440-MS

Heydarabadi, F.R., Moghadasi, J., Safian, G. and Ashena, R., 2010. Criteria for Selecting a Candidate Well for Hydraulic Fracturing, Nigeria Annual International Conference and Exhibition. Society of Petroleum Engineers, Tinapa - Calabar, Nigeria, pp. 7 doi:https://doi-org.ezproxy.lib.ou.edu/10.2118/136988-MS

Holdaway, K.R., 2013. Data Mining Methodologies enhance Probabilistic Well Forecasting, SPE Middle East Intelligent Energy Conference and Exhibition. Society of Petroleum Engineers doi:https://dx.doi.org/10.2118/167428-MS

Holditch, S.A., Holcomb, D.L. and Rahim, Z., 1993. Using Tracers To Evaluate Propped Fracture Width, SPE Eastern Regional Meeting. Society of Petroleum Engineers, Pittsburgh, Pennsylvania, pp. 8 doi:https://dx.doi.org/10.2118/26922-MS

Horne, R.N., 1995. Modern well test analysis. Petroway Inc

Horne, R.N., 2000. Modern well test analysis, A Computer-Aided Approach. Petroway, Incorporated, 79-81 pp.

Houze, O., Viturat, D. and Fjaere, O.S., 2016. Dynamic Data Analysis, 558 pp.

Hsu, Y. et al., 2012. New Physics-Based 3D Hydraulic Fracture Model, SPE Hydraulic Fracturing Technology Conference. Society of Petroleum Engineers, The Woodlands, Texas, USA, pp. 15 doi:http://dx.doi.org/10.2118/152525-MS

Huckabee, P.T., 2009. Optic Fiber Distributed Temperature for Fracture Stimulation Diagnostics and Well Performance Evaluation, SPE Hydraulic Fracturing Technology Conference. Society of Petroleum Engineers, The Woodlands, Texas, pp. 21 doi:https://doi-org.ezproxy.lib.ou.edu/10.2118/118831-MS

Hurtig, E., 1993. Borehole temperature measurements using distributed fibre optic sensing. Scientific Drilling, 3: 283-286

Huseby, O., Valestrand, R., Nævdal, G. and Sagen, J., 2010. Natural and Conventional Tracers for Improving Reservoir Models Using the EnKF Approach. SPE Journal, 15(04): 1047-1061 doi:https://dx.doi.org/10.2118/121190-PA

Ilk, D., Rushing, J.A., Perego, A.D. and Blasingame, T.A., 2008. Exponential vs. hyperbolic decline in tight gas sands: understanding the origin and implications for reserve estimates using Arps' decline curves, SPE annual technical conference and exhibition. Society of Petroleum Engineers doi:https://dx.doi.org/10.2118/116731-MS

Jacobs, T., 2020. Sealed Wellbores and the Unlikely "Breakthrough" Behind Cheap, Accurate Fracture Diagnostics. Journal of Petroleum Technology, 72(04): 29-33 doi:10.2118/0420-0029-JPT

Jahanbani, A. and Aguilera, R., 2008. Well Testing of Tight Gas Reservoirs, Canadian International Petroleum Conference. Petroleum Society of Canada

James, J. and Alex, V., 2003. Distributed temperature sensing-A DTS primer for oil and gas production. May

Joshi, K. and Lee, W.J., 2013. Comparison of various deterministic forecasting techniques in shale gas reservoirs, SPE Hydraulic Fracturing Technology Conference. Society of Petroleum Engineers doi:https://dx.doi.org/10.2118/163870-MS

Jousset, P. et al., 2018. Dynamic strain determination using fibre-optic cables allows imaging of seismological and structural features. Nature communications, 9(1): 1-11 doi:https://doi.org/10.1038/s41467-018-04860-y

Kanfar, M. and Wattenbarger, R., 2012. Comparison of empirical decline curve methods for shale wells, SPE Canadian Unconventional Resources Conference. Society of Petroleum Engineers doi:https://dx.doi.org/10.2118/162648-MS

Kanfar, M.S. and Clarkson, C.R., 2016. Reconciling flowback and production data: A novel history matching approach for liquid rich shale wells. Journal of Natural Gas Science and Engineering, 33: 1134-1148 doi:https://doi.org/10.1016/j.jngse.2016.04.042

Kim, T.H. and Lee, K.S., 2015. Pressure-transient characteristics of hydraulically fractured horizontal wells in shale-gas reservoirs with natural-and rejuvenated-fracture networks. Journal of Canadian Petroleum Technology, 54(04): 245-258 doi:https://dx.doi.org/10.2118/176027-PA

King, G.E., Haile, L., Shuss, J.A. and Dobkins, T., 2008. Increasing Fracture Path Complexity and Controlling Downward Fracture Growth in the Barnett Shale, SPE Shale Gas Production Conference. Society of Petroleum Engineers, Fort Worth, Texas, USA, pp. 8 doi:https://dx.doi.org/10.2118/119896-MS

Kuchuk, F., Onur, M. and Hollaender, F., 2010a. PRESSURE TRANSIENT FORMATION AND WELL TESTNG. Dev. in Petr. Science, 57

Kuchuk, F.J., Onur, M. and Hollaender, F., 2010b. Pressure transient formation and well testing: convolution, deconvolution and nonlinear estimation, 57. Elsevier.

Kuchuk, F.J. and Tarek, H., 1997. Pressure behavior of laterally composite reservoirs. SPE Formation Evaluation, 12(1): 47-56 doi:10.2118/24678-PA

Kumar, A., Seth, P., Shrivastava, K., Manchanda, R. and Sharma, M.M., 2020. Integrated Analysis of Tracer and Pressure-Interference Tests To Identify Well Interference. SPE Journal, 25(04): 1623-1635 doi:10.2118/201233-PA

Laastad, H. et al., 2000. Water-Based Formation Imaging and Resistivity Logging in Oil-Based Drilling Fluids- Today's Reality, SPE Annual Technical Conference and Exhibition. Society of Petroleum Engineers, Dallas, Texas, pp. 16 doi:https://dx.doi.org/10.2118/62977-MS

Lange, A., Bourbiaux, B.J. and Bouzian, J., 2005. Tracer-Test Simulation on Discrete Fracture Network Models for the Characterization of Fractured Reservoirs, SPE Europec/EAGE Annual Conference. Society of Petroleum Engineers, Madrid, Spain, pp. 10 doi:https://dx.doi.org/10.2118/94344-MS

Lecampion, B. and Gunning, J., 2007. Model selection in fracture mapping from elastostatic data. International journal of solids and structures, 44(5): 1391-1408 doi:https://doi.org/10.1016/j.ijsolstr.2006.06.022

Lecampion, B., Jeffrey, R. and Detournay, E., 2005. Resolving the geometry of hydraulic fractures from tilt measurements. Pure and Applied Geophysics, 162(12): 2433-2452 doi:https://doi.org/10.1007/s00024-005-2786-4

Lee, W.J., 2015. Critique of Simple Decline Models. SPE webinar

Lee, W.J. and Sidle, R., 2010. Gas-Reserves Estimation in Resource Plays. SPE Economics & Management, 2(02): 86-91 doi:http://dx.doi.org/10.2118/130102-PA

Levitan, M.M., 2003. Practical application of pressure-rate deconvolution to analysis of real well tests, SPE Annual Technical Conference and Exhibition. Society of Petroleum Engineers

Levitan, M.M., 2005. Practical application of pressure-rate deconvolution to analysis of real well tests, SPE Annual Technical Conference and Exhibition. Society of Petroleum Engineers doi:https://dx.doi.org/10.2118/84290-MS

Levitan, M.M. and Wilson, M.R., 2012. Deconvolution of pressure and rate data from gas reservoirs with significant pressure depletion. SPE Journal, 17(03): 727-741 doi:https://dx.doi.org/10.2118/134261-PA

Majer, E., Baria, R. and Fehler, M., 2005. Cooperative research on induced seismicity associated with enhanced geothermal systems. Geotherm. Resour. Counc. Trans, 29: 99-101

Marquart, G., Vogt, C., Klein, C. and Widera, A., 2013. Estimation of geothermal reservoir properties using the Ensemble Kalman Filter. Energy Procedia, 40: 117-126 doi:https://doi.org/10.1016/j.egypro.2013.08.015

Masoudi, A., Belal, M. and Newson, T.P., 2013. A distributed optical fibre dynamic strain sensor based on phase-OTDR. Measurement Science and Technology, 24(8): 085204 doi:https://dx.doi.org/10.1088/0957-0233/24/8/085204

Mattar, L. and Anderson, D.M., 2003. A Systematic and Comprehensive Methodology for Advanced Analysis of Production Data, SPE Annual Technical Conference and Exhibition. Society of Petroleum Engineers, Denver, Colorado, pp. 14 doi:https://dx.doi.org/10.2118/84472-MS

Mattar, L. and Moghadam, S., 2009. Modified Power Law Exponential Decline for Tight Gas, Canadian International Petroleum Conference. Petroleum Society of Canada, Calgary, Alberta, pp. 11 doi:http://dx.doi.org/10.2118/2009-198

Mayerhofer, M.J., Stutz, H.L., Davis, E.J. and Wolhart, S.L., 2006. Optimizing Fracture Stimulation Using Treatment-Well Tiltmeters and Integrated Fracture Modeling. SPE Production & Operations, 21(02): 222-229 doi:https://dx.doi.org/10.2118/84490-PA

McDaniel, R.R. et al., 2009. Determining Propped Fracture Width from a New Tracer Technology, SPE Hydraulic Fracturing Technology Conference. Society of Petroleum Engineers, The Woodlands, Texas, pp. 16 doi:https://dx.doi.org/10.2118/119545-MS

McNeil, R., Jeje, O. and Renaud, A., 2009. Application of the Power Law Loss-Ratio Method of Decline Analysis, Canadian International Petroleum Conference. Petroleum Society of Canada, Calgary, Alberta, pp. 7 doi:http://dx.doi.org/10.2118/2009-159

Meyet Me Ndong, M.P., Dutta, R. and Burns, C., 2013. Comparison of Decline Curve Analysis Methods with Analytical Models in Unconventional Plays, SPE Annual Technical Conference and Exhibition. Society of Petroleum Engineers, New Orleans, Louisiana, USA, pp. 32 doi:http://dx.doi.org/10.2118/166365-MS

Mittag-Leffler, G.M., 1903. Sur la nouvelle fonction Eα (x). CR Acad. Sci. Paris, 137(2): 554-558

Mohaghegh, S.D., 2020. Subsurface analytics: Contribution of artificial intelligence and machine learning to reservoir engineering, reservoir modeling, and reservoir management. Petroleum Exploration and Development, 47(2): 225-228 doi:https://doi.org/10.1016/S1876-3804(20)60041-6

Moreno, J., Tarrahi, M., Gildin, E. and Gonzales, S., 2014. Real-Time Estimation of Hydraulic Fracture Characteristics From Production Data, SPE/AAPG/SEG Unconventional Resources Technology Conference. Unconventional Resources Technology Conference, Denver, Colorado, USA, pp. 11 doi:https://dx.doi.org/10.15530/URTEC-2014-1923687

Munoz, A.V., Asadi, M., Woodroof, R.A. and Morales, R., 2009. Long-term post-frac performance analysis based on flowback analysis using chemical frac-tracers, Latin American and Caribbean Petroleum Engineering Conference. Society of Petroleum Engineers

Nagel, N.B., Sanchez, M.A. and Lee, B., 2012. Gas Shale Hydraulic Fracturing: A Numerical Evaluation of the Effect of Geomechanical Parameters, SPE Hydraulic Fracturing Technology Conference. Society of Petroleum Engineers, The Woodlands, Texas, USA, pp. 19 doi:https://dx.doi.org/10.2118/152192-MS

O'Brien, D.G. et al., 2011. Using Real-Time Downhole Microseismic to Evaluate Fracture Geometry for Horizontal Packer-Sleeve Completions in the Bakken Formation, Elm Coulee Field, Montana, SPE Hydraulic Fracturing Technology Conference. Society of Petroleum Engineers, The Woodlands, Texas, USA, pp. 22 doi:https://dx.doi.org/10.2118/139774-MS

Olivier Houze, Didier Viturat and Fjaere, O.S., 2016. Dynamic Data Analysis. In: Kappa (Editor). Kappa, pp. 708

Palmer, I.D. and Sparks, D.P., 1991. Measurement of Induced Fractures by Downhole TV Camera in Black Warrior Basin Coalbeds. Journal of Petroleum Technology, 43(03): 270-328 doi:https://doi-org.ezproxy.lib.ou.edu/10.2118/20660-PA

Pan, Z., 2016. Revised productivity index equation to improve transient history match for the Capacitance Resistance Model. Thesis, University of Texas at Austin doi:https://dx.doi.org/2152/46243

Pandurangan, V., Peirce, A., Chen, Z.R. and Jeffrey, R.G., 2018. Tiltmeter Mapping of Measured Nonsymmetric Hydraulic-Fracture Growth in a Conglomerate/Sandstone Formation Using the Implicit Level-Set Algorithm and the Extended Kalman Filter. SPE Journal, 23(01): 172-185 doi:https://dx.doi.org/10.2118/186100-PA

Parney, R., Cladouhos, T., La Pointe, P., Dershowitz, W. and Curran, B., 2000. Fracture and Production Data Integration Using Discrete Fracture Network Models for Carbonate Reservoir Management, South Oregon Basin Field, Wyoming, SPE Rocky Mountain Regional/Low-Permeability Reservoirs Symposium and Exhibition. Society of Petroleum Engineers, Denver, Colorado, pp. 7 doi:https://dx.doi.org/10.2118/60306-MS

Paryani, M., Ahmadi, M., Awoleke, O. and Hanks, C., 2016. Using Improved Decline Curve Models for Production Forecasts in Unconventional Reservoirs, SPE Eastern Regional Meeting. Society of Petroleum Engineers, Canton, Ohio, USA, pp. 15 doi:http://dx.doi.org/10.2118/184070-MS

Perkins, T.K. and Kern, L.R., 1961. Widths of Hydraulic Fractures. Journal of Petroleum Technology, 13(09): 937-949 doi:http://dx.doi.org/10.2118/89-PA

PetroWiki, 2020. Borehole Imaging. Society of Petroleum Engineers

Peyret, O. et al., 2012. Subsurface To Surface Microseismic Monitoring for Hydraulic Fracturing, SPE Annual Technical Conference and Exhibition. Society of Petroleum Engineers, San Antonio, Texas, USA, pp. 15 doi:https://dx.doi.org/10.2118/159670-MS

Poston, S.W. and Poe, B.D., 2008. Analysis of production decline curves. Society of Petroleum Engineers Richardson, TX.

Raab, T., Reinsch, T., Aldaz Cifuentes, S.R. and Henninges, J., 2019. Real-Time Well-Integrity Monitoring Using Fiber-Optic Distributed Acoustic Sensing. SPE Journal, 24(05): 1997-2009 doi:https://dx.doi.org/10.2118/195678-PA

Rahman, M.K., Hossain, M.M. and Rahman, S.S., 2002. A shear-dilation-based model for evaluation of hydraulically stimulated naturally fractured reservoirs. International Journal for Numerical and Analytical Methods in Geomechanics, 26(5): 469-497 doi:https://doi.org/10.1002/nag.208

Ravikumar, A. and Lee, J., 2019. Robust Estimation of Arps Decline Parameters Using Regularizing Priors, SPE Eastern Regional Meeting. Society of Petroleum Engineers doi:https://dx.doi.org/10.2118/196576-MS

Reinsch, T. and Henninges, J., 2010. Temperature-dependent characterization of optical fibres for distributed temperature sensing in hot geothermal wells. Measurement Science and Technology, 21(9): 094022 doi:https://dx.doi.org/10.1088/0957-0233/21/9/094022

Reinsch, T., Henninges, J. and Ásmundsson, R., 2013. Thermal, mechanical and chemical influences on the performance of optical fibres for distributed temperature sensing in a hot geothermal well. Environmental earth sciences, 70(8): 3465-3480 doi:https://doi.org/10.1007/s12665-013-2248-8

Reinsch, T., Thurley, T. and Jousset, P., 2017. On the mechanical coupling of a fiber optic cable used for distributed acoustic/vibration sensing applications—a theoretical consideration. Measurement Science and Technology, 28(12): 127003 doi:https://dx.doi.org/10.1088/1361-6501/aa8ba4

Robertson, S., 1988. Generalized Hyperbolic Equation. Society of Petroleum Engineers, pp. 20

Salman, A., Kurtoglu, B. and Kazemi, H., 2014. Analysis of Chemical Tracer Flowback in Unconventional Reservoirs, SPE/CSUR Unconventional Resources Conference – Canada. Society of Petroleum Engineers, Calgary, Alberta, Canada, pp. 22 doi:https://dx.doi.org/10.2118/171656-MS

Satter, A. and Iqbal, G.M., 2016. 3 - Reservoir rock properties. In: A. Satter and G.M. Iqbal (Editors), Reservoir Engineering. Gulf Professional Publishing, Boston, pp. 29-79.

Seller, D., Edmiston, C., Torres, O. and Goetz, J., 1990. Field Performance Of A New Borehole Televiewer Tool And Associated Image Processing Techniques, SPWLA 31st Annual Logging Symposium. Society of Petrophysicists and Well-Log Analysts, Lafayette, Louisiana, pp. 20

Seller, D., King, G. and Eubanks, D., 1994. Field test of a six arm microresistivity borehole imaging tool. Society of Petrophysicists and Well-Log Analysts

Seshadri, J.N. and Mattar, L., 2010. Comparison of Power Law and Modified Hyperbolic Decline Methods, Canadian Unconventional Resources and International Petroleum Conference. Society of Petroleum Engineers, Calgary, Alberta, Canada, pp. 17 doi:http://dx.doi.org/10.2118/137320-MS

Shatalin, S.V., Treschikov, V.N. and Rogers, A.J., 1998. Interferometric optical time-domain reflectometry for distributed optical-fiber sensing. Applied optics, 37(24): 5600-5604 doi:https://doi.org/10.1364/AO.37.005600

Siebrits, E. et al., 2000. Refracture Reorientation Enhances Gas Production in Barnett Shale Tight Gas Wells, SPE Annual Technical Conference and Exhibition. Society of Petroleum Engineers, Dallas, Texas, pp. 7 doi:https://dx.doi.org/10.2118/63030-MS

Silber, R., Martin, J., Willis, S. and Kozera, G., 2003. Comparing Fracture Simulation Design to Radioactive Tracer Field Results: A Case History, SPE Eastern Regional Meeting. Society of Petroleum Engineers, Pittsburgh, Pennsylvania, pp. 9 doi:https://dx.doi.org/10.2118/84842-MS

Smith, B., Beall, J. and Stark, M., 2000. Induced seismicity in the SE Geysers field, California, USA, pp. 2887-2892

Smith, L., Mase, C.W. and Schwartz, F.W., 1987. Estimation Of Fracture Aperture Using Hydraulic And Tracer Tests, The 28th U.S. Symposium on Rock Mechanics (USRMS). American Rock Mechanics Association, Tucson, Arizona, pp. 12

Smith, M.B., Rosenberg, R.J. and Bowen, J.F., 1982. Fracture Width-Design vs. Measurement, SPE Annual Technical Conference and Exhibition. Society of Petroleum Engineers, New Orleans, Louisiana, pp. 9 doi:https://doi-org.ezproxy.lib.ou.edu/10.2118/10965-MS

Sneddon, I.N., 1946. The Distribution of Stress in the Neighborhood of a Crack in an Elastic Solid. Philosophical Transactions of the Royal Society of London, Series A, 187(1009): 1934-1990

Spivey, J.P. and Lee, W.J., 2013. Applied well test interpretation. Society of Petroleum Engineers Richardson, TX.

Stegent, N.A., Ferguson, K. and Spencer, J., 2011. Comparison of frac valves vs. plug-and-perf completion in the oil segment of the Eagle Ford Shale: a case study, Canadian Unconventional Resources Conference. Society of Petroleum Engineers

Sutton, R.P., Cox, S.A. and Barree, R.D., 2010. Shale Gas Plays: A Performance Perspective, Tight Gas Completions Conference. Society of Petroleum Engineers, San Antonio, Texas, USA, pp. 12 doi:https://dx.doi.org/10.2118/138447-MS

Tan, L., Zuo, L. and Wang, B., 2018. Methods of decline curve analysis for shale gas reservoirs. Energies, 11(3): 552

Valko, P.P., 2009. Assigning value to stimulation in the Barnett Shale: a simultaneous analysis of 7000 plus production hystories and well completion records, SPE hydraulic fracturing technology conference. Society of Petroleum Engineers

Valkó, P.P. and Lee, W.J., 2010. A better way to forecast production from unconventional gas wells, SPE annual technical conference and exhibition. Society of Petroleum Engineers doi:https://dx.doi.org/10.2118/134231-MS

Veatch, R.W., Jr. and Crowell, R.F., 1982. Joint Research/Operations Programs Accelerate Massive Hydraulic Fracturing Technology. Journal of Petroleum Technology, 34(12): 2763-2775 doi:https://dx.doi.org/10.2118/9337-PA

Wang, K. et al., 2017. Predicting production and estimated ultimate recoveries for shale gas wells: A new methodology approach. Applied Energy, 206: 1416-1431

Wang, X., Ding, Y.H., Xiu, N.L., Wang, Z.D. and Yan, Y.Z., 2013. A New Method to Interpret Hydraulic Fracture Complexity in Unconventional Reservoir by Tilt Magnitude, International Petroleum Technology Conference. International Petroleum Technology Conference, Beijing, China, pp. 15 doi:https://dx.doi.org/10.2523/IPTC-17094-MS

Warpinski, N., 2009. Microseismic Monitoring: Inside and Out. Journal of Petroleum Technology, 61(11): 80-85 doi:https://dx.doi.org/10.2118/118537-JPT

Warpinski, N.R., 1996. Hydraulic Fracture Diagnostics. Journal of Petroleum Technology, 48(10): 907-910 doi:https://dx.doi.org/10.2118/36361-JPT

Warpinski, N.R. (Editor), 2019. Fracture Diagnostics. Hydraulic Fracturing Fundamentals and Advancements, Volume 1. Society of Petroleum Engineers, Richardson, Texas, 625-655 pp.

Warpinski, N.R., Du, J. and Zimmer, U., 2012. Measurements of Hydraulic-Fracture-Induced Seismicity in Gas Shales, SPE Hydraulic Fracturing Technology Conference. Society of Petroleum Engineers, The Woodlands, Texas, USA, pp. 19 doi:https://dx.doi.org/10.2118/151597-MS

Wasaki, A. and Akkutlu, I.Y., 2015. Permeability of organic-rich shale. Spe Journal, 20(06): 1,384-1,396 doi:https://dx.doi.org/10.2118/170830-MS

Weijers, L. and De Pater, H. (Editors), 2019. Hydraulic Fracture Modeling. Hydraulic Fracturing Fundamentals and Advancements, Volume 1. Society of Petroleum Engineers, Richardson, Texas, 76-142 pp.

Weng, X., Kresse, O., Cohen, C.-E., Wu, R. and Gu, H., 2011. Modeling of Hydraulic-Fracture-Network Propagation in a Naturally Fractured Formation. SPE Production & Operations, 26(04): 368-380 doi:https://dx.doi.org/10.2118/140253-PA

Wesson, R.L. and Nicholson, C., 1987. Earthquake hazard associated with deep well injection; a report to the US Environmental Protection Agency. 2331-1258, US Geological Survey doi:https://doi.org/10.3133/ofr87331

Whittle, T.M. and Gringarten, A.C., 2008. The determination of minimum tested volume from the deconvolution of well test pressure transients, SPE Annual Technical Conference and Exhibition. Society of Petroleum Engineers doi:https://dx.doi.org/10.2118/116575-MS

Williams-Kovacs, J.D., 2017. Quantitative Analysis of Multi-Phase Flowback From Multi-Fractured Horizontal Wells. http://dx.doi.org/10.11575/PRISM/27503 doi:http://dx.doi.org/10.11575/PRISM/27503

Wolhart, S.L., McIntosh, G.E., Zoll, M.B. and Weijers, L., 2007. Surface Tiltmeter Mapping Shows Hydraulic Fracture Reorientation in the Codell Formation, Wattenberg Field, Colorado, SPE Annual Technical Conference and Exhibition. Society of Petroleum Engineers, Anaheim, California, U.S.A., pp. 8 doi:https://dx.doi.org/10.2118/110034-MS

Woodroof Jr, R.A., Asadi, M. and Warren, M.N., 2003. Monitoring fracturing fluid flowback and optimizing fracturing fluid cleanup using chemical frac tracers, SPE European Formation Damage Conference. Society of Petroleum Engineers

Woodroof, R.A., Jr., Asadi, M. and Warren, M.N., 2003. Monitoring Fracturing Fluid Flowback and Optimizing Fracturing Fluid Cleanup Using Chemical Frac Tracers, SPE European Formation Damage Conference. Society of Petroleum Engineers, The Hague, Netherlands, pp. 12 doi:https://dx.doi.org/10.2118/82221-MS

Wright, C.A. et al., 1998. Surface Tiltmeter Fracture Mapping Reaches New Depths - 10,000 Feet and Beyond?, SPE Rocky Mountain Regional/Low-Permeability Reservoirs Symposium. Society of Petroleum Engineers, Denver, Colorado, pp. 12 doi:https://dx.doi.org/10.2118/39919-MS

Wu, X. and Childers, D.R., 2020. Forecasting Shale Gas Performance Using the Connected Reservoir Storage Model. Journal of Natural Gas Science and Engineering, https://doi.org/10.1016/j.jngse.2020.103499: 103499 doi:https://doi.org/10.1016/j.jngse.2020.103499

Wu, X., Humphrey, K. and Liao, T.T., 2012a. Enhancing Production Allocation in Intelligent Wells via Application of Models and Real-Time Surveillance Data, SPE International Production and Operations Conference & Exhibition. Society of Petroleum Engineers doi:https://dx.doi.org/10.2118/155031-MS

Wu, X., Humphrey, K. and Liao, T.T., 2012b. Enhancing Production Allocation in Intelligent Wells via Application of Models and Real-Time Surveillance Data, SPE International Production and Operations Conference & Exhibition. Society of Petroleum Engineers doi:https://dx.doi.org/10.2118/155031-MS

Wu, Y.-S., 2015. Multiphase fluid flow in porous and fractured reservoirs. Gulf Professional Publishing.

Xu, W. et al., 2010. Wiremesh: A Novel Shale Fracturing Simulator, International Oil and Gas Conference and Exhibition in China. Society of Petroleum Engineers, Beijing, China, pp. 6 doi:https://dx.doi.org/10.2118/132218-MS

Xu, W., Thiercelin, M.J. and Walton, I.C., 2009. Characterization of Hydraulically-Induced Shale Fracture Network Using An Analytical/Semi-Analytical Model, SPE Annual Technical Conference and Exhibition. Society of Petroleum Engineers, New Orleans, Louisiana, pp. 7 doi:https://dx.doi.org/10.2118/124697-MS

Xu, Y., Cavalcante Filho, J.S.A., Yu, W. and Sepehrnoori, K., 2017. Discrete-Fracture Modeling of Complex Hydraulic-Fracture Geometries in Reservoir Simulators. SPE Reservoir Evaluation & Engineering, 20(02): 403-422 doi:https://doi.org/10.2118/183647-PA

Yao, F., Weng, D., Li, Y., Yu, Y. and Hou, F., 2007. Reorientation Refracturing Case Study, Production and Operations Symposium. Society of Petroleum Engineers, Oklahoma City, Oklahoma, U.S.A., pp. 6 doi:https://dx.doi.org/10.2118/106595-MS

Zemanek, J. et al., 1969. The Borehole TeleviewerA New Logging Concept for Fracture Location and Other Types of Borehole Inspection. Journal of Petroleum Technology, 21(06): 762-774 doi:https://dx.doi.org/10.2118/2402-PA

Zemanek, J., Glenn, E.E., Norton, L.J. and Caldwell, R.L., 1970. Formation evaluation by inspection with the borehole televiewer. Geophysics, 35(2): 254-269 doi:https://doi.org/10.1190/1.1440089

Zemel, B., 1995. Tracers in the oil field. Elsevier.

Zhang, H., Rietz, D., Cagle, A., Cocco, M. and Lee, J., 2016. Extended exponential decline curve analysis. Journal of Natural Gas Science and Engineering, 36: 402-413

Zheltov, A.K., 1955. 3. Formation of Vertical Fractures by Means of Highly Viscous Liquid, 4th World Petroleum Congress. World Petroleum Congress, Rome, Italy, pp. 8

Zhou, J., Zeng, Y., Jiang, T., Zhang, B. and Zhang, X., 2015. Tiltmeter Hydraulic Fracturing Mapping on a Cluster of Horizontal Wells in a Tight Gas Reservoir, SPE/IATMI Asia Pacific Oil & Gas Conference and Exhibition. Society of Petroleum Engineers, Nusa Dua, Bali, Indonesia, pp. 9 doi:https://dx.doi.org/10.2118/176371-MS

Zhu, D., Hill, D. and Zhang, S., 2018. Using Temperature Measurements From Production Logging/Downhole Sensors To Diagnose Multistage Fractured Well Flow Profile, SPWLA 59th Annual Logging Symposium. Society of Petrophysicists and Well-Log Analysts, London, UK, pp. 13 doi:https://www.onepetro.org/conference-paper/SPWLA-2018-PP

Zuo, L., Yu, W. and Wu, K., 2016. A fractional decline curve analysis model for shale gas reservoirs. International Journal of Coal Geology, 163: 140-148

Appendix A: CRSM Derivations

Liquid Production:

For a vertical well without mechanical skin factor, see figure (A–1), Economides et al. (2013) gave the general expression for the inflow performance relationship under PSS condition in oil field units:

$$\overline{P}_r - P_{wf} = \frac{141.2 q_o \mu_o B_o}{kh} \left(\frac{1}{2} \ln \left[\frac{4A}{C_A \gamma r_w^2} \right] \right) \qquad \text{A-(1)}$$

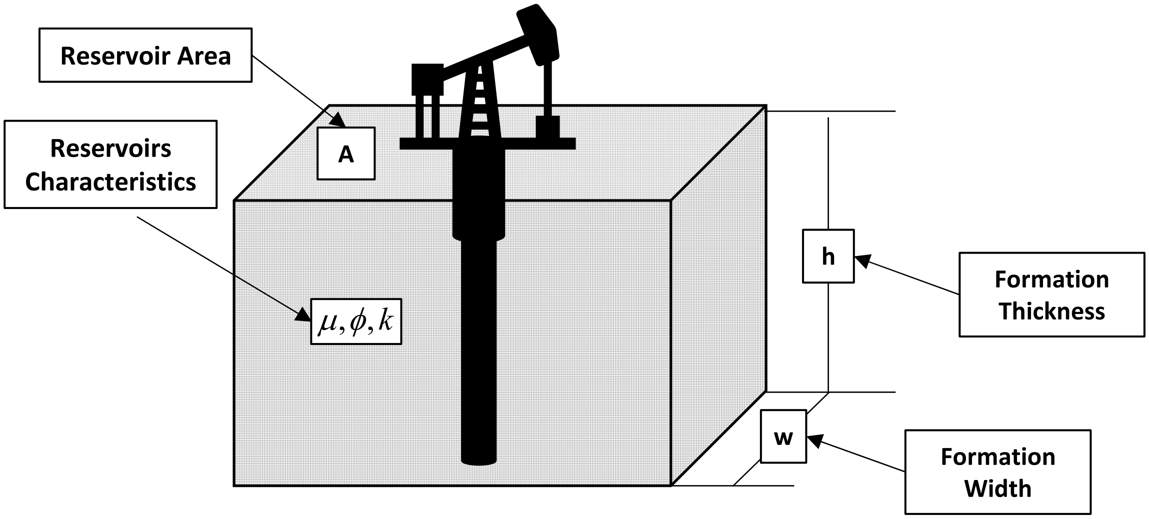

Figure A - 1: Schematic of a vertical well that is used as the basis of the derivations of the Connected Reservoir Storage Model (CRSM).

Assumptions:

1. Vertical well
2. Constant production rate
3. No mechanical skin effects
4. No non-Darcy flow effects

Where the parameters of Eq. A-(1) are as follows: $\overline{P}_r$ is the average reservoir pressure in psi , P_{wf} is the flowing bottomhole pressure in psi, q_o is the production rate in STB/d, k is permeability in md, B_o is the oil formation volume factor in bbls/STB, A is drainage area in ft^2, C_A is the shape factor which is dimensionless, γ is Euler constant equal to 1.78, and r_w is the wellbore radius in feet as illustrated in (Economides et al., 2013).

Defining the reservoir storage as:

$$E(t) = V_p(t)c_t \qquad \text{A-(2)}$$

Assuming the reservoir is cylindrical in shape with constant porosity and thickness, then we have Eq. A-(2) can be expressed as:

$$E(t) = Ah\phi c_t \qquad \text{A-(3)}$$

Where $V_P(t)$ and c_t are the proven volume and total compressibility as it relates to liquid. Rearranging Eq. A-(3) and solving for the drainage area and substituting this equation into equation Eq. A-(1) and simplifying, the PSS solution to the radial diffusivity equations becomes,

$$\bar{P}_r - P_{wf} = \frac{70.6 q_{osc} \mu_o B_o}{kh} \ln\left[\frac{4V_p(t)}{C_A \gamma \phi h r_w^2}\right] \qquad \text{A-(4)}$$

Total compressibility is defined as:

$$c_t = c_w S_W + c_o S_o + c_g S_g + c_f \qquad \text{A-(5)}$$

where the parameters of Eq. A-(5) are as follows: c_t total compressibility in psi^{-1}, c_w is the water compressibility in psi^{-1}, S_w is water saturation fraction, c_o is the oil compressibility in psi^{-1}, S_o is oil saturation fraction, c_g is the gas compressibility in psi^{-1}, S_g is gas saturation fraction, and c_f is the pore volume compressibility in psi^{-1}.

From material balance and assuming pseudosteady state (PSS) conditions Eq. A-(5) takes the following form:

$$c_t = -\frac{1}{V}\frac{\Delta V}{\Delta P} = -\frac{1}{V_p(t)}\frac{Q_o(t)}{\overline{P}_r - P_i} \qquad \text{A-(6)}$$

where $Q_o(t) = \int_0^t q_o(\tau) B_o d\tau$

Rearrange Eq. A-(6) to solve for the average reservoir pressure will yield the following equation:

$$\overline{P}_r(t) = -\frac{1}{V_p(t)}\frac{Q_o(t)}{c_t} + P_i \qquad \text{A-(7)}$$

Plugging Eq. A-(7) into equation Eq. A-(4) will yield the following equation Eq. A-(8), which is the differential pressure across the sand face.

$$P_i - P_{wf} = \frac{70.6 q_{osc} \mu_o B_o}{kh} \ln\left[\frac{4V_p(t)}{C_A \gamma \phi h r_w^2}\right] + \frac{1}{V_p(t)}\frac{Q_o(t)}{c_t} \qquad \text{A-(8)}$$

Note that $E(t) = V_p(t) c_t$ and plugging this expression into Eq. A-(8) and further simplifying becomes:

$$P_i - P_{wf} = \frac{70.6 q_o \mu_o B_o}{kh} \ln\left[\frac{4E(t)}{C_A \gamma \phi h c_t r_w^2}\right] + \frac{Q_o(t)}{E(t)} \qquad \text{A-(9)}$$

Simplifying Eq. A-(9) and defining the following normalized rate and cumulative production terms Eq. A-(11) and A-(12) the new equation is as follows:

$$1 = \frac{70.6\mu_o}{kh} \ln\left[\frac{4E(t)}{C_A \gamma \phi h c_t r_w^2}\right] q_N(t) + \frac{Q_N(t)}{E(t)} \qquad \text{A-(10)}$$

Defining: $\varepsilon = \frac{70.6\mu_o}{kh}$, $\sigma = \frac{4E(t)}{C_A \gamma \phi h c_t r_w^2}$

$$Q_N(t) = \frac{Q_o(t)}{P_i - P_{wf}} \qquad \text{A-(11)}$$

$$q_N(t) = \frac{q_o(t)}{P_i - P_{wf}} \qquad \text{A-(12)}$$

where $Q_N(t)$ is in units of bbls/psi, and $q_N(t)$ is in units of bbls/psi/day.

The normalized PSS solution to the radial diffusivity equation for liquid reservoirs is defined as follows.

$$1 = \varepsilon \ln[\sigma] q_N(t) + \frac{Q_N(t)}{E(t)} \qquad \text{A-(13)}$$

Gas Production:

Similarly, we can derivate the gas connected reservoir storage model by introducing the normalized or adjusted pseudopressure term. Defining pseudopressure as follows:

$$m(P) = 2\int_0^P \frac{P}{\mu(P_{ref}) z(P_{ref})} dP \qquad \text{A-(14)}$$

Defining the normalized pseudopressure as illustrated from (Olivier Houze et al., 2016).

$$\delta = \frac{P_{ref}}{m(P_{ref})} m(P_j) \qquad \text{A-(15)}$$

Plugging Eq. A-(14) and A-(15) into Eq. A-(1) and solving Eq. A-(1) similar to the procedure as outlined in Spivey and Lee (2013) will yield the gas well initial production rate (IPR) using the normalized pseudopressure for gas production form as follows:

$$\bar{\delta}_r - \delta_{wf} = \frac{141.2 q_g \mu_g B_g}{kh}\left(\frac{1}{2}\ln\left[\frac{4A}{C_A \gamma r_w^2}\right]\right) \qquad \text{A-(16)}$$

where $\bar{\delta}_r$ is the normalized average reservoir pressure in psi , δ_{wf} is the normalized flowing bottomhole pressure in psi, q_g is the production rate in Mscf/d, k is permeability in md, B_g is the gas formation volume factor in bbls/Mscf, A is drainage area in ft^2, C_A is the shape factor which is dimensionless

Simplifying Eq. A-(16) and plugging in Eq. A-(3) the new form of Eq. A-(16) is as follows:

$$\bar{\delta}_r - \delta_{wf} = \frac{70.6 q_g \mu_g B_g}{kh}\ln\left(\frac{4V_P(t)}{C_A \gamma \phi h r_w^2}\right) \qquad \text{A-(17)}$$

Defining total compressibility equation A-(6) in the form of pseudopressure as well as taking the derivative yields the following relationship for total compressibility for gas:

$$c_t = -\frac{1}{V}\frac{\Delta V}{\Delta P} = -\frac{1}{V_p(t)}\frac{Q_g(t)}{\partial m(P)}\frac{\partial m(P)}{\partial P} = -\frac{1}{V_p(t)}\frac{Q_g(t)}{m(\bar{P}_r) - m(P)_i}\frac{2P}{\mu_g z} \qquad \text{A-(18)}$$

where $Q_g(t) = \int_0^t q_g(\tau) B_g d\tau$

Expressing the form of A-(18) in terms of normalized pressures, and note that δ_i is the normalized initial reservoir pressure in psi:

$$c_t = -\frac{1}{V_p(t)}\frac{Q_g(t)}{\overline{\delta}_r - \delta_i} = -\frac{1}{Ah\varphi}\frac{Q_g(t)}{\overline{\delta}_r - \delta_i} \qquad \text{A-(19)}$$

Where ΔV is the cumulative gas production volume in reservoir condition, in terms of surface production Q_g. Rewriting Eq. A-(19) in the form of average normalized reservoir pressure will yield the following expression:

$$\overline{\delta}_r = -\frac{Q_g(t)}{Ah\phi c_t} + \delta_i \qquad \text{A-(20)}$$

Plugging Eq. A-(20) into equation Eq. A-(19) will yield the following equation, which is the differential pressure across the sand face.

$$\delta_i - \delta_{wf} = \frac{70.6 q_g \mu_g B_g}{kh}\ln\left(\frac{4V_P(t)}{C_A \gamma \phi h r_w^2}\right) + \frac{Q_g(t)}{Ah\phi c_t} \qquad \text{A-(21)}$$

Recall that $E(t) = V_p(t)c_t$ then Eq. A-(21) becomes:

$$\delta_i - \delta_{wf} = \frac{70.6 q_g \mu_g B_g}{kh}\ln\left(\frac{4E(t)}{C_A \gamma \phi h c_t r_w^2}\right) + \frac{Q_g(t)}{E(t)} \qquad \text{A-(22)}$$

Simplifying Eq. A-(22) and defining the following normalized rate and cumulative production terms of gas Eq. A-(24) and A-(25):

$$1=\frac{70.6\mu_g}{kh}\ln\left(\frac{4E(t)}{C_A\gamma\phi hc_t r_w^2}\right)q_{N_g}(t)+\frac{Q_{N_g}(t)}{E(t)} \quad \text{A-(23)}$$

Defining: $\zeta=\frac{70.6\mu_g}{kh}$ and $\sigma=\frac{4E(t)}{C_A\gamma\phi hc_t r_w^2}$

$$Q_{N_g}(t)=\frac{Q_g(t)}{\delta_i-\delta_{wf}} \quad \text{A-(24)}$$

$$q_{N_g}(t)=\frac{q_g(t)}{\delta_i-\delta_{wf}} \quad \text{A-(25)}$$

where $Q_{N_g}(t)$ is in units of bbls/psi, and $q_{N_g}(t)$ is in units of bbls/psi/day. The normalized PSS solution to the radial diffusivity equation for gas reservoirs is defined as follows:

$$1=\zeta\ln(\sigma)q_{N_g}(t)+\frac{Q_{N_g}(t)}{E(t)} \quad \text{A-(26)}$$

Fracture Volume via Unit Pressure Response and Wellbore Storage for Gas Reservoirs:

Using the definition for wellbore storage Eq. A-(27), assuming gas compressibility is constant and no liquid dropout, as defined in (Spivey and Lee, 2013), which is the product of the gas compressibility (psi^{-1}) and wellbore volume (ft^3):

$$C=c_g V_{wb} \quad \text{A-(27)}$$

Defining the differential pressure across the sand face at standard conditions:

$$\Delta P = \frac{1000 q_g B_g t}{24C} \qquad \text{A-(28)}$$

where C is the wellbore storage in cf/psi, q_g is the production rate in Mscf/d, B_g is the gas formation volume factor in cf/Mscf, and t is production time in hours.

Solving Eq. A-(28) in terms of wellbore storage:

$$C = \frac{1000 q_g B_g t}{24\Delta P} \qquad \text{A-(29)}$$

Defining the formation volume factor for gas as follows and note that B_g in Eq. A-(30) has units of cf/scf; therefore, B_g will be converted to scf/Mscf once substituted into A-(29):

$$B_g = \frac{P_{sc}}{T_{sc}}\left(\frac{zT}{P}\right) = 0.028269\frac{zT}{P} \qquad \text{A-(30)}$$

Expanding Eq. A-(30) and subbing in Eq. A-(29) the following expression for wellbore storage is as follows:

$$C = \frac{1000 q_g B_g t}{24\Delta P} = 1.178\frac{q_g t}{P_i - P_{wf}}\frac{zT}{P} \qquad \text{A-(31)}$$

Manipulating and rearranging Eq. A-(31) is as follows:

$$C = \frac{1000 q_g B_g t}{24\Delta P} = \frac{1.178 q_g t T}{\mu_g}\frac{1}{\frac{P\left(P_i - P_{wf}\right)}{\mu_g z}} = \frac{2.36 q_g t T}{\mu_g}\frac{1}{\frac{2P}{\mu_g z}\left(P_i - P_{wf}\right)} \qquad \text{A-(32)}$$

Using the average gas viscosity and gas deviation factor in place of the gas viscosity and gas deviation factor terms in Eq. A-(32) reduces as follows:

$$C = \frac{2.36 q_g t T}{\mu_g} \frac{1}{\frac{2P}{\bar{\mu}_g \bar{z}}\left(P_i - P_{wf}\right)} \qquad \text{A-(33)}$$

Recall Eq. A-(14) and A-(15) for the definition of pseudopressure and normalized pseudopressure respectively Eq. A-(33) reduces to the following:

$$C = \frac{2.36 q_g T}{\mu_g}\left(\frac{t}{\Delta\delta}\right) \qquad \text{A-(34)}$$

Defining normalized differential pressure in dimensionless form, where q_g is the production rate in Mscf/d, $\overline{B}_g$ is the average gas formation volume factor in cf/Mscf, $\overline{\mu}_g$ is the average gas viscosity in cP, k is the permeability in md, h is the formation thickness in feet, and $P_D(t)$ is the dimensionless pressures, for gas as follows:

$$\Delta\delta = \frac{141.2 q_g \overline{B}_g \overline{\mu}_g}{kh} P_D(t) \qquad \text{A-(35)}$$

Defining the unit pressure response in dimensionless form as follows:

$$P_{Unit_g}(t) = \frac{141.2 \overline{B}_g \overline{\mu}_g}{kh} P_D(t) \qquad \text{A-(36)}$$

Plugging Eq. A-(35) into Eq. A-(36) yields the following:

$$\Delta\delta = q_g P_{Unit_g}(t) \qquad \text{A-(37)}$$

Plugging Eq. A-(37) into Eq. A-(34) and simplifying, the wellbore storage is now a function of the unit pressure response.

$$C_{gas} = \frac{2.36T}{\mu_g}\left[\frac{t}{P_{Unit_g}}\right] \qquad \text{A-(38)}$$

Connected Reservoir Storage Curve Derivations:

The connected reservoir storage at any time t_i can be determined from the intercept on the abscissa of the normalized cumulative production of the tangent line going through $q_N(t)_i$ and $Q_N(t)_i$. The equational form is as follows, where "i" represents the ith time step and the "int." represents the normalized production rate intercept, on the ordinate, at the ith time step.

$$q_N(t)_i = \left(\frac{dq_N(t)}{dQ_N(t)}\right)_i Q_{N_i} + q_N(t)_{\text{int}} \qquad \text{A-(39)}$$

To determine the connected reservoir storage from Eq. A-(39) the normalized rate at the ith time step will be zero and this will yield the connected reservoir storage for the ith time step as follows:

$$E(t)_i = \frac{-q_N(t)_{\text{int}}}{\left({dq_N(t)} \big/ {dQ_N(t)} \right)_i} \qquad \text{A-(40)}$$

Where the derivative can be obtained numerically for discrete points.

Once the connected reservoir storage is determined, the connected pore volume of the well can be determined at any time by the following:

$$V_p(t) = \frac{E(t)}{c_t} \qquad \text{A-(41)}$$

Appendix B: Superposition for Variable Rate

Discretize the production history into $q_1, q_2, \ldots q_n$ in the duration of $t_1, t_2, \ldots t_n$ using variable production-rate scheduling as illustrated in figure (B - 1) and using eq. 2.60 from (Horne, 1995) to solve the flow rate at the N$^{\text{th}}$ step from equation B-(1):

$$P_{wf}(t) = P_i - \frac{141.2 B_o \mu_o}{kh} \left[q_1 P_D(t) + \sum_{j=2}^{N} \left(q_j - q_{j-1} \right) P_D\left(t - t_j \right) \right] \qquad \text{B-(1)}$$

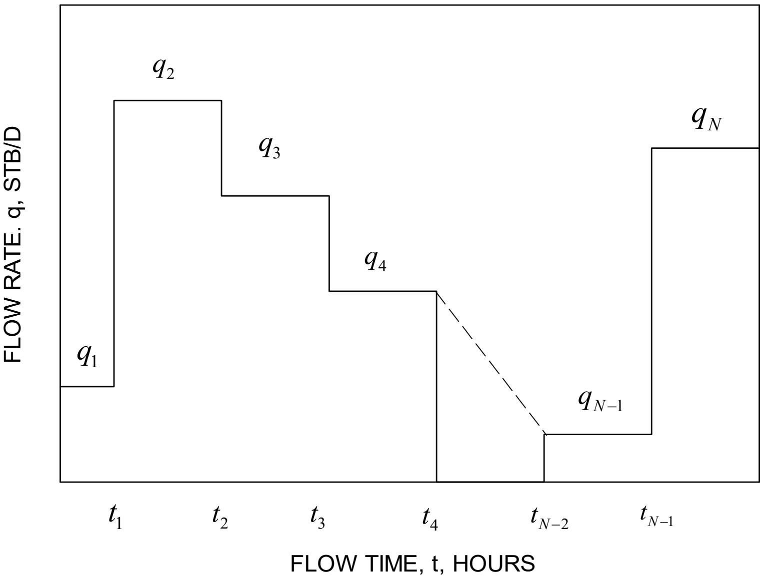

Figure B - 1: Schematic representation of a variable production-rate schedule, pg. 191 (Earlougher, 1977)

Introducing $\alpha = \frac{141.2 B_o \mu_o}{kh}$ gives:

$$P_{wf}(t) = P_i - \alpha \left[q_1 P_D(t) + \sum_{j=2}^{N} \left(q_j - q_{j-1} \right) P_D\left(t - t_j \right) \right] \qquad \text{B-(2)}$$

Next solving the flow rate for the Nth step.

$$\frac{P_i - P_{wf}(t)}{\alpha} = \left[q_1 P_D(t) + \sum_{j=2}^{N} \left(q_j - q_{j-1}\right) P_D\left(t - t_j\right) \right] \qquad \text{B-(3)}$$

Let $\Delta P(t) = P_i - P_{wf}(t)$

$$\frac{\Delta P(t)}{\alpha} = \left[q_1 P_D(t) + \sum_{j=2}^{N} (q_j - q_{j-1}) P_D(t - t_j) \right] \qquad \text{B-(4)}$$

Expanding the right-hand side of Eq. B-(4) for Nth series.

$$\frac{\Delta P(t)}{\alpha} = \left[q_1 P_D(t) + \left(q_N - q_{N-1}\right) P_D\left[t - t_j\right] + \sum_{j=2}^{N-1} (q_j - q_{j-1}) P_D(t - t_j) \right] \qquad \text{B-(5)}$$

Eq. B-(5) gives the flow rate at the Nth step for a given flowing bottomhole pressure is as follows.

$$q_N = q_{N-1} + \frac{1}{P_D\left[t - t_j\right]} \left[\frac{\Delta P(t)}{\alpha} - \sum_{j=1}^{N-1} (q_j - q_{j-1}) P_D(t - t_j) \right] \qquad \text{B-(6)}$$

Defining unit pressure as follows:

$$P_{Unit}(t) = \frac{141.2\mu_o}{kh} P_D(t) = \frac{\alpha}{B_o} P_D(t) \qquad \text{B-(7)}$$

$$P_{Unit}(t - t_j) = \frac{141.2\mu_o}{kh} P_D(t - t_j) = \frac{\alpha}{B_o} P_D(t - t_j) \qquad \text{B-(8)}$$

Rewriting Eq. B-(6) in terms of unit pressure and simplifying:

$$q_N = q_{N-1} + \frac{1}{P_{Unit}\left[t - t_j\right]}\left[\Delta P(t) - \sum_{j=1}^{N-1}(q_j - q_{j-1})P_{Unit}(t - t_j)\right] \qquad \text{B-(9)}$$

Equation B-(9) is the production rate prediction based on deconvolution and superposition. Unit pressure response is determined from the deconvolution of the normalized cumulative and production rate as a function of time.

Appendix C: CRSM Process Flow

Applying the CRSM procedure, an eight-step implementation process:

Step 1: Gather BHFP and production rate historical data. The data should be tabulated as follows:

Table C - 1 Tabulated data format for a producing well. The three main parameters needed for the CRSM is production time, BHFP and production flow rate.

Time	Bottomhole Flowing Pressure	Flow Rate
t_1	P_{wf1}	q_1
t_2	P_{wf2}	q_2
...	...	...
...	...	...
t_i	$P_{wf\,i}$	q_i

Step 2: Generate the Normalized Decline Curve (NDC) using the normalized cumulative production Eq. A-(13), liquid production, Eq. A-(26), gas production, and the normalized cumulative and production rate Eq. A-(11) and A-(12), liquid production, Eq A-(24) and A-(25) for gas production.

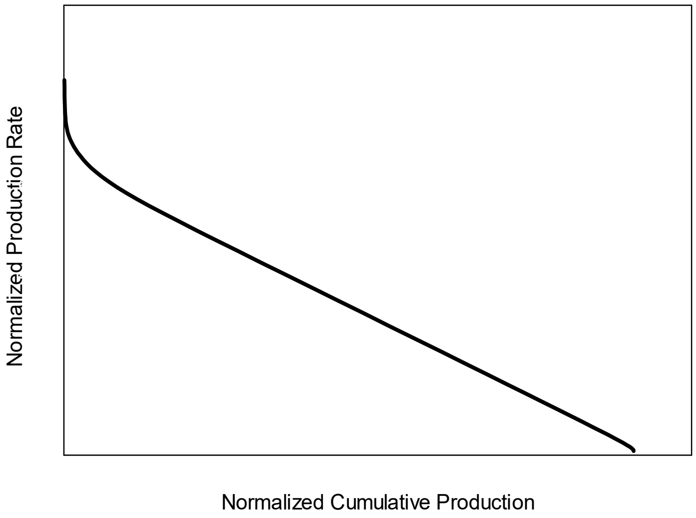

Figure C - 1: Normalized Decline Curve determined from the BHFP and flow rate production history. The NDC curve is generated from Eq. A-(11) and Eq. A-(12), liquid production, Eq. A-(24) and Eq. A-(25), gas production, of the normalized production and normalized cumulative production, respectively.

The NDC curve, figure (C - 1), is used to diagnose the well performance and flow region of a producing well.

Step 3: Using numerical differentiation for discrete points, the data that governs NDC, represents the tangent at any point on the NDC. Eq. A-(40) is used to determine the linear line that is tangent at any time on the NDC. Using equation A-(40) the tangent for a given moment in time on the NDC, where $E(t_l)$ is the CRS value at time t_l of well life can be determined from the intercept of the abscissa line of the normalized cumulative production. This is illustrated in Figure (C - 2) as follows:

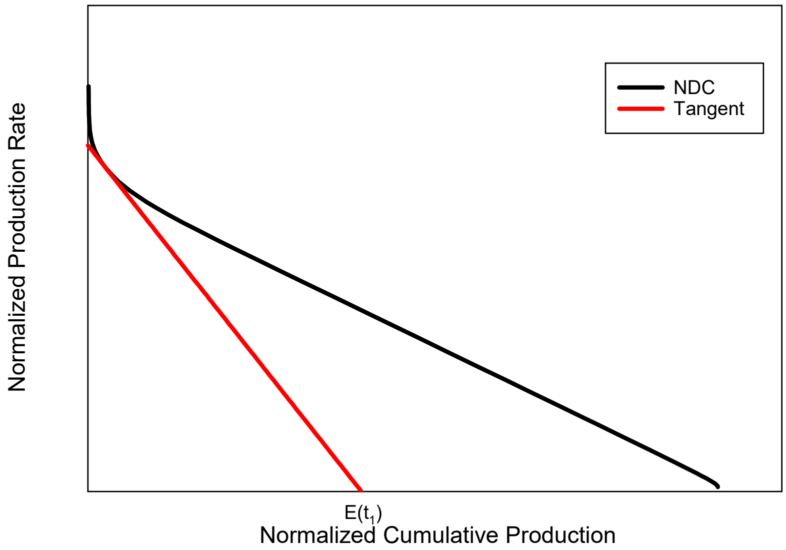

Figure C - 2: Any point tangent along the NDC can be extrapolated to the normalized cumulative production intercept, abscissa axis, which determines the reservoir storage.

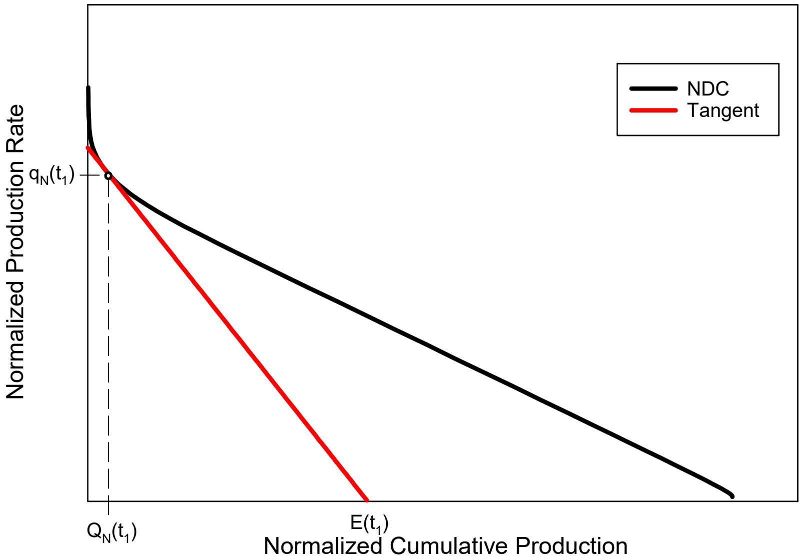

Figure C - 3: The reservoir storage E(t) can be determine from the tangent to the NDC for any value of time for a given set of normalized production rate and cumulative production parameters, respectively.

Step 4: During the transient flow regime, the CRS value changes until PSS flow regime is reached. Once PSS flow regime is reached, the CRS value will be approximately constant. The CRS value is related to the normalized production rate and normalized cumulative production for a given time interval and is illustrated in Figure (C - 3).

Step 5: Determine the CRS, Eq. A-(40) and it should be noted that the CRS is also referred to as the proven energy (PrE). The CRS curve, Figure (C - 4), is illustrated as a function of time and shows the transition that occurs from the transient flow regime to PSS flow regime. During the transient flow regime CRS is not constant, whereas CRS is approximately constant during the PSS flow regime.

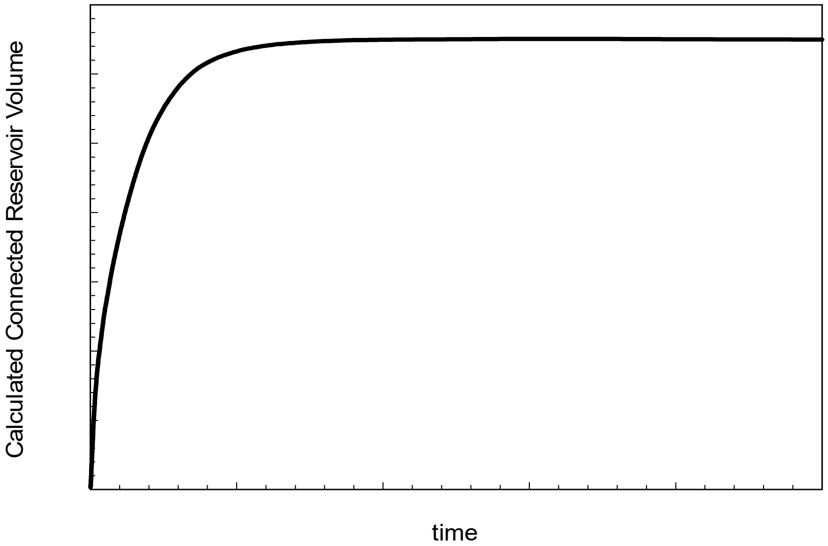

Figure C - 4: Connected Reservoir Storage Volume can be determined for any time through Eq. A-(40), which is the reciprocal of negative normalized production rate intercept to the derivative of the NDC

Step 6: Finding the connected pore volume at various stages of well life, the proven volume can be determined at any given time Eq. A-(41).

Step 7: Using deconvolution methods, user's preference, to determine the unit pressure response curve, figure (C - 5), the deconvolved pseudopressure drop curve and deconvolved pseudopressure derivative curve, figure (C - 6). The pseudopressure drop curve can be used to predict the production rate for complex reservoirs and zonal rate allocations and monitor well productivity change and skin history. The derivative curve states the boundary conditions and flow regimes in the reservoir.

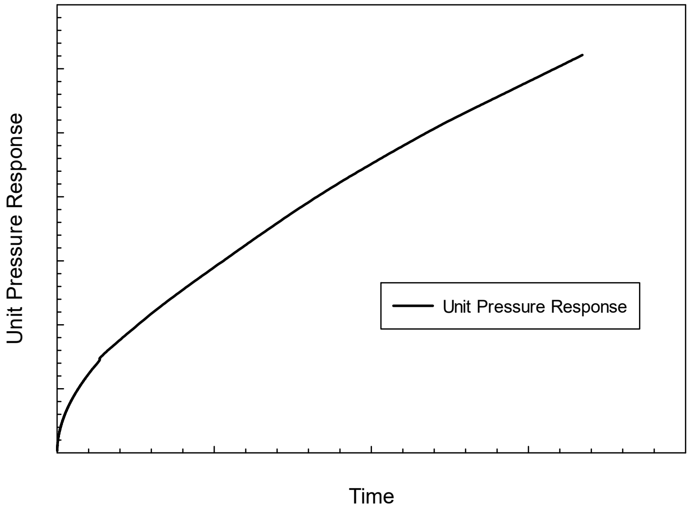

Figure C - 5: Deconvolved unit pressure response curve that is determined from historical production data.

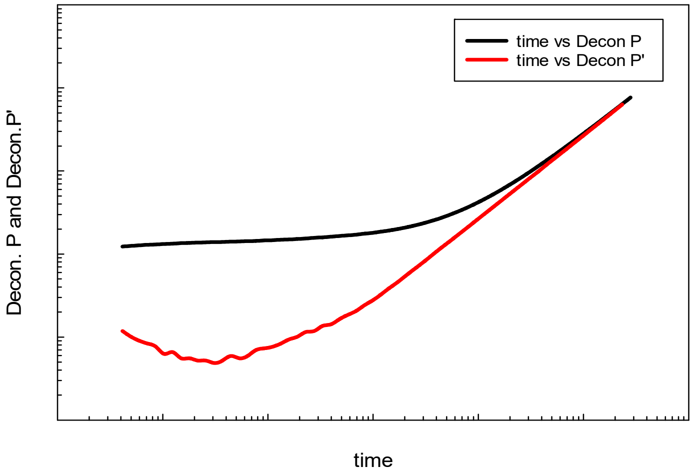

Figure C - 6: Deconvolved pseudopressure and pseudopressure derivative curve. This curve can be used for reservoir characterization and flow regime determination.

Step 8: Using CRSM along with figures (C - 1) through (C - 6), one can estimate and forecast reserves along with determining reservoir characteristics and original fluids in place by only utilizing bottom hole flowing pressure and rate production historical profiles.

Appendix D: CRSM Derived with ROI and Time

This section will demonstrate how the CRSM can be derived as function of the radius of investigation (ROI) and time. Starting off with the definition of the Ei(-x) function where Ei(-x) is defined as follows:

$$Ei(-x) = \int_{x}^{-\infty} \frac{e^{-y}}{y} dy \qquad \text{D-(1)}$$

Where "x" is defined as follows:

$$x = \frac{948 \varphi \mu c_t r^2}{kt} \qquad \text{D-(2)}$$

Since the diffusivity equation is linear and a 2nd order partial derivative equation, the principle of superposition can be used to compute solutions for complex boundary conditions using only linear solution combinations for relatively simple boundary conditions. In fact, horizontal wells can be characterized as the superposition of multiple vertical wells where each completion stage is assumed to be a vertical well.

Since the logarithmic approximation to the Ei(-x) function is zero when the argument of the logarithm is "1" then the following can be assumed $1.781x = 1$; therefore, Eq. D-(1) can be expressed as follows:

$$Ei(-x) \sim -\ln(1.781x), x \leq 0.01 \qquad \text{D-(3)}$$

and Eq. D-(2) can be solved for time by setting "x" equal to $x = \frac{1}{1.781}$, then the equation for time is as follows:

$$t = \frac{1688 \varphi \mu c_t r_{inv}{}^2}{k} \qquad \text{D-(4)}$$

Solving Eq. D-(4) in terms of the radius of investigations is as follows:

$$r_{inv} = 0.0243 \sqrt{\frac{kt}{\varphi \mu c_t}} \qquad \text{D-(5)}$$

Using Eq. A-(2) and expanding the connected reservoir storage equation with time dependent pore volume and assuming for a special case of a cylindrical reservoir with constant thickness and porosity, the connected reservoir storage can be expressed:

$$E(t) = c_t V_P(t) = c_t \pi r_{inv}^2 h \varphi \qquad \text{D-(6)}$$

Plugging Eq. D-(5) into Eq. D-(6) and simplifying then the CRS will become:

$$E(t) = \pi \left[0.0243^2 \frac{kt}{\mu} \right] h \qquad \text{D-(7)}$$

Mobility is defined as $\lambda = {}^{k}\!/_{\mu}$ and setting $a = 0.0243^2 \pi$; therefore, Eq. D-(7) can be simplified where $E(t)$ is a function of mobility and time with uniform thickness.

$$E(t) = a \lambda h t \qquad \text{D-(8)}$$

Eq. D-(8) shows that for the special case, the connected reservoir storage has a linear relationship with the increase of time. This conclusion is very critical for rate forecast before the radius of investigation is less than the external reservoir boundary. This linear relationship can be used to extrapolate the connected reservoir storage growth, even for the case of changing reservoir thickness, permeability, and viscosity. Moreover, from Eq. D-(8) one can use geological parameters to predict production performance without the actual production history, which is a topic that will be further researched in the future.